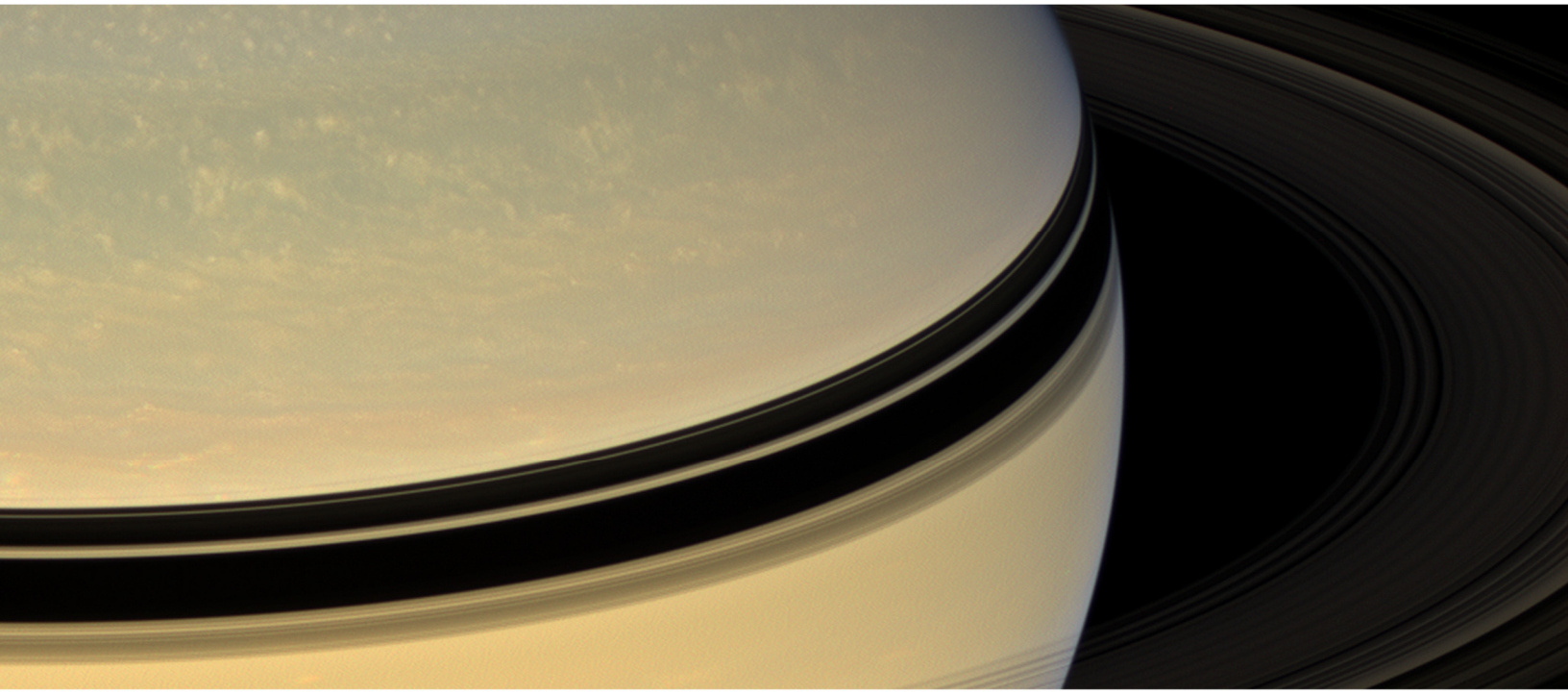

SATURN

Before Cassini, scientists viewed Saturn's unique features only from Earth and from a few spacecraft flybys. During more than a decade orbiting the gas giant, Cassini studied the composition and temperature of Saturn's upper atmosphere as the seasons changed there. Cassini also provided up-close observations of Saturn's exotic storms and jet streams, and heard Saturn's lightning, which cannot be detected from Earth. The Grand Finale orbits provided valuable data for understanding Saturn's interior structure and magnetic dynamo, in addition to providing insight into material falling into the atmosphere from parts of the rings.

Cassini's Saturn science objectives were overseen by the Saturn Working Group (SWG). This group consisted of the scientists on the mission interested in studying the planet itself and phenomena which influenced it. The Saturn Atmospheric Modeling Working Group (SAMWG) was formed to specifically characterize Saturn's uppermost atmosphere (thermosphere) and its variation with time, define the shape of Saturn's 100 mbar and 1 bar pressure levels, and determine when the Saturn safely eclipsed Cassini from the Sun. Its membership consisted of experts in studying Saturn's upper atmosphere and members of the engineering team.

CONTENTS

Figures

Tables

EXECUTIVE SUMMARY

The Executive Summary is organized into the 10 major discoveries that Cassini made about the planets during its 13 years at Saturn and its months-long flyby of Jupiter.

The planets themselves were an important scientific objective of the Cassini mission, and they are the focus of this Saturn Discipline Working Group (DWG) science results. The Executive Summary is organized into the 10 major discoveries that Cassini made about the planets during its 13 years at Saturn and its months-long flyby of Jupiter. Measurements for the future, after Cassini, are given at the end. The main parts are organized by objectives listed in the Cassini Announcement of Opportunity (AO) and the Traceability Matrix (TM) of the Cassini Solstice Mission (CSM). The bold items in parenthesis that appear with the 10 major discoveries in the Executive Summary refer to the sub-sections in the Saturn DWG Science Results and Saturn DWG Non-Saturn Science Results sections. Figures are found in these sub-sections.

1. **Great Storm on Saturn – (Storms (SN1b, SN2a))**

   a. **Storm Evolution.** Saturn's weather is generally quieter and blander than Jupiter's and Earth's, but every few decades a latitude band erupts with turbulent clouds, high winds, and lightning. Typically the disturbed region spreads eastward or westward around the planet and fades after a few months of violent activity. Five such eruptions, sometimes called great white spots, were observed from Earth during the period 1876–1990. Cassini was fortunate to be in orbit, routinely taking images and searching for radio signals from Saturn lightning, when the great storm of 2010–2011 began. The storm appeared on December 5, 2010 as a small dot in an Imaging Science Subsystem (ISS) image and a sudden start of lightning activity recorded by the Radio and Plasma Wave Science (RPWS) instrument. Within a few days, amateur astronomers were tracking its progress from Earth, and within a month a new set of observing commands had been uploaded onto the Cassini spacecraft to bring its powerful instruments to bear on the new target. Figure SATURN-7 shows an ISS image of the storm on February 25, 2011, after the storm's head, trailing westward, had wrapped around the planet and caught the tail. The giant storm of 2010–2011 is extensively reviewed by Sanchez-Lavega et al. [2018].

   b. **Lightning.** For months or years at a time, Saturn does not emit the broad-band radio signals called atmospherics (sferics) that are produced by lightning. In contrast, the great storm of 2010–2011 was emitting constantly, often faster than the RPWS counting rate of ten per second. The ISS is only ON when the shutter is open, for about 0.1 second depending on the filter, but sometimes it detects lightning. Figure SATURN-8 shows a color image, a superposition of three ISS

images in different filters taken in rapid succession. The blue filter happened to capture a lightning flash, which shows up as a blue dot near the right edge of the image. Further to the right, a second color image taken 30 minutes later at the same location failed to capture a lightning flash. The size of the observed flash is comparable to the depth from the tops of the clouds down to the light source, which is probably in the water cloud. This data could give an estimate of the amount of water on Saturn, and the analysis is ongoing.

c. **Ammonia Precipitation.** The great storm affected all levels in the atmosphere. Figure SATURN-9 [Janssen et al. 2013] shows images from 2009, 2010, and 2011 taken by the Cassini Titan Radar Mapper (RADAR) with its transmitter turned OFF. Operated this way, the instrument sees thermal radiation coming up through dry spots, which are gaps in the otherwise uniform distribution of ammonia vapor. The gaps show up as bright areas, and on March 20, 2011 the great storm, at 30–40° planetocentric latitude, shows up as a low-ammonia band [Sromovsky et al. 2016]. This tells us something about the updrafts and downdrafts, since the vapor falls out when the air is rising. The first models of this process have been published [Li and Ingersoll 2015], and the research is ongoing.

d. **Upward-Propagating Waves.** The great storm sent waves propagating up into the stratosphere, where they break and deposit their energy. The heating is strong enough to cause chemical changes of the stratospheric gases, which are still somewhat of a mystery. Figure SATURN-10 [Fletcher et al. 2011] shows an Earth-based image, left, and two infrared images taken by Cassini Composite Infrared Spectrometer (CIRS) on January 19, 2011. The center image records temperature in the upper troposphere, at the 200–500 mbar level, and the right image shows temperatures at the 1–10 mbar level. The stratospheric beacon stands out in the right image.

e. **Temperatures, Molecular Hydrogen, and Heat Budget.** Figure SATURN-11 [Achterberg et al. 2014], from Cassini CIRS, shows evidence of air being dredged up from below. The top two panels show tropospheric temperature before and after the storm, and the band from 30–40° planetographic has warmed by several degrees. The bottom two panels show the two chemical states (nuclear spins parallel and nuclear spins anti-parallel) of molecular hydrogen H_2 before and after the great storm. The 30–40° band shows a low para fraction, which indicates that the air has risen from below cloud base. Figure SATURN-4 [Li et al. 2015] shows the thermal emission of the planet, in units of W m^{-2}, also from Cassini CIRS. Comparing the years before and after 2011, it is clear that the storm increased the thermal emission by 5–10% in the 30–40° latitude band, and that the anomaly persisted for several years. These details are important for understanding why Saturn erupts and are a necessary test of atmospheric models.

2. Saturn's Rotation and Interior – (Saturn's Rotation Rate (SN1a))

a. **Rotation.** The giant planets reveal their rotation in several ways—from cloud motions in the atmosphere, from the wobble of the internally-driven magnetic field, from radio waves, from the equatorial bulge, and for Saturn at least, from internal oscillations revealed in slight eccentricities in the orbits of ring particles. Cloud motions have two problems. Different latitudes give different periods ranging from about 10 h 12 m to about 10 h 40 m, and the atmosphere can slide relative to deeper levels. Saturn's internally-driven magnetic field is aligned within 0.06° of the rotation axis [Cao et al. 2011], so it does not wobble. As a random event, such alignment is highly improbable, given that the other giant planets are misaligned by tens of degrees and the probability goes as the area on the surface of the sphere rather than the angle from the pole. Voyager detected radio waves with a period of 10 h 39 m 22 s, but the radio periods turned out to vary over the years in ways that strongly suggested they originated in the upper atmosphere and magnetosphere.

b. **Gravity.** The other methods, involving gravity, are being developed and tested. Rotation causes the planet to bulge at the equator, but to interpret the shape it is necessary to know the equation of state to high accuracy. The shape of the atmosphere just gives the rotation of the atmosphere. The axisymmetric components of the gravity field indicate that the zonal winds extend 9000 km down into the fluid interior [Iess et al. 2019; Galanti et al. 2019]. The depth is greater than that for Jupiter, and that is consistent with the greater depth on Saturn at which magnetic drag reduces the winds to zero. The method involves tracking the orbit of the spacecraft using the Doppler shift of the craft's radio signal, which is observed to high precision.

c. **Ring seismology.** The orbits of Saturn's ring particles are exquisitely sensitive to non-axisymmetric (tesseral) harmonics of the gravity field. These could be due to normal mode oscillations in Saturn's interior or masses floating in the interior and rotating with it. Figure SATURN-15 [Hedman and Nicholson 2014] shows observed periods that are close to the atmospheric periods and are therefore likely be the signature of floating masses. The observed periods are just as diverse as those derived from cloud motions, which may indicate floating masses moving at different speeds. The frequencies of the normal modes depend on the planet's rotation. The implied rotation period turns out to be intermediate between the shortest and longest atmospheric periods defined from cloud motions at different latitudes [Mankovich et al. 2019]. Although the possibility of using the rings as a seismometer was predicted before Cassini, there was no guarantee that the irregularities inside the planet would be large enough.

3. **Energy for the Zonal Jet Streams – (Atmospheric dynamical processes (S_AO2))**

    a. **Mean Zonal Winds.** The eastward-flowing and westward-flowing jet streams are an iconic feature of giant planet atmospheres. They are remarkably fast and remarkably steady in time by terrestrial standards. Figure SATURN-18 [Porco et al. 2003] shows the zonal jet streams for Jupiter. The black curve is from Cassini ISS data in late 2000, and the red curve is from Voyager data in mid-1979. The jets are remarkably steady over this interval of 21 years. Figure SATURN-5 [Garcia-Melendo et al. 2011b] shows Saturn data from Cassini ISS. The black curve represents data from the 350 to 700 mbar levels, and the red curve represents data from 100 to 200 mbar. The differences are small except for a latitude band within ±15° of the equator. This could be part of a 15-year periodicity that resembles the quasi-biennial oscillation in the stratosphere of Earth. We have more to say about that oscillation in the section entitled Saturn DWG Non-Saturn Science Results.

    b. **Eddy Input.** Figure SATURN-13 [Del Genio and Barbara 2012] and Figure SATURN-19 [Salyk et al. 2006] show how eddies are pumping energy and momentum into the jets for Saturn and Jupiter, respectively. Both studies use Cassini ISS data. An eddy in this context is a departure of wind from the zonal mean. The eddy eastward wind u′ is the residual after the mean zonal wind has been subtracted off, and similarly for the eddy northward wind v′. The zonal means of u′ and v′ are zero by definition, but the mean of their product, $\overline{u'v'}$, may be non-zero. Multiplied by the density, this quantity is the northward flux of eastward momentum. If this quantity has the same sign as $\partial\bar{u}/\partial y$, which is the increase of the mean eastward wind with latitude, then the eddies are putting energy into the jets and not the reverse. Figures SATURN-13 and SATURN-19 show that this is the case. The data are less noisy for Jupiter because Jupiter has more small-scale features with which to measure winds from a series of images. This type of eddy mean-flow interaction is an important topic in fluid dynamics and atmospheric science, and the giant planets provide the best examples.

4. **Elemental Abundances and Chemical Tracers – (Composition and chemistry (SN1c); Saturn Formation and Evolution (S_AO5))**

    a. **Helium.** For the Sun, the abundances of major elements relative to hydrogen are known to better than ±10%. Jupiter and Saturn come close to solar composition, but the actual ratios range from less than 1 to at least 10. Each element tells its own story of how and when it was incorporated into the giant planet when it was forming and how the atmospheric ratio has evolved since then. Helium, being the second most abundant element after hydrogen, has special relevance. Direct detection by mass spectrometry when the spacecraft is dipping into the

exosphere on its final proximal orbits is possible, but the determination of the planet's He/H ratio involves extrapolating down to the well-mixed troposphere and is difficult. Remote sensing is difficult because helium has no spectral signature at visible or infrared wavelengths, so one has to use its effect on the molecular mass. Traditionally this is done by finding temperature as a function of pressure from infrared radiometry and then finding density as a function of altitude by preforming an occultation. Hydrostatic equilibrium then gives density as a function of pressure. With T, P, and density, one can solve for the molecular mass. Another approach uses the difference between He and H_2 in their effects on the infrared spectrum of hydrogen itself. The most recent estimate [Koskinen and Guerlet 2018] uses Cassini UVIS for the occultations and CIRS for temperature versus pressure. They get a helium mass fraction Y of 0.16−0.22, which is about 70% of the protosolar mass fraction of 0.27, implying that a certain amount of settling has occurred in Saturn's interior.

b. **Carbon.** The C/H ratio is perhaps the most accurately known ratio of all elements beyond helium. This is because its molecular form, methane, does not condense at Saturn temperatures and is not readily destroyed in chemical reactions. Cassini CIRS probes the far-infrared rotational lines of the molecule and has determined a volume mixing ratio of $(4.7 \pm 0.2) \times 10^{-3}$, corresponding to a C/H enrichment relative to solar of 10.4. This is more than a factor of 2 greater than that for Jupiter and points to a fundamental difference between the gas giants' origin and evolution. The O/H ratio is largely unknown because its molecular form, water, condenses out at the 15–20 bar level, which is well below the levels reachable by remote sensing. CO and H_2O, which are observed in trace amounts in the upper atmosphere, are probably supplied by comets. Without direct observation, the best one can do is to assume that the enrichment factor relative to solar of O/H is the same as that of C/H.

c. **Phosphorus, Arsenic, and Nitrogen.** Although phosphine, PH_3, is also enriched relative to solar by a factor of ~10, its abundance is highly variable and is often used as tracer of vertical motion. The standard view is that PH_3 is brought up from below on updrafts and is destroyed by sunlight in the upper troposphere and stratosphere. Arsine (AsH_3) is supposed to work the same way, and so is ammonia, although it is removed from the upper troposphere by precipitation rather than destruction by sunlight. However, Figure SATURN-2, from Cassini Visual and Infrared Mapping Spectrometer (VIMS) [Fletcher et al. 2011], does not tell a consistent story according to this picture. NH_3 shows a high mole fraction at the equator, consistent with upwelling there and downwelling on either side at 10–12° latitude, but PH_3 and AsH_3 show low abundances at the equator. Low para fraction, discussed in connection with Figure SATURN-11, also implies upwelling at the equator—an observation dating back to Voyager. On the other hand, the Cassini CIRS data [Fletcher et al. 2009a] show a maximum of PH_3 at the equator, which seems to contradict the Cassini VIMS data (Figure SATURN-

2). All the data are good, and the resolution may be that there are two circulations, one on top of the other, with rising motion at high altitude and sinking motion deeper down. This is compatible with all the data, since VIMS is sensitive to deeper levels, 1.3 to 4 bars, where the equatorial downwelling might occur, and CIRS is sensitive above the 1.3 bar level, where the equatorial upwelling might occur. These complications are one of the surprises of the Cassini mission, and tell us important things about how atmospheres work. Upwelling and downwelling are what drive atmospheric circulations and give energy to the winds.

5. **Hexagon and Polar Vortex – (Storms (SN1b, SN2a); Atmospheric dynamical processes (S_AO2))**

a. **Discovery.** Saturn has five or six eastward jets in each hemisphere, but only the one at 75° meanders in latitude, forming a six-lobed pattern. Small clouds within the jet move eastward along the hexagonal pattern at 100 m s^{-1}, but the pattern stays stationary in a reference frame close to Saturn's radio emissions. There is no consensus on why only this jet meanders, although there are numerical models and laboratory experiments that can simulate the phenomenon, given the right boundary and initial conditions. The hexagon was discovered in images taken by the two Voyager spacecraft as they flew past Saturn in 1980 and 1981. It was re-discovered in infrared VIMS images in 2006. ISS images had to wait until the start of spring in the northern hemisphere when the North Pole was in full sunlight. Figure SATURN-12 shows a false color image taken on November 27, 2012. The MT3 and MT2 images, which are dark where the light is passing through methane gas, are projected as blue and green, respectively. The CB2 image, which is not sensitive to methane absorption, is projected as red. The color balance is chosen to make the planet's atmosphere look realistic. The rings look bright blue because there is no methane gas between the rings and the spacecraft.

The hexagon was discovered in images taken by the two Voyager spacecraft as they flew past Saturn in 1980 and 1981.

b. **Polar Cyclone.** The red spot in the center of Figure SATURN-12 extends from the pole to a latitude of 88–89°. It looks red in the false-color image because the clouds are deep and methane gas absorbs the sunlight before it can reflect off the clouds and reach the spacecraft. There is a similar zone in the south, and there the clouds just outside the zone appear to cast shadows, either because they are 50–70 km higher than the clouds inside [Dyudina et al. 2009] or because there is a step-wise poleward decrease in optical depth of the overlying haze [Sromovsky et al. 2019]. The outer ring of clouds circulates counterclockwise around the pole at a speed of 100 m s^{-1}. In these respects the structure is like a

tropical cyclone on Earth—a hurricane—but it is not in the tropics and it is not drawing energy from an ocean underneath. It is known that cyclonic vortices drift poleward, but how they originate and why there is only one on Saturn is still being investigated.

6. Equatorial Oscillation – (Saturn's Winds (SC1b))

a. **Quasi-biennial oscillation.** On Earth, waves generated by storms in the troposphere propagate into the stratosphere and break, depositing energy and momentum there. A symmetry-breaking instability develops in which the eastward waves break preferentially at altitudes where the mean zonal wind is eastward, and similarly for the westward waves and the westward wind. The result is that the mean zonal wind forms an oscillation with altitude that propagates downward with time. The amplitude of the waves sets the period, and on Earth it averages out to 22 months and is known as the quasi-biennial oscillation (QBO). The period of the oscillation on Jupiter is ~4 years, and on Saturn it is ~15 years. Figure SATURN-6 [Fouchet et al. 2008], from Cassini CIRS, documents the oscillation in greater detail, as reflected both in the temperature field, upper panel, and its associated zonal velocity, lower panel. The wave generation mechanism is still uncertain, but presumably the longer period as one moves out in the solar system is due to the lower energy flux available to drive the waves.

7. Upper Atmosphere – (Seasonal Variations (SC1a); Upper atmosphere (SC2a); Aurora (SC2a); (SN1c))

a. **Stratosphere.** Upwelling and downwelling in the stratosphere are detected by chemical tracers as in the troposphere. For both Saturn and Jupiter, the best tracers are probably ethane and acetylene, C_2H_6 and C_2H_2, respectively. Both gases are formed from photodissociation of methane at mbar levels and are destroyed in the troposphere where they revert back to methane. Thus an enhancement at the 200 mbar level is indicative of downwelling.
Figure SATURN-20 [Nixon et al. 2007] shows the picture for Jupiter, as derived from Cassini CIRS data. C_2H_2 has a shorter lifetime once it is formed than C_2H_6 does, so it decays on the downdrafts faster than C_2H_6. Thus the lower panel of Figure SATURN-20 shows downdrafts at the pole and updrafts at the equator. The upper panel shows that the time constant of this circulation is longer than the lifetime of the C_2H_2 molecule, because it has decayed before reaching the 200 mbar level.

b. **Thermosphere.** An ongoing mystery is why the thermosphere is so warm outside the polar auroral zones. The problem is illustrated in Figure SATURN-16 [Koskinen et al. 2015], which compares Cassini Ultraviolet Imaging Spectrograph (UVIS) observations with Voyager observations and with a 3-D general

circulation model. The model result is represented by the smooth dot-dashed line, and it is significantly low (colder) equatorward of ±60° in both hemispheres. The problem is that the air from the polar regions, heated by auroral currents, cools before it reaches the lower latitudes. One proposal is that drag forces due to atmospheric gravity waves, which are often overlooked in the models, could speed up the pole-to-equator circulation [Müeller-Wodarg et al. 2019]. The Cassini data confirm that the observations are good and not restricted to the Voyager era.

8. **Seasonal Change, Energy Budget and Temperatures – (Temperature and clouds (S_AO1); Saturn Formation and Evolution (S_AO5))**

   a. **Radiation.** Seasonal change begins with the changing distribution of sunlight falling on the two hemispheres. The rings amplify this effect by putting the winter hemisphere in shadow, but the effect on temperatures is moderated by the large heat capacity of Saturn's deep atmosphere and the small radiative fluxes far out in the solar system. Figure SATURN-4 [Li et al. 2015], which we have already discussed in connection with the great storm, also shows the reduction of emitted long-wave radiation in the south and increase in the north as the latter changed from early winter in 2004 to late spring in 2013.These changes in the emitted radiation reflect changes in temperature at the emitting levels, but they also could reflect changes in gaseous and cloud opacity.

   b. **Temperature Change.** The emitted radiation of Figure SATURN-2 includes the radiation at all wavelengths. Radiation at specific wavelengths allows one to probe to different levels and deduce temperature as a function of latitude and altitude. Figure SATURN-3 [Fletcher et al. 2010] shows this for years 2005 and 2008, also using CIRS data. The south is warmer than the north in both years, although most of the hemispheric contrast and most of the difference between 2005 and 2008 is confined to high altitudes. There the sunlight is strongest and the atmospheric density is low, so the seasonal effect on temperature is greatest.

   c. **Chemical Change.** The other seasonal effect is on the chemistry of the atmosphere. Figure SATURN-1 was taken by the ISS in 2004 as Cassini was approaching Saturn. It was summer in the south, and the sunlight was driving a rich hydrocarbon chemistry, resulting in an orange haze of small particles. The north was mostly shielded from sunlight, and the skies were blue, as shown by the sliver of atmosphere visible above the ring. Toward the end of the mission, the colors reversed. The rate of the shift reveals much about the photochemical processes that produce the haze.

9. **Lightning – (Saturn Lightning Sources and Morphology (S_AO6, SN2a))**

    a. **Quiet Times.** We have already mentioned that the Cassini RPWS recorded lightning strikes from the 2010–2011 great storm at rates exceeding 10 s^{-1}. But normally Saturn is a quiet place, with no lightning storms at all, which contrasts starkly with Earth's average of 2000 storms per day. Figure SATURN-14 [Dyudina et al. 2007] shows the Saturn electrostatic discharge counts, SED's, which are roughly equivalent to lightning strikes, over a 2-year period starting in 2004. The SED's are detected by the RPWS instrument, which is ON continuously. The lower panel shows ISS coverage of latitudes −34° to −36°, where all the storms were occurring, and it is clear that no storms were present when the RPWS was detecting nothing.

10. **Jupiter Colors and Movies – (Jupiter atmospheric dynamics (J_AO1))**

    a. **Chromophores.** The agent that colors the particles in Jupiter's clouds has been a mystery for decades. The principal cloud-forming gases are NH_3, H_2S, and H_2O, but they form particles that are white. Disequilibrium species involving phosphorus, sulfur, and/or hydrocarbons have been suggested, and it is difficult to choose one candidate over another. A new, Cassini-era candidate, a red (blue-absorbing) chromophore made from ammonia reacting with acetylene has been proposed [Carlson et al. 2016; Baines et al. 2019]. It seems to account for almost all of the color variation on the planet [Sromovsky et al. 2017]. Figure SATURN-17 shows the highest-resolution, full-disk color mosaic of Jupiter ever taken.

    b. **Movies.** With its powerful imaging system, Cassini took images continuously during its 70-day approach to Jupiter at the end of year 2000. A 70-day movie shows the clouds in motion at all longitudes and latitudes up to within ~10 degrees of the poles. The movie can be seen at these site(s): https://photojournal.jpl.nasa.gov/catalog/PIA03452; https://photojournal.jpl.nasa.gov/catalog/PIA03453; https://photojournal.jpl.nasa.gov/catalog/PIA03454. It is a modern sequel to the successful Voyager approach movie and an important research tool for measuring winds and the evolution of cloud features.

11. **For the Future, the Next Generation**

    a. **Water.** Measure the global water abundance and determine its role in bringing heat to the surface. Determine the role of moist convection in maintaining the large-scale motions. A Saturn probe to the base of the water cloud is a challenging but possible objective. Juno-type microwave remote sensing, in addition, is potentially valuable.

b. **Ammonia.** Determine the global ammonia abundance, and map its distribution with depth over the planet. Currently available data are good down to only about 3 bars, which do not necessarily represent the deep well mixed abundance of ammonia. A Saturn probe to 10 bars could make this measurement, and microwave remote sensing is potentially valuable.

c. **Noble Gases.** Determine Saturn's noble gas abundances including helium, and their isotopic ratios, as done for Jupiter by the Galileo probe. A Saturn probe could measure noble gases to exquisite precision.

d. **Interior Motions.** Determine Saturn's rotation period if such a number exists, or determine the spread of periods if differential motions persist into the interior. Document the time dependence of motions in Saturn's interior.

e. **Weather Layer.** Determine the vertical profiles of temperature, winds, clouds, condensable gases, longwave and shortwave radiation, and turbulence levels. A cloud-resolving model like those used in tropical meteorology, but tailored to the giant planets, is both timely and valuable. Again, a Saturn probe is needed.

f. **Interior.** Using the power of ring seismometry and gravity sounding, improve the understanding of Saturn's internal equation of state, mass distribution, composition, and temperature distribution. Develop a fully coupled interior/weather-layer model as done for Earth's oceans and atmosphere.

SATURN DWG SUMMARY

Cassini's Saturn science objectives were overseen by the Saturn DWG. This group consisted of the scientists on the mission interested in studying the planet itself and phenomena which influenced it. Leadership consisted of Interdisciplinary Scientists (IDS). The Saturn DWG would meet roughly three times a year at the Project Science Group (PSG) meetings and occasionally via telecon to discuss the executed and upcoming planned Saturn science, in addition to any high-priority science issues that the Project Scientist would request. This group would participate in tour selection (Prime, Equinox, and Solstice, and Grand Finale), define campaigns for focused Saturn science and define activities that eventually become the highest-priority observations—Pre Integration Event (PIE) and Cassini Apoapses for Kronian Exploration (CAKE)—to be negotiated with other Cassini DWGs.

The day-to-day work of the Saturn DWG was carried out by the Saturn Target Working Team (TWT). The Saturn TWT consisted of a subset of Saturn scientists who were interested in negotiating on a weekly basis with other scientists to layout a timeline of observations to be conducted in Saturn-centric windows of time (segments) within the constraints of the

Cassini's Saturn science objectives were overseen by the Saturn DWG.

spacecraft and of the mission. Its leadership consisted of an appointed Saturn scientist, a supporting Investigation Scientist, and one or more Science Planning Engineers. This group would implement both individual stand-alone team observations and campaign templates involving multiple of Cassini's instruments. Most issues were nicely negotiated and resolved during the weekly (and ultimately monthly) telecons. Where there were major science conflicts to be resolved amongst the scientists, the Saturn DWG would offer recommendations for their resolution.

The SAMWG was formed by the Project Scientist to specifically answer the following three questions: 1) characterize Saturn's uppermost atmosphere (thermosphere) and its variation with time; 2) define the shape of Saturn's 100 mbar and 1 bar pressure levels; and 3) determine when the Saturn safely eclipsed Cassini from the Sun. Its membership consisted of experts in studying Saturn's upper atmosphere and members of the engineering team. The SAMWG reported to the Saturn DWG on a periodic basis.

Saturn Key Objectives

Cassini's Saturn and Jupiter science objectives originate from those spelled out in the AO and CSM TMs. They are briefly called out here.

- **Saturn Temperature, Clouds, Composition (S_AO1)**
  - **Temperature and clouds (S_AO1)** – Determine temperature field, cloud properties, and composition of the atmosphere of Saturn.
  - **Composition and chemistry (SN1c)** – Measure the spatial and temporal variability of trace gases and isotopes.
- **Saturn Winds and Weather (S_AO2)**
  - **Seasonal Variations (SC1a)** – Observe seasonal variations in temperature, clouds, and composition in three spatial dimensions.
  - **Saturn's Winds (SC1b)** – Observe seasonal changes in the winds at all accessible altitudes coupled with simultaneous observations of clouds, temperatures, composition, and lightning.
  - **Storms (SN1b, SN2a)** – Observe the aftermath of the 2010–2011 storm. Study the life cycles of Saturn's newly discovered atmospheric waves, south polar hurricane, and rediscovered north polar hexagon. Monitor the planet for new storms and respond with observations when they occur.
  - **Atmospheric dynamical processes (S_AO2)** – Measure the global wind field, including wave and eddy components; observe synoptic cloud features and processes.

  - **Saturn Lightning Sources and Morphology (S_AO6, SN2a)** – Investigate the sources and the morphology of Saturn lightning—Saturn Electrostatic Discharges (SED)—lightning whistlers.
- **Saturn Interior Structure and Rotation (S_AO3)**
  - **Saturn's Rotation Rate (SN1a)** – Determine Saturn's rotation rate and internal structure despite the planet's unexpected high degree of axisymmetry.
  - **Saturn Formation and Evolution (S_AO5)** – Provide observational constraints (gas composition, isotope ratios, heat flux, …) on scenarios for the formation and the evolution of Saturn.
- **Aurora, Chemistry, and Upper Atmosphere (SC2a)** – Observe the upper atmosphere and the aurora as it changes on all time scales—minutes to years—and is affected by seasonal and solar cycle forcing.
- **Jupiter atmospheric dynamics (J_AO1)** – Extend the time for studies of atmospheric dynamics beyond the period accessible to the Galileo nominal mission.
- **Jupiter Global Atmospheric Structure and Composition (J_AO2)** – Infer global atmospheric thermal structure and composition with instrumentation not carried by the Galileo Orbiter, complementing the local in situ measurements of the Galileo Probe.
- **Venus atmosphere observations** – No specific objectives were called out.
- **Cruise Planetary and Stellar Internal Oscillations (C_AO5)** – Attempt to detect internal oscillations of Saturn, Jupiter, and some stars.
- **Saturn Ionosphere-Magnetospheric Interaction (S_AO4)** – Study the diurnal variations and magnetic control of the ionosphere of Saturn.

Saturn Science Assessment

Table SATURN-1 is an assessment of data collected to satisfy an objective. It is not as assessment of the status of data analysis/publications.

Table SATURN-1. Science Assessment.

Fully/Mostly Accomplished: **Partially Accomplished:** **Not Accomplished:**

Saturn DWG Science Objectives	AO and TM Science Objectives	Saturn DWG Assessment	Comments (if yellow, partially fulfilled)
Saturn Temperature, Clouds, Composition	S_AO1		
– Temperature and clouds	S_AO1		
– Composition and chemistry	SN1c		
Saturn Winds and Weather	S_AO2		
– Seasonal variations	SC1a		

Table SATURN-1. Science Assessment.

Fully/Mostly Accomplished: **Partially Accomplished:** **Not Accomplished:**

Saturn DWG Science Objectives	AO and TM Science Objectives	Saturn DWG Assessment	Comments (if yellow, partially fulfilled)
– Saturn's winds	SC1b		
– Storms	SN1b, SN2a		
– Atmospheric dynamical processes	S_AO2		
– Saturn lightning	S_AO6, SN2a		
Saturn Interior Structure and Rotation	S_AO3		
– Saturn's rotation rate	S_AO3, SN1a		
– Saturn formation and evolution	S_AO3, S_AO5		
Aurorae, Chemistry, and Upper Atmosphere	SC2a		
– Upper atmosphere	SC2a		
– Aurora	SC2a		
Jupiter Atmospheric Dynamics	J_AO1		
– Dynamics observations	J_AO1		
– Dynamics modeling and theory	J_AO1		
Jupiter Global Atmospheric Structure and Composition	J_AO2		
– Thermal and cloud structure	J_AO2		
– Composition and chemistry	J_AO2		
Venus Atmosphere Observations	N/A		
Cruise Planetary and Stellar Internal Oscillations	C_AO5		NOTE: Planetary and stellar cruise observations were not conducted.
Saturn Ionosphere-Magnetosphere Interaction	S_AO4		NOTE: This is primarily a MAPS WG objective. See their objectives MN1b, MN1c, MN2a, and MC1a. The green assessment reflects the status of both WG's data analysis.

SATURN DWG SCIENCE RESULTS

Saturn Temperature, Clouds, Composition (S_AO1)

- **Temperature and clouds (S_AO1)** – Determine temperature field, cloud properties, and composition of the atmosphere of Saturn.

The temperature field, cloud properties, and composition are an interacting system that controls the energy budget of the planet and the clouds and haze that we see in the planet's atmosphere (Figure SATURN-1). Clouds are a tracer of the motion. They form on updrafts, which are part of the energy cycle that controls the zonal winds. Also, clouds interact with the temperature field through condensation and evaporation. Cassini, with its comprehensive array

of instruments and unique perspective from different positions in the orbit, has contributed critical data on all of these objectives. In addition, Cassini has spawned exploration of Saturn from Earth-based telescopes.

Timed with the start of Cassini's exploration of the Saturn system, Beebe [2005] presented the case for comparative study of the outer planets. Papers on the Cassini instruments and their ability to measure clouds and haze include: Baines et al. [2005] on VIMS; Porco et al. [2005] on ISS; Flasar et al. [2005] and Jennings et al. [2017] on CIRS; and Janssen et al. [2013] on the Cassini RADAR radiometer. Schinder et al. [2015] give the techniques for probing the electron density and temperature structure with radio occultations.

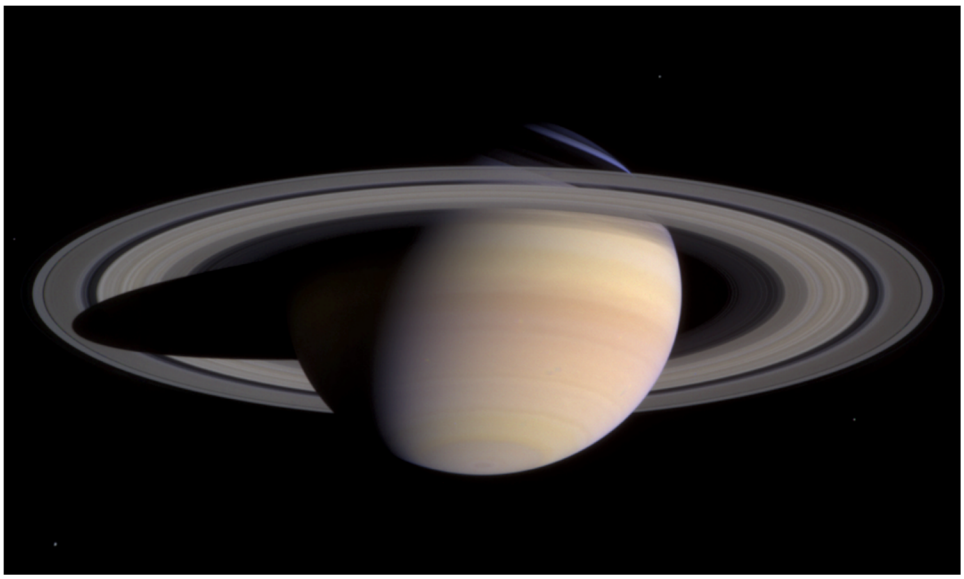

Figure SATURN-1. Image taken by the ISS in 2004 as Cassini was approaching Saturn. It was summer in the south, and the sunlight was driving a rich hydrocarbon chemistry, resulting in an orange haze of small particles. The north was mostly shielded from sunlight, and the skies were blue, as shown by the sliver of atmosphere visible above the ring (PIA05389).

Banfield et al. [1998] described the use near-infrared (IR) spectroscopy from the 5-m Hale telescope at Palomar, California, to measure the altitudes and scattering properties of clouds and haze. Similarly, Sanchez-Lavega et al. [2004] described Hubble Space Telescope observations of cloud morphology in Saturn's atmosphere. Temma et al. [2005] used Earth-based telescopic observations to probe the vertical structure of Saturn's cloud layers. Using Hubble Space Telescope (HST) data, Perez-Hoyos et al. [2006] documented short-term variability (weeks to months) associated with cloud reflectivity of the belts and zones. West et al. [2009] gives a comprehensive survey of clouds and haze in Saturn's atmosphere as inferred from Cassini VIMS and ISS, as well as HST and other Earth-based telescopes. Ingersoll et al. [2018] present images taken during the last few months of the mission at resolutions down to 0.5 km per pixel. The interesting features include filamentary clouds coherent over 20,000 km and puffy clouds resembling terrestrial cumulus.

Fletcher et al. [2007b] used Cassini CIRS data to probe the vertical and horizontal temperature structure and its relation to the belt and zone cloud structure. Roman et al. [2013] used ISS data to probe the layered cloud structure from the haze layers at 40 mbar to tropospheric clouds at 2.5 bar. Laraia et al. [2013] used Cassini RADAR radiometer data to probe the vertical distribution of NH_3 to depths below its nominal cloud base. Barstow et al. [2016] used Cassini VIMS to document a photochemical origin for the stratospheric haze and either NH_3 or NH_4SH for the deeper tropospheric cloud. Using Cassini ISS data, Dyudina et al. [2016] and Perez-Hoyos et al. [2016] quantified the way the atmosphere scatters light, including the phase function and the spherical and Bond albedos.

Del Genio et al. [2009] give a comprehensive review of Saturn's atmospheric structure and dynamics. The early data come from the Voyager flybys and Earth-based telescopes and then from the remote-sensing instruments on Cassini. The review covers the deep atmosphere, the troposphere, the stratosphere, and dynamical features such as the jets, waves, discrete features. Del Genio and Barbara [2016] provide a classification scheme based on cloud morphology for revealing the underlying dynamics.

- **Composition and chemistry (SN1c)** – Measure the spatial and temporal variability of trace gases and isotopes

The gaseous composition of a giant planet atmosphere varies due to several processes: condensation and precipitation that remove the particles from the gas, updrafts and downdrafts that alter the chemical equilibrium of the various reacting species, and photochemical reactions that lead to dissociation and/or ionization (Figure SATURN-2). The reacting species include CH_4, NH_3, PH_3, and their chemical byproducts like C_2H_2 and C_2H_6. In addition, the upper atmosphere may receive molecules and solid particles from the rings and satellites.

Fouchet et al. [2009] give a comprehensive review of Saturn composition and chemistry. Fletcher et al. [2011a] review the elements that appear in simple compounds that are detectable in VIMS spectra, including PH_3, NH_3, AsH_3, GeH_3, CO, CH_3D, and $^{13}CH_4$. Howett et al. [2007] and [Guerlet et al. 2009] focus on C_2H_2, C_2H_6, and C_3H_8, which are produced in the stratosphere by photodissociation of methane. They use Cassini CIRS data to infer a stratospheric circulation from south to north during the southern summer. Guerlet et al. [2010] added C_3H_8 and CH_3C_2H to the list of tracers and again found evidence of upwelling in the south and downwelling in the north. Fletcher et al. [2007a] also used CIRS data, focusing on phosphine, PH_3. It is in chemical equilibrium below the cloud tops and is destroyed by photolysis in the stratosphere. The altitudes of sources and sinks are opposite to that of C_2H_2 and C_2H_6, but the inferred circulation is similar.

Cassini CIRS data stimulated photochemical modeling in order to quantify the inferred circulations [Dobrijevic et al. 2011; Hue et al. 2015]. The data also stimulated laboratory measurements [Auwera et al. 2007; Devi et al. 2014] to refine the infrared absorptions of these gases. Gases like CH_4, C_2H_2, and C_2H_6 absorb and emit in the infrared, and their spatial and temporal variations create temperature variations, which in turn affect the circulation. These

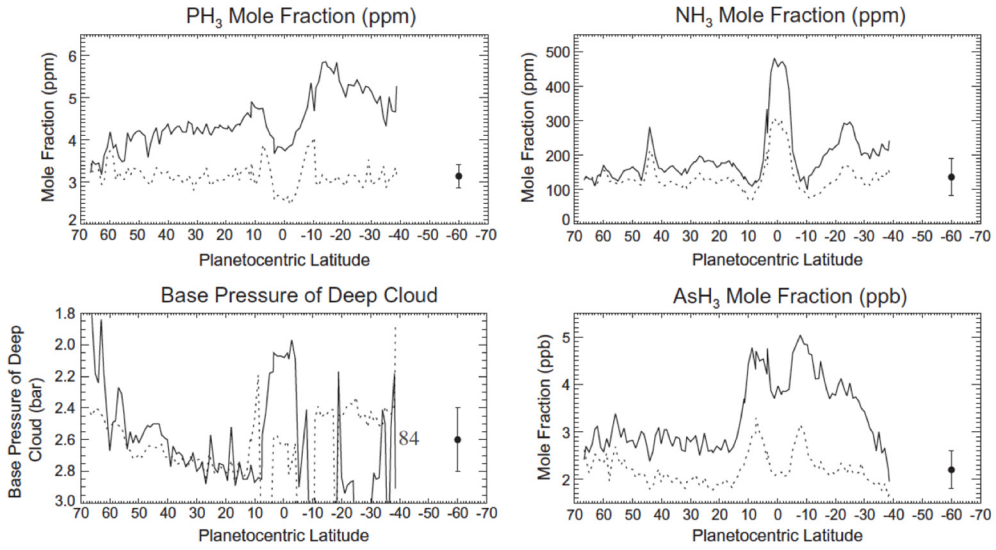

Figure SATURN-2. Tropospheric chemical abundances from Cassini VIMS. The profiles do not tell a consistent story according to this picture. NH_3 shows a high mole fraction at the equator, consistent with upwelling there and downwelling on either side at 10–12° latitude, but PH_3 and AsH_3 show low abundances at the equator, consistent with downwelling. The data may be indicating a double Hadley cell, with rising motion at the higher altitudes at the equator and sinking motion deeper down [Fletcher et al. 2011a].

interactions are studied with 2-D photochemical models, which have been another desirable outgrowth of Cassini observations [Hue et al. 2016].

Intensified Earth-based observations are a further desirable result of Cassini's mission to Saturn. Some of the observations immediately preceded the outpouring of Cassini data [Kim and Geballe 2005; Tejfel 2005], both to extend the range of temporal variability and to compare inferences based on different data sets. For instance, microwaves are sensitive to ammonia vapor at deeper levels than those probed by infrared radiation. The Cassini RADAR used in passive mode collects thermal radiation at 2.2 cm wavelength. With laboratory measurements of the ammonia opacity [Hanley et al. 2009], the Cassini 2.2 cm data were used to infer depletion of ammonia below the expected base of the ammonia cloud [Janssen et al. 2013; Laraia et al. 2013]. This depletion is observed on Jupiter as well and has not been fully explained. The NH_3 abundance is controlled mostly by condensation and evaporation, which is more tied to the cloud structure, so it reveals different aspects of the circulation [Hurley et al. 2012b] than that of the hydrocarbons.

In giant planet atmospheres, the principal oxygen-bearing molecules are H_2O and CO, with the latter in equilibrium at higher temperatures and pressures than the former. However, water is frozen out at high altitudes, so the presence of CO_2 at the 1 mbar level suggests a source outside the planet. Cassini CIRS observations were used to show that the source is probably interstellar dust grains [Abbas et al. 2013].

Saturn Winds and Weather (S_AO2)

- **Seasonal Variations (SC1a)** – Observe seasonal variations in temperature, clouds, and composition in three spatial dimensions.

Two opposing effects control the amplitude of seasonal variations on Saturn (Figure SATURN-3). The obliquity is 26.73°, which is larger than that of Earth, and is tending to produce large seasonal variations in incident sunlight. These variations are augmented by the rings, which block sunlight from reaching large parts of the winter hemisphere. On the other hand, Saturn's troposphere is massive, with clouds of water down to the 20-bar level, assuming the enrichment of water relative

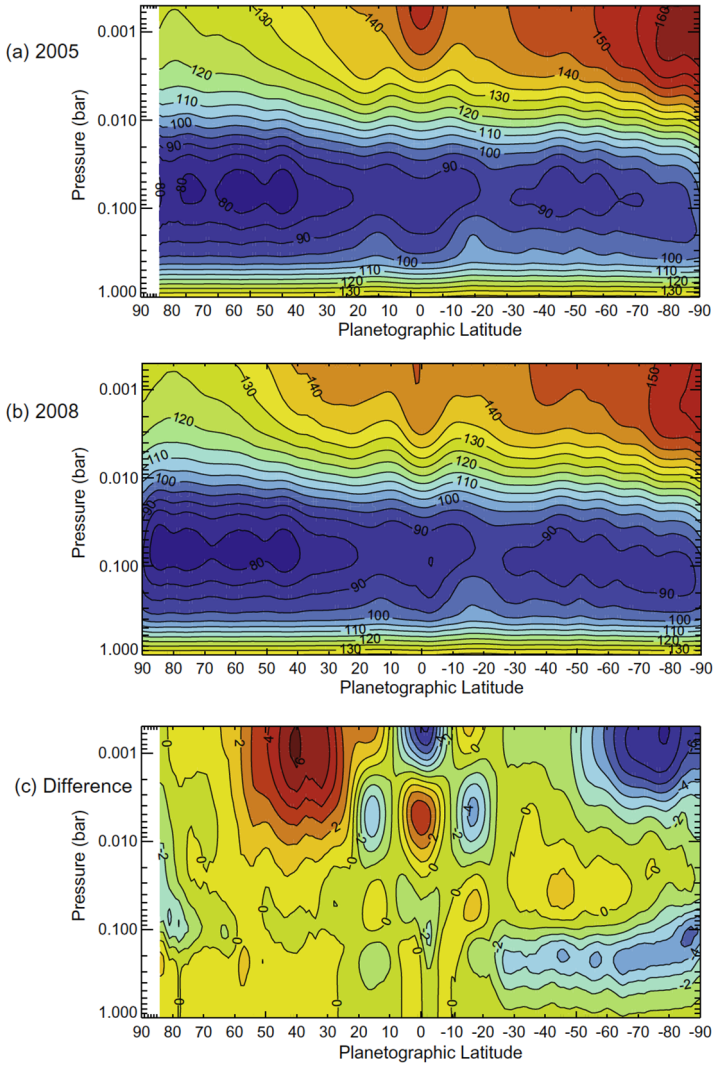

Figure SATURN-3. Temperature as a function of latitude and altitude from Cassini CIRS. In 2005 the season was early winter in the north, and in 2008 the season was mid-winter. The south is warmer than the north in both years, although most of the hemispheric contrast and most of the difference between 2005 and 2008 is confined to high altitudes [Fletcher et al. 2010].

to solar composition is the same as that of methane, whose abundance can be measured spectroscopically. Further, the high specific heat of hydrogen gives the troposphere a huge thermal inertia, so the atmosphere tends to average over the seasonal cycle rather than respond to it. Seasonal averaging is reduced in the stratosphere, because it has less thermal inertia than the troposphere. Seasonal change is reflected in the emitted power as a function of latitude [Li et al. 2015], as the northern hemisphere season changed from winter to late spring over the period 2004-2013 (Figure SATURN-4).

Using Cassini CIRS data Fletcher et al. [2010] showed that the stratosphere has a greater range of temperatures than the troposphere, which is consistent with the greater thermal inertia of the latter. They point out that a photochemical haze develops in the spring/summer hemisphere (Figure SATURN-1). Fletcher et al. [2015] observed polar cooling and depletion of acetylene in the southern hemisphere during fall and winter. Tropospheric temperature variations are small [Fletcher et al. 2016] and show a substantial seasonal lag time, as expected. These seasonal changes are superposed on a general upwelling in the tropics and downwelling at the poles, as revealed by the two states (ortho and para) of the H_2 molecule [Fletcher et al. 2016, 2017]. Sinclair et al. [2013] and Sylvestre et al. [2015] compare CIRS observations of temperature, C_2H_2, C_2H_6, and C_3H_8 with a static photochemical model and find substantial effects of circulation and transport in addition to variations due to chemistry. Seasonal change of thermal structure, composition and aerosol is extensively reviewed by Fletcher et al. [2018].

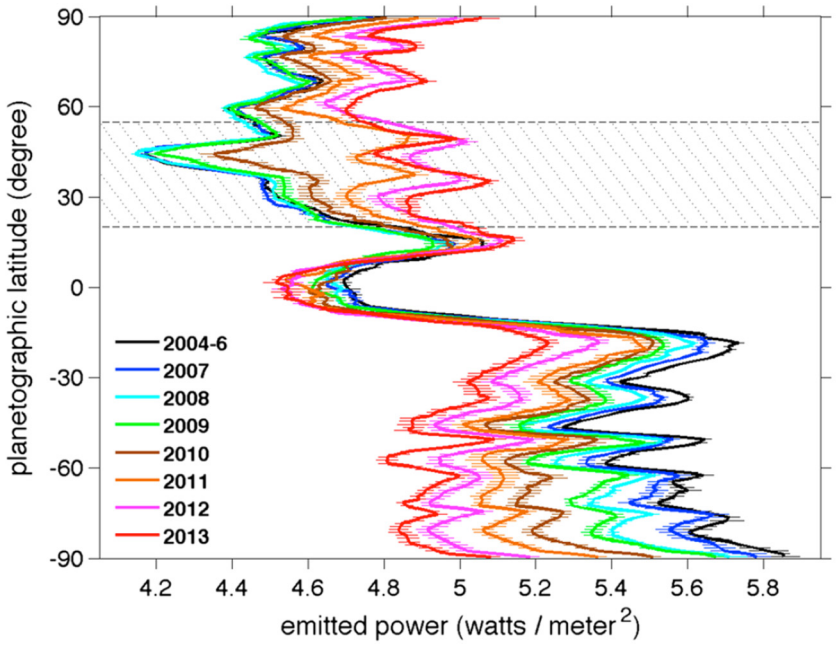

Figure SATURN-4. Thermal emission of the planet in units of W m^{-2} from Cassini CIRS. In the south the season was early summer in 2004 and mid fall in 2013. The decrease in thermal emission in the south was due to cooling of the atmosphere. Comparing the years before and after 2011, it is clear that the great storm increased the thermal emission by 5–10% in the 30–40° latitude band, and that the anomaly persisted for several years [Li et al. 2015].

- **Saturn's Winds (SC1b)** – Observe seasonal changes in the winds at all accessible altitudes coupled with simultaneous observations of clouds, temperatures, composition, and lightning.

Tracking small clouds in sequences of images is the principal way of measuring the winds (Figure SATURN-5). Both ISS and VIMS can measure the winds directly. CIRS can measure the gradient of the wind with respect to altitude by measuring the horizontal gradient of temperature and applying the thermal wind equation. Except at the equator, the mean zonal winds—the

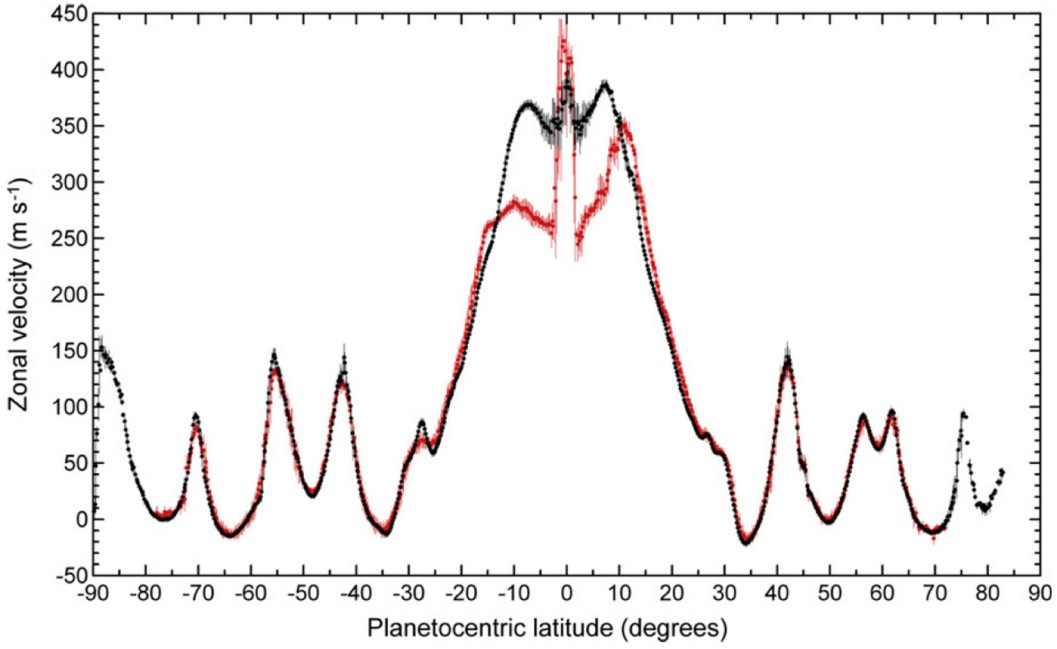

Figure SATURN-5. Atmospheric zonal velocity for Saturn from Cassini ISS. The black curve is data from the 350 to 700 mbar levels, and the red curve is data from 100 to 200 mbar. The differences are small except for a latitude band ±15° from the equator [Garcia-Melendo et al. 2011b].

eastward winds averaged with respect to longitude—are remarkably steady. This conclusion follows, in part, by comparing the mean zonal winds during Voyager times with those measured by Cassini 25–30 years later [Antunano et al. 2015; Choi et al. 2009; Li et al. 2011, 2013; Vasavada et al. 2006]. Images taken at wavelengths where methane is a strong absorber tend to sample higher altitudes than those where methane is transparent. Vertical shears show up in the eastward jets [Garcia-Melendo et al. 2009, 2011], which is consistent with the horizontal temperature gradient and the thermal wind equation.

At the equator, the speed of the zonal wind in the upper troposphere and stratosphere oscillates with a 15-year period [Fouchet et al. 2008] (Figure SATURN-6). Similar oscillations occur in the stratospheres of Earth and Jupiter. On Earth the period is about 22 months, and the oscillation is called QBO. On Jupiter, the period is about four years. On Earth, the mechanism is feedback between the wind profile and the altitude where waves propagating up from the troposphere deposit their zonal momentum. The period is inversely related to the intensity of the waves. A similar

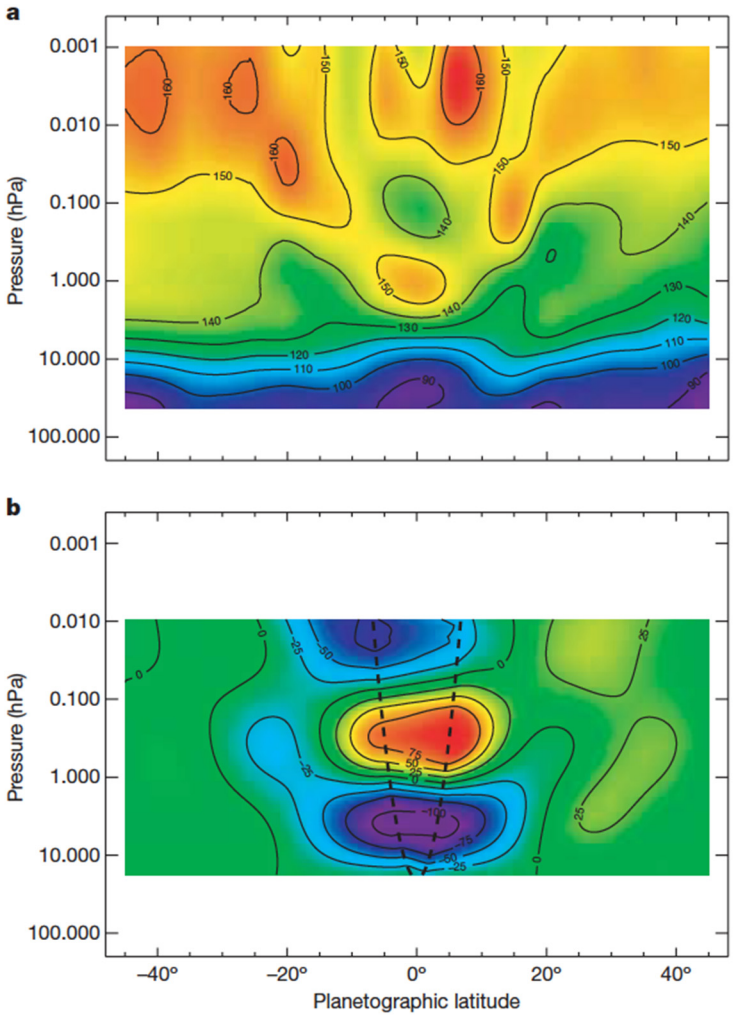

Figure SATURN-6. Oscillation of temperature (upper panel) and mean zonal wind (lower panel) at the equator from Cassini CIRS. The pattern moves down with time and has a ~15-year period. A similar pattern on Earth has a ~22 month period and is known as the QBO. The period of the oscillation on Jupiter is ~4 years. The longer period as one moves out in the solar system is probably due to the lower energy available to drive the oscillation [Fouchet et al. 2008].

mechanism is likely to operate on Jupiter and Saturn. Since vertical shear in the zonal wind is related to horizontal gradients of temperature through the thermal wind equation, the oscillation reveals itself in the temperatures on either side of the equator.

In preparation for the Cassini encounter, Voyager and Hubble Space Telescope observations were used to document the variability of the zonal wind in the equatorial stratosphere [Perez-Hoyos and Sanchez-Lavega 2006; Sanchez-Lavega et al. 2000]. Sanchez-Lavega et al. [2007] and Garcia-Melendo et al. [2010] used Cassini ISS images in the methane bands to further document the vertical wind shear and its temporal variability. Li et al. [2008] used Cassini CIRS data, where the oscillation is revealed in stratospheric temperatures, and Li et al. [2011] showed that the temperatures and cloud-tracked winds are consistent with the QBO oscillation mechanism.

Schinder et al. [2011] used radio occultations by the Cassini spacecraft to measure temperature and showed that the zonal wind profile propagates downward as on Earth, consistent with the wave forcing mechanism of the QBO. Downward propagation also shows up in the thermal infrared maps based on CIRS data [Fouchet et al. 2008; Guerlet et al. 2011]. Sanchez-Lavega et al. [2016] used ISS data to track individual features in the upper haze and clouds and further demonstrated the intense vertical shears and temporal variability.

- **Storms (SN1b, SN2a)** – Observe the aftermath of the 2010–2011 storm. Study the life cycles of Saturn's newly discovered atmospheric waves, south polar hurricane, and rediscovered north polar hexagon. Monitor the planet for new storms and respond with observations when they occur.

Saturn is prone to large-scale eruptions (Figure SATURN-7). They start with a small cloud that grows rapidly during its first week and expands zonally, until after two or three months the

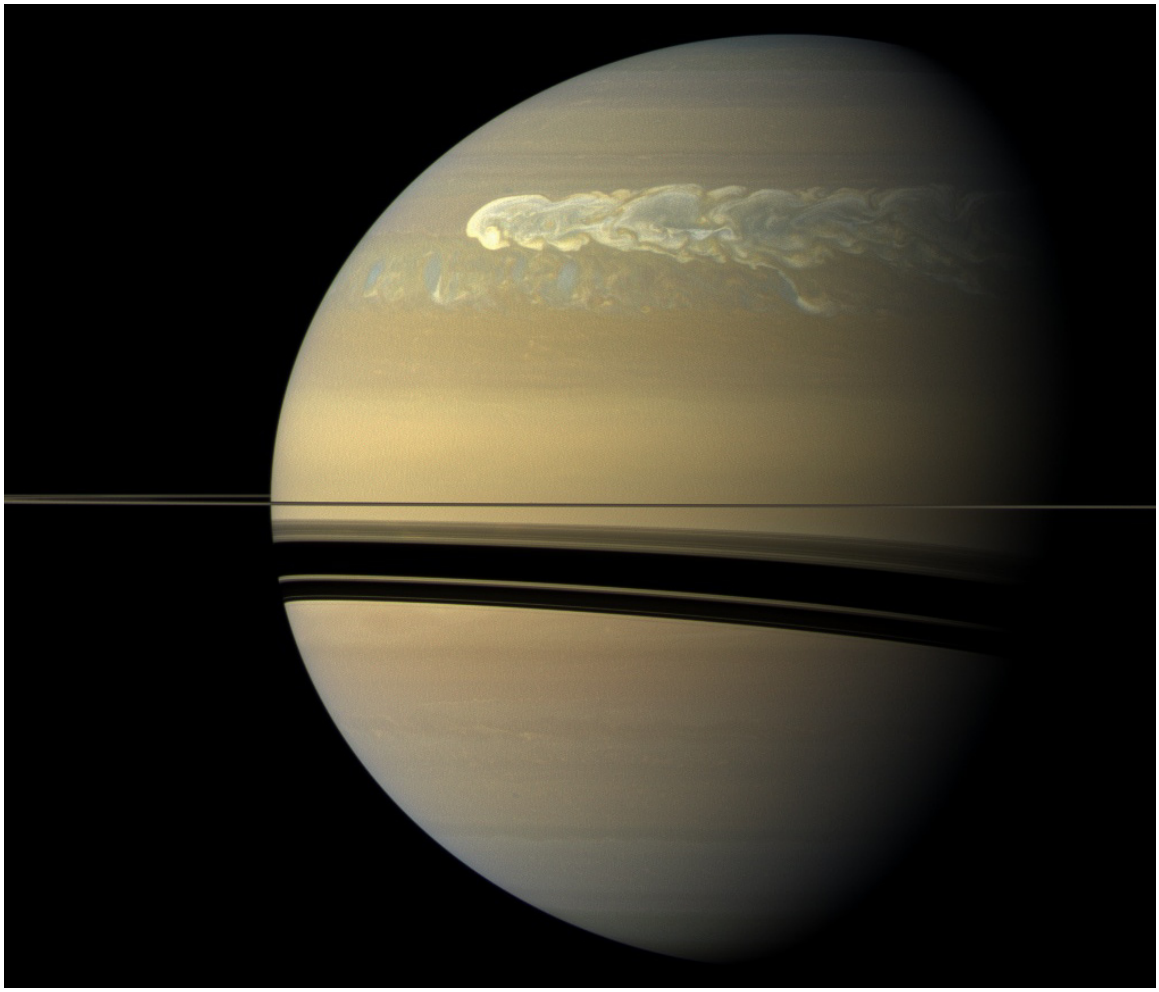

Figure SATURN-7. Saturn imaged by Cassini ISS on February 25, 2011. The great storm of 2010–2011 is clearly visible in a band centered at 30–40° latitude. Since its appearance on December 5, 2010, the head of the storm had drifted west and overtaken the tail.

disturbance has fully encircled the planet within its latitude band. The paper by Sanchez-Lavega [1994] is the definitive pre-Cassini review of these phenomena. He calls them Great White Spots, and he lists five of them before the Cassini era: 1876, 1903, 1933, 1960, and 1990. This gives an average periodicity of 28.5 Earth years, which is close to Saturn's year of 29.46 Earth years. The corresponding latitude bands of these storms are 8 ±3°, 36 ±2°, 2 ±3°, 58 ±1°, and 12 ±1°, all in the northern hemisphere. Whether the disturbances are in a unique class or just the largest in a continuous distribution of sizes is uncertain. And whether the disturbances are locked in phase to Saturn's year is also uncertain, because within each latitude band the period is much longer than a Saturn year. And the great storm of 2010–2011 came 10 years too early to satisfy the annual cycle hypothesis.

Saturn's great storm of 2010–2011 was a singular event in Cassini's 13 year tour of the Saturn system [Sanchez-Lavega et al. 2018]. It began as a small (~1000 km) spot captured in a routine ISS image on December 5, 2010. Cassini RPWS had been detecting lighting discharges (Figure SATURN-8) from the storm for a few hours when the image was taken [Fischer et al. 2011]. The lightning continued for the ~7 month lifetime of the storm as the westward-moving head left behind a tail that eventually wrapped around the planet. In its mature phase, the storm filled a latitude band 10,000 km wide that was centered at a planetocentric latitude of 35°. Earth-based telescopes were following the storm within days of its appearance [Sanchez-Lavega et al. 2011], and systematic Cassini imaging began in January 2011.

Visible-light images of clouds in the troposphere [Sanchez-Lavega et al. 2012; Sayanagi et al. 2013] showed that the head spawned large (10,000 km diameter) anticyclones that drifted off to the east and became part of the tail. The storm seems to have originated from a feature called the string of pearls, a train of cyclones at the latitude of the great storm [Sayanagi et al. 2014]. Garcia-Melendo et al. [2013] are able to reproduce many of the observed morphological features of the storm with a prescribed heat source moving at a prescribed velocity. Li and Ingersoll [2015] present a theory that reproduces the observed drying (low mixing rate of ammonia) of the storm's latitude band (Figure SATURN-9) [Janssen et al. 2013; Laraia et al. 2013] as well as the multi-decadal

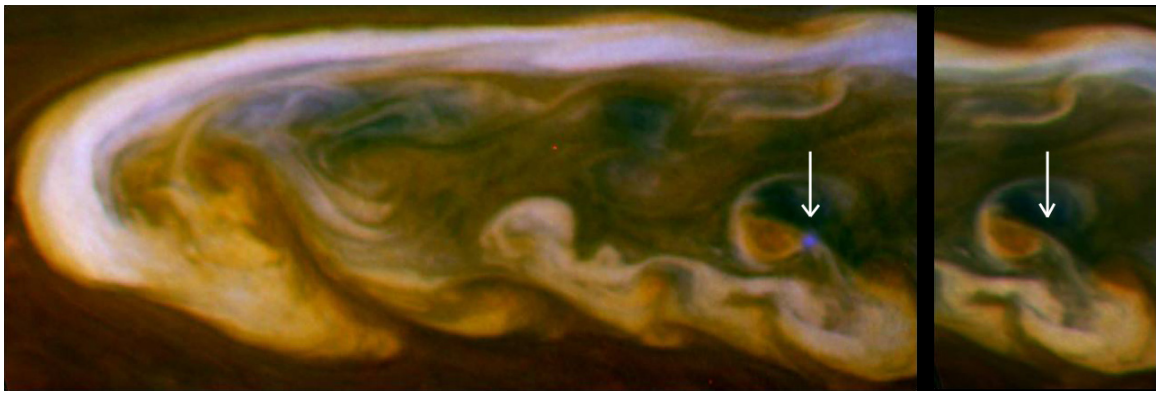

Figure SATURN-8. Lightning flash in Saturn's great storm of 2010–2011. The color composite consists of three images taken in rapid succession at three different wavelengths. A lightning flash occurred while the blue-filtered image was taken, making a blue spot in the composite image, left. The same region was imaged 30 minutes later and did not see a lightning flash, right (PIA14921).

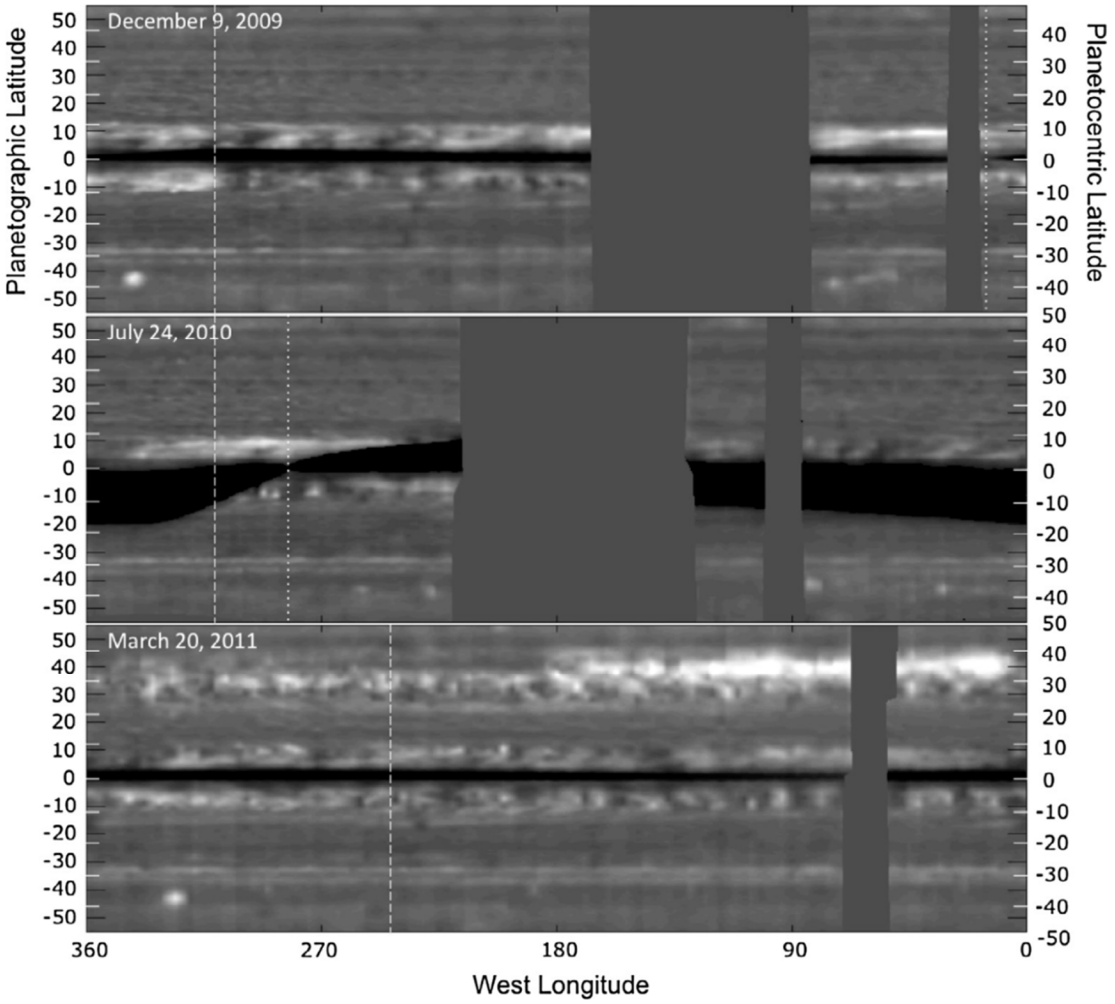

Figure SATURN-9. Cylindrical projection of Jupiter thermal emission at 2.2 cm wavelength, obtained by the Cassini RADAR in passive (non-transmitting) mode. The dark band at the equator is due to the rings, which are colder than the planet itself. The top two panels show the planet before the great storm. The lower panel shows warm emission at the location of the storm. Ammonia is the principal absorber at 2.2 cm wavelength, so the warm emission is due to ammonia depletion allowing radiation from deeper levels to reach the detector [Janssen et al. 2013].

interval between great storms. The latter is tied to mass loading, i.e., the stabilizing effect of water and ammonia condensation in a low molecular weight (H_2 and He) atmosphere. Above a critical abundance of the condensates, the atmosphere becomes stable after a convective event, and the time needed to destabilize the atmosphere is decades. Based on the C/H ratios for Jupiter and Saturn, assuming the same enrichment factors relative to solar for O/H, Saturn is above the critical value and Jupiter is below it, which could explain why only Saturn has these great storms.

Thermal infrared spectroscopy by Cassini CIRS revealed effects of the storm that penetrated into the stratosphere to the 1 mbar level [Fletcher et al. 2011b]. Subsidence of air in the stably-stratified stratosphere produced beacons as much as 16 K warmer than their surroundings

(Figure SATURN-10). By May 5, 2011, the beacons had reached temperatures of 226 K, about 80 K warmer than the surrounding stratosphere [Fletcher et al. 2012; Fouchet et al. 2016]. The storm produced a 100-fold increase of ethylene in the stratosphere near the beacon [Hesman et al. 2012]. Photochemical models cannot explain this increase, so some dynamical mechanism must be at work [Cavalie et al. 2015; Moses et al. 2015]. Temperatures in the troposphere at the latitude of the storm increased by 3 K, and the para fraction of H_2 decreased by about 0.4, indicating warm air upwelling from below (Figure SATURN-11) [Achterberg et al. 2014].

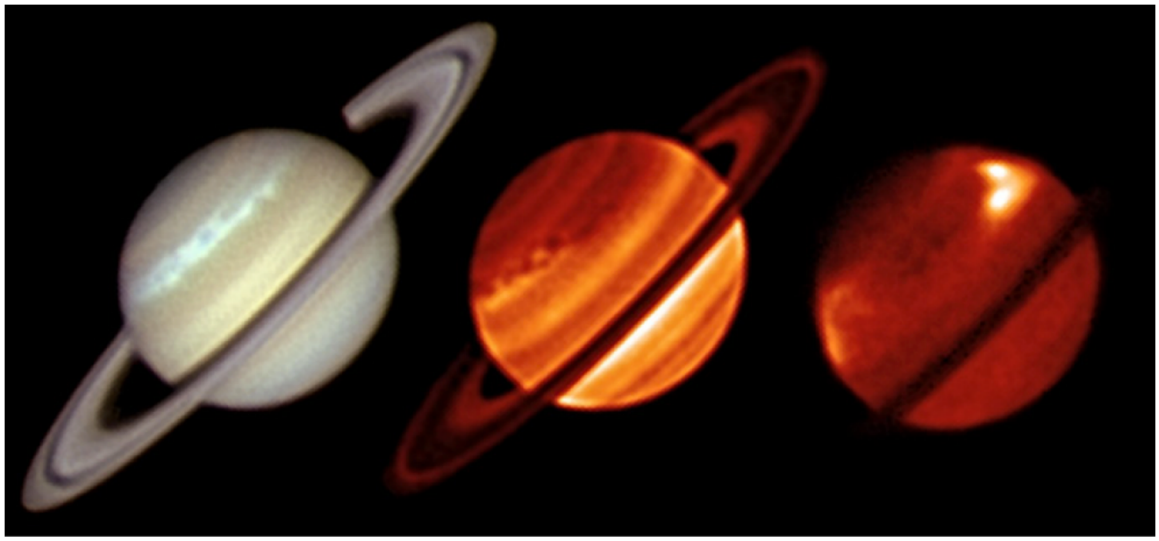

Figure SATURN-10. Earth-based image, left, and two infrared images taken by Cassini CIRS on January 19, 2011. The center image records temperature in the upper troposphere, at the 200–500 mbar level, and the right image shows temperatures at the 1–10 mbar level. The stratospheric beacon stands out in the right image [Fletcher et al. 2011b].

The 2010–2011 storm seems to have affected clouds and haze, both at the latitude of the storm and farther away. Sromovsky et al. [2013] used VIMS spectra to study the composition of the cloud particles lofted by the storm, and found evidence of ammonia ice, water ice, and ammonium hydrosulfide. This is the first spectroscopic evidence of water ice in Saturn's atmosphere and indicates upwelling from 200 km below the tops of the ammonia clouds. Further study of the aftermath of the storm reveals clearing of the ammonia cloud with some residual particles of other species [Sromovsky et al. 2016]. According to an analysis of VIMS data, a residual haze layer persisted in the upper troposphere and lower stratosphere as well [Oliva et al. 2016]. The great storm seems to have caused a 10 K warming of the middle atmosphere (0.5-5 mbar) at the equator, providing evidence of teleconnections between latitudes [Fletcher et al. 2017].

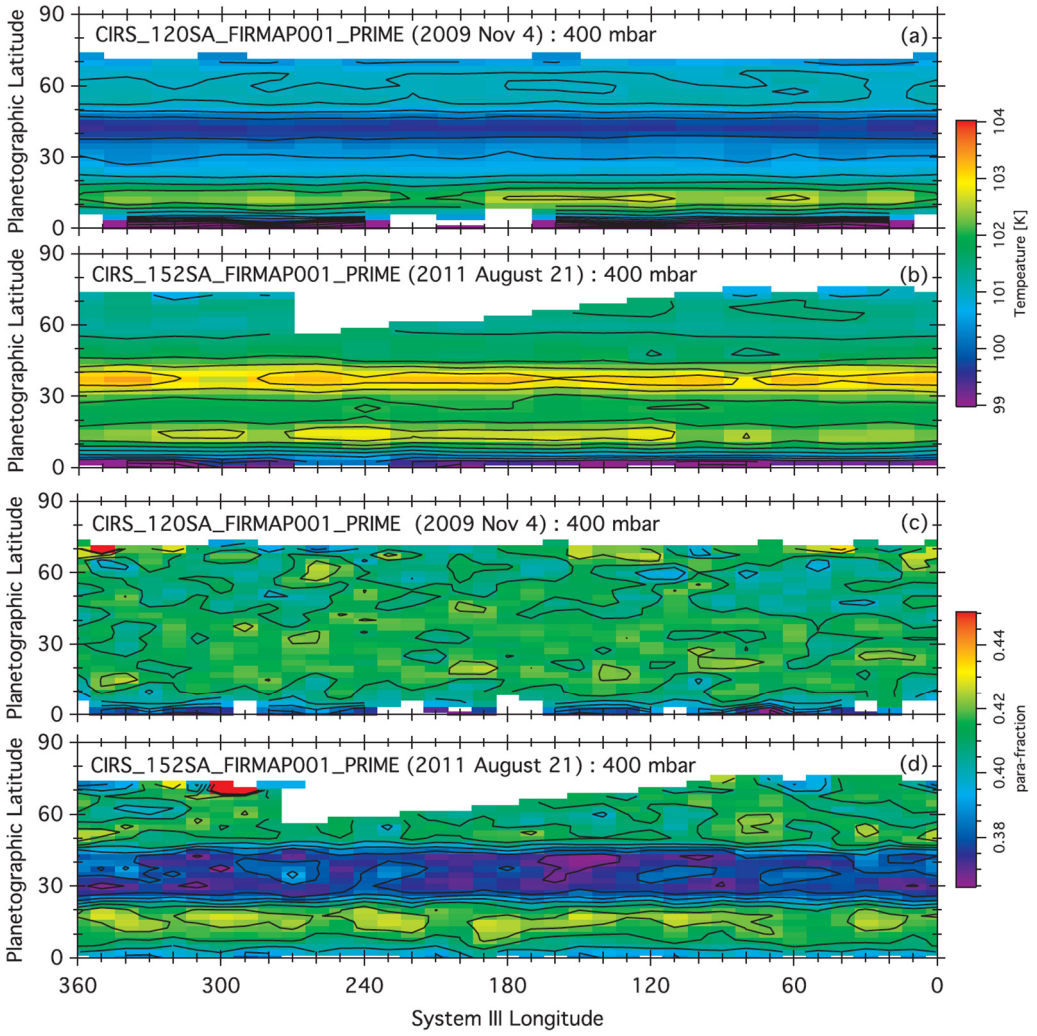

Figure SATURN-11. Cassini CIRS cylindrical projections showing evidence of air being dredged up from below. The top two panels show tropospheric temperature before and after the storm and the band from 30–40° planetographic has warmed by several degrees. The bottom two panels show the two chemical states (nuclear spins parallel and nuclear spins anti-parallel) of molecular hydrogen H_2 before and after the great storm. The 30–40° band shows a low para fraction, which indicates that the air has risen from below cloud base [Achterberg et al. 2014].

Saturn's hexagon is a six-lobed meandering pattern in an eastward jet centered at 75° north latitude (Figure SATURN-12). The excursions in latitude are approximately ±1°, which gives the structure its polygonal shape. Larger excursions would give it a more sinusoidal, wave-like shape. The hexagon was discovered in Voyager images taken in 1980 and was discovered again by Cassini VIMS, before the spring equinox when the North Pole was still in darkness [Baines et al. 2009b]. Its effects extend into the stratosphere to altitudes of 0.5 mbar [Adriani et al. 2015]. Based on ISS and VIMS imaging, the clouds on either side of the jet move slowly or not at all relative to the nominal rotation rate for Saturn, which was defined following the Voyager encounter [Desch and Kaiser 1981]. Relative to these clouds and to the hexagon pattern, the jet's speed is

~125 m s^{-1}. Thus the hexagon is like a road fixed in the Voyager reference frame, and the clouds in the jet move along it. Based on the hexagon's long-term stability, Sanchez-Lavega et al. [2014] argue that it is a deep-seated feature that could reveal the true rotation of the planet.

Each pole of Saturn is occupied by a single isolated cyclonic vortex with peak winds of ~150 m s^{-1} [Dyudina et al. 2008, 2009; Sanchez-Lavega et al. 2006]. The latitude of the peak winds

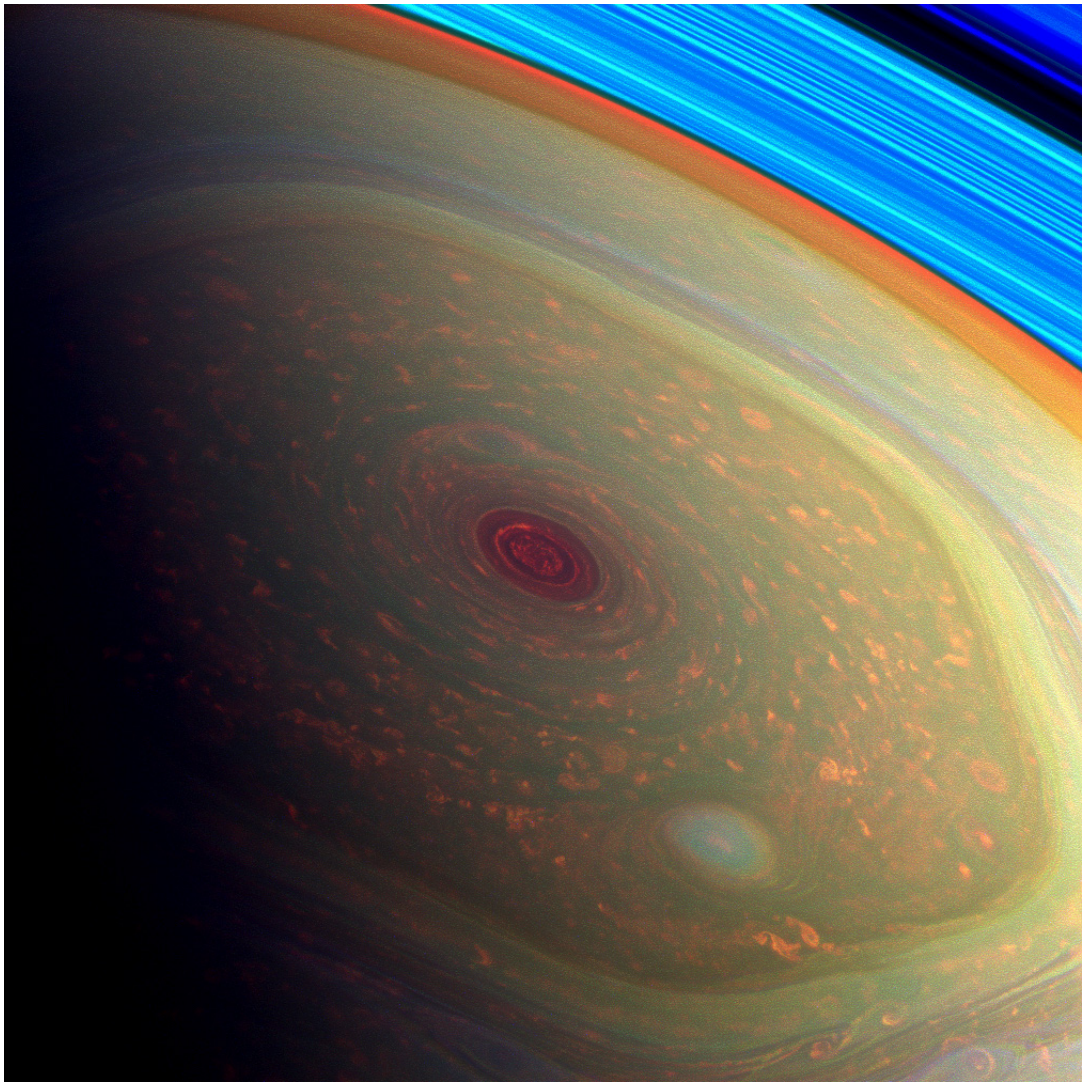

Figure SATURN-12. Saturn's north polar hexagon and polar cyclone. This false color image was taken on November 27, 2012 by the Cassini ISS. The MT3 and MT2 images, which are sensitive to absorption by methane gas in the atmosphere, are projected as blue and green, respectively. The CB2 image, which is not sensitive to methane absorption, is projected as red. The color balance is chosen to make the planet's atmosphere look realistic. The rings look bright blue because there is no methane gas between the rings and the spacecraft. The red spot in the center extends from the pole to a latitude of 88–89°. It looks red in the false-color image because the clouds are deep and methane gas absorbs the sunlight before it can reflect off the clouds and reach the spacecraft. The spot is a cyclone with winds of ~100 m s^{-1}.

is ~88°, which means that the average relative vorticity within 2° of the poles is equal to 0.4 times the local planetary vorticity. Based on Cassini ISS, VIMS, and CIRS data, Dyudina et al. [2008] and Dyudina et al. [2009] interpreted the vortex as a hurricane-like eye with eyewall clouds at 88° extending 20–70 km above the clouds at the pole. Sromovsky and Fry [2019] argued that an abrupt change of optical thickness could mimic the apparent eyewalls. The region has a 4–7 K warm core extending from the upper troposphere into the stratosphere [Achterberg et al. 2018]. The warm core and stable stratification implies downwelling, which is consistent with low phosphine abundance in the core [Fletcher et al. 2008]. Outside the eyewall are numerous anticyclonic vortices suggesting a convective origin [Dyudina et al. 2009]. Sayanagi et al. [2017] compared the north and south polar cyclones and attributed the differences to seasonal effects. Polar phenomena are extensively reviewed by Sayanagi et al. [2018].

- **Atmospheric dynamical processes (S_AO2)a**

Giant planet atmospheres are a superb laboratory for studying the dynamics of rotating fluids. Cloud tracking provides estimates of the winds, and the lack of continents and oceans provides a simpler setting than on Earth. The Cassini mission advanced this field, not only by providing 13 years of observations of Saturn but also by providing a 3-month flyby of Jupiter with an upgraded suite of instruments compared with those on the Voyager flybys. The Jupiter observations are discussed in the section entitled Saturn DWG non-Saturn science results. Here we focus on observations and models of the jets and vortices in Saturn's atmosphere. Saturn's atmospheric dynamics is extensively reviewed by Showman et al. [2018].

The zonal wind profile is a fundamental observation. ISS provided the first data at the start of the Cassini mission [Garcia-Melendo et al. 2011b; Porco et al. 2005; Vasavada et al. 2006] and a valuable comparison with Voyager 25 years earlier. The second fundamental observation is the eddy momentum flux (Figure SATURN-13). Eddies are the time- and longitude-dependent motions that carry heat and momentum across latitude circles. Using ISS data, Del Genio et al. [2007] and Del Genio and Barbara [2012] found a clear positive correlation between eddy momentum fluxes and meridional shear of the zonal wind, implying that eddies supply eastward momentum to the eastward jets and westward momentum to the westward jets. Similar correlations are found on Jupiter and Earth, although the energy supply for Earth's eddies could be different from that for Saturn and Jupiter.

> The eddies north and south of the equator supply positive angular momentum to the equator, so the meridional circulation replaces it with air from higher latitudes on both sides, implying convergence.

Since the eddies supply positive angular momentum to the eastward jets, the meridional circulation must replace it with low angular momentum air, which is found at higher latitudes. Conversely, the westward jets must have flow from lower latitudes. The result is that the meridional circulation diverges in the latitude bands that have westward jets on their poleward sides and eastward jets on their equatorward sides. These are the cyclonic shear zones—called belts on Jupiter.

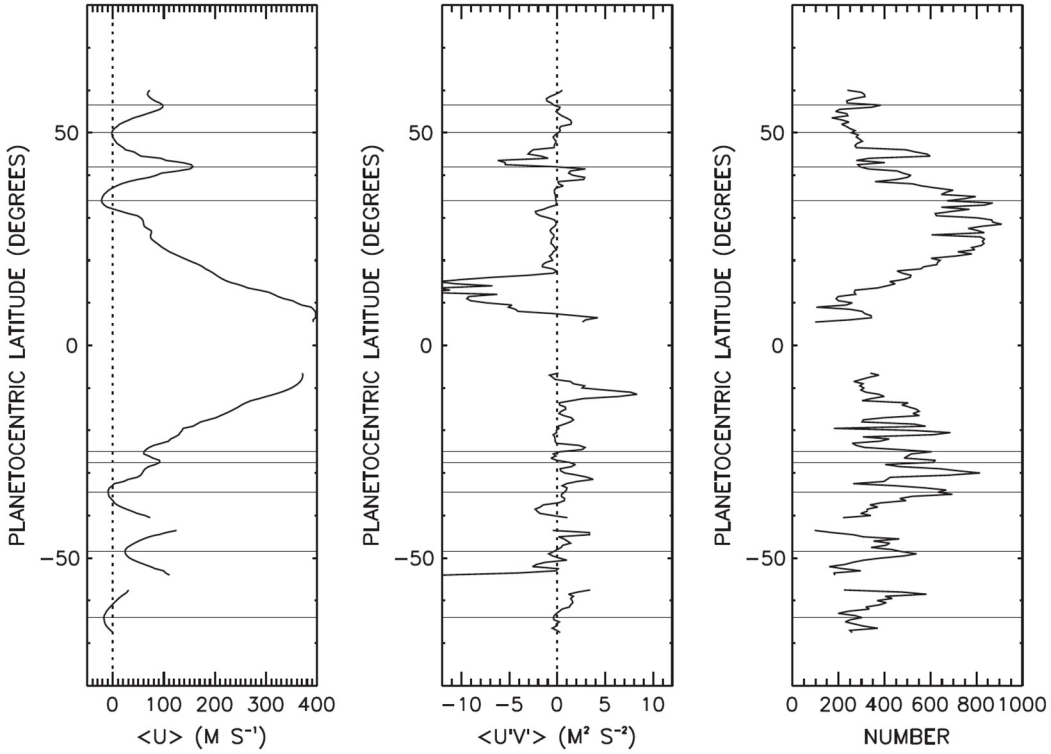

Figure SATURN-13. Eddy momentum transport for Saturn from Cassini ISS. The eastward and northward eddy winds u′ and v′ are the departures from the zonal means. Their product $\overline{u'v'}$ averaged over longitude and multiplied by density is the northward eddy flux of eastward momentum. The fact that this quantity has the same sign as $\partial\bar{u}/\partial y$, which is the increase of the mean eastward wind with latitude, says that the eddies are putting energy into the jets and not the reverse [Del Genio and Barbara 2012].

Anticyclonic shear zones—called zones on Jupiter—are the reverse, so they have convergence. The eddies north and south of the equator supply positive angular momentum to the equator, so the meridional circulation replaces it with air from higher latitudes on both sides, implying convergence. Horizontal convergence implies vertical divergence—either upwelling into the stratosphere or downwelling into the deep troposphere, or both. Using CIRS data Fletcher et al. [2009a] observed phosphine (PH_3), which is destroyed by photochemistry in the upper troposphere, to infer upwelling at the equator above the 0.5 bar level. However using VIMS data, which is sensitive to deeper levels, Fletcher et al. [2011a] inferred downwelling at the equator below the 1.3 bar level. Zuchowski et al. [2009] showed how this pair of stacked, oppositely-directed Hadley cells could arise from a balance between the effects of radiative heating and eddy momentum flux convergence. There is evidence of stacked Hadley cells on Jupiter as well [Gierasch et al. 2000; Ingersoll et al. 2000, 2017; Showman and de Pater 2005], but the subject of upwelling and downwelling is still open.

Zonal jet stability is the third important observation. Stability depends on the potential vorticity [Antunano et al. 2019], which depends on vertical structure, both of temperature and wind, but a simple but relevant criterion is that the flow is stable if the curvature of the zonal wind profile with respect to latitude does not exceed β, which is twice the planet's angular velocity times the cosine

of latitude divided by the planetary radius. Interestingly, this stability criterion is violated on Saturn near the peaks of the westward jets, especially at high latitudes, indicating that the zonal jets could be unstable [Antunano et al. 2015; Read et al. 2009a]. That does not mean the flow is unstable, however, as there are other stability criteria that involve vertical structure [Dowling 1995]. Liao et al. [2007] argue that a statistical equilibrium occurs as the zonal flow saturates. In their global vortex analysis, Trammell et al. [2014] find a correlation between the number of vortices and the westward jet peaks, implying at least some degree of instability at those latitudes.

Waves and vortices are another important feature of giant planet atmospheres. Saturn currently has nothing like the Great Red Spot, which has endured for over 100 years, but it has similar structures. Generally, anticyclones last longer than cyclones, but del Rio-Gaztelurrutia et al. [2010, 2018] document a cyclone that lasted for four years. Convective storms can generate waves that transport westward momentum away from their source regions, helping to accelerate eastward jets at the latitudes of the convection [Gunnarson et al. 2018; Liu and Schneider 2015; Sayanagi and Showman 2007]. This acceleration must be balanced somewhere, and [Schneider and Liu 2009] argue that the balance occurs through magneto-hydrodynamic drag at 0.3 to 1.4 Mbar where the atmosphere becomes electrically conducting [Liu et al. 2014; Liu and Schneider 2015].

Saturn's north polar hexagon at 75° latitude has inspired several modeling studies, both in the laboratory [Aguiar et al. 2010] and on the computer [Morales-Juberias et al. 2011, 2015]. Saturn's ribbon at 47° latitude is a less dramatic relative of the hexagon [Sayanagi et al. 2010] since both seem to represent a steady meandering pattern on an eastward jet stream. The models do not explain why the conditions necessary for a long-lived meandering jet stream exist only at certain latitudes on Saturn or why there are no such jet streams on Jupiter. O'Neill et al. [2015, 2016] propose a model of Saturn's polar cyclones in which convection at mid latitudes produces a vortex that is cyclonic at the bottom and anticyclonic at the top. The two halves separate, and the cyclonic vortex drifts to the pole and merges with other cyclonic vortices to make a single polar vortex. Brueshaber et al. [2019] one-layer shallow-water simulations also show that poleward drifting cyclonic vortices merge to form polar vortices, and also revealed a mechanism that separates the polar dynamical regimes of Jupiter, Saturn, and Uranus/Neptune. On the other hand, Antunano et al. [2018] report no meridional migration in the region north of the hexagon, and suggest that mergers do not contribute to the maintenance of the polar vortex. Sanz-Requena et al. [2018, 2019] describe the haze and cloud structure in the north pole and hexagon region.

Saturn's great storm has also inspired modeling studies. One model uses an imposed heat pulse and studies its interaction with the ambient zonal flow [Garcia-Melendo and Sanchez-Lavega 2017]. Another model studies how precipitation of water, which has a high molecular mass relative to hydrogen, from the troposphere, can inhibit convection for decades due to the long radiative time constant of Saturn's atmosphere [Li and Ingersoll 2015]. A third model uses a long-term numerical integration of moist convection in a giant planet atmosphere [Sugiyama et al. 2014]. The simulations are conducted using a two-dimensional cloud-resolving model that explicitly represents the convective motions and microphysics of NH_3, NH_4SH, and H_2O. It produces intermittent cumulonimbus activity. The time scale is ~60 days, although it is proportional to the water abundance and is therefore likely to be greater for Saturn than for Jupiter.

Numerical models of Saturn's jets and vortices fall into two categories. One is the conventional general circulation model (GCM), which uses hydrostatic balance in the vertical and is valid for large horizontal scales and small vertical scales [Friedson and Moses 2012; Garcia-Melendo et al. 2007; Trammell et al. 2016]. The other is the fluid sphere model in which the vertical and horizontal scales are comparable and the flow takes place in thick spherical shells [Aurnou et al. 2008; Heimpel and Aurnou 2007; Liu et al. 2014]. Computational limitations make it difficult to develop a single model that includes both small and large vertical scales, although the effort is being made [Heimpel et al. 2016]. More often, the practitioners divide in separate camps and work with different tools.

- **Saturn Lightning Sources and Morphology (S_AO6, SN2a)** – Investigate the sources and the morphology of Saturn lightning SED, lightning whistlers.

The Cassini RPWS detects the radio waves from lightning at frequencies starting at 1.3 MHz and ranging up to 40 MHz [Fischer et al. 2006a; Fischer et al. 2006b; Fischer et al. 2007; Fischer et al. 2008]. A single flash is called a SED, and it lasts for less than the 35.2 ms integration time of the RPWS instrument (Figure SATURN-14). Fundamentally, the duration of an SED is unknown [Farrell et al. 2007]. An SED is not a whistler; it is a freely-propagating radio wave that follows a straight-line path from the source. Although the RPWS is listening virtually all the time, sometimes it detects nothing for months. SED activity is often from a single storm, with SEDs every few seconds for a 5-hour ON period followed by a 5-hour OFF period, when the storm is hidden behind Saturn. Often the storm itself is visible, both in ISS images [Dyudina et al. 2007] and in the images gathered by amateur astronomers at Earth. Criteria used to identify the storm are that it appeared within a day or two after the onset of SED activity and it was always on the side of the planet facing the spacecraft when the RPWS was detecting signals. Thus the number of lightning storms at any one time is likely to be either 0 or 1. In contrast, Earth has ~2000 lightning storms over the globe at all times, and Jupiter has dozens of storms at all times [Little et al. 1999].

Cassini ISS eventually detected the lightning flashes [Dyudina et al. 2010], even on the day side despite the bright background of clouds in sunlight. The secret is to take many short exposures, since a short exposure reduces the background but not the lightning; it does reduce the probability of capturing a flash, so one needs to take many exposures. The diameter of the illuminated spot is about 200 km, indicating that the lightning is 125–250 km below cloud tops. This depth is above the liquid H_2O–NH_3 cloud and may be either in the NH_4SH cloud or the H_2O ice cloud.

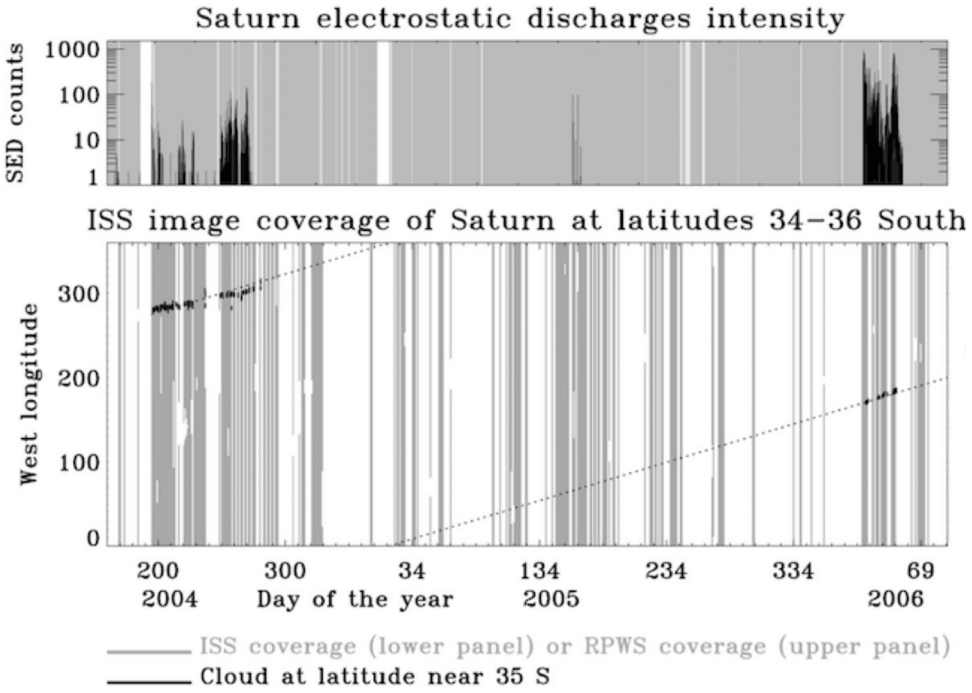

Figure SATURN-14. Saturn electrostatic discharge counts, SEDs, which are roughly equivalent to lightning strikes, over a 2-year period starting in 2004. The SEDs are detected by the RPWS instrument, which is ON continuously. The lower panel shows ISS coverage of latitudes −34° to −36°, where all the storms were occurring, and it is clear that storms were seen only when the RPWS was detecting SED's [Dyudina et al. 2007].

The great northern storm of 2010–2011 was a copious lightning emitter [Dyudina et al. 2013; Fischer et al. 2011]. The RPWS recorded flashes every 0.2 s. The optical energy per flash was about equal to that of the radio energy [Dyudina et al. 2013], although there is considerable uncertainty in both. The optical energy in single flashes ranged up to 8×10^9 J. The flash rate and total power were hundreds of times greater than those of the smaller southern storms that had been appearing intermittently since the start of Cassini observations. Fischer et al. [2014] proposed that the northern storm could account for a change in the Saturn kilometric radiation (SKR) frequency through its effect on thermospheric winds.

The Saturn lighting results stimulated two reviews of planetary lightning [Yair et al. 2008; Yair 2012]. Lightning is an agent of chemical change. Based on VIMS observations, Baines et al. [2009a] proposed that the dark and spectrally featureless clouds associated with giant planet thunderstorms represent small particles of elemental carbon. The particles are postulated to arise from atmospheric methane exposed to high temperatures during the lightning discharge, but Sromovsky et al. [2018] argue that the dark features are more likely regions of reduced optical depth. Dubrovin et al. [2014] studied the effect of lightning on the lower ionosphere of Saturn finding that H_3^+ ions are rapidly produced from the parent H_2^+ ion. On the other hand [Hurley et al. 2012a] searched for but found no correlation between acetylene and thunderstorm activity on Saturn. The Saturn results also

stimulated lightning searches throughout the solar system and on exoplanets from Earth-based radio telescopes and from spacecraft [Hodosan et al. 2016; Zarka et al. 2008].

Saturn Interior Structure and Rotation (S_AO3)

- **Saturn Formation and Evolution (S_AO5)** – Provide observational constraints (gas composition, isotope ratios, heat flux, …) on scenarios for the formation and the evolution of Saturn

The internal heat coming out of the planet is a fundamental quantity relevant to formation and evolution. Because giant planets in our solar system are massive and their surfaces are cold, they cool off slowly. Their interiors are still warm, and they are still releasing some of their heat of formation. To measure the internal power one takes the difference between the emitted infrared power and the absorbed solar power, which is the difference between the incident and reflected sunlight. Using Voyager data, Hanel et al. [1983] estimated the effective emission temperature as 95.0 ±0.4 K, corresponding to an average emitted heat flux of 4.62 ±0.8 W m^{-2}, and the ratio of emitted power to absorbed power as 1.78 ±0.09. Thus the internal power divided by the absorbed solar power is 0.78. Using data from Cassini CIRS, Li et al. [2010] estimated the emitted heat flux as 4.952 ±0.035 W m^{-2} during 2004–2009, although it decreased by 2% during that time and was 16% higher in the southern hemisphere than in the northern hemisphere. These were likely seasonal changes associated with the approach of vernal equinox in 2009. Li et al. [2015] measured the emitted power vs. latitude from 2004 to 2013 and documented the 2010 great storm's effect, which was to increase the global emitted power by 2% and the power at the latitude of the storm by 9% (Figure SATURN-4). These changes were in addition to a seasonal warming of the north and cooling of the south from 2004 to 2013.

The settling releases gravitational potential energy, which affects the cooling history and planetary evolution.

The helium to hydrogen ratio in the atmosphere reflects the value in the solar nebula when the planets were forming as well as the degree to which helium has settled toward the core. Settling is thought to happen because helium becomes immiscible in metallic hydrogen, which is the dominant constituent at megabar pressures. The settling releases gravitational potential energy, which affects the cooling history and planetary evolution. In principle, helium is detected by remote sensing through its effect on the molecular weight of the gas. One uses occultation data to get density vs. altitude, and from the hydrostatic equation one gets density vs. pressure. Then one uses infrared data to get temperature vs. pressure, and with the equation of state one can solve for the molecular weight. The method was used for Jupiter and Saturn using Voyager data [Conrath et al. 1984], but the Galileo probe gave a different result for Jupiter and forced a reanalysis for Saturn [Conrath and Gautier 2000]. Cassini has collected excellent data using CIRS for the temperature and occultations by several instruments—radio science, VIMS, and UVIS, but getting a consistent estimate of the helium abundance is difficult. The occultation result depends on the ray path, and that depends on unknown winds and temperatures above the

occultation point. The most recent estimate [Koskinen and Guerlet 2018] uses Cassini UVIS for the occultations and CIRS for temperature versus pressure. They get a helium mass fraction Y of 0.16−0.22, which is about 70% of the protosolar mass fraction of 0.27, implying that a certain amount of settling has occurred in Saturn's interior.

Before Cassini reached Saturn, the C/H abundance ratio was known to be higher on Saturn than on Jupiter, which was known to be higher than that on the Sun [Atreya et al. 1999, 2003; Owen and Encrenaz 2003]. The C/H ratio is perhaps the most accurately known ratio of all the heavy elements because its molecular form, methane, doesn't condense at Saturn temperatures and isn't readily destroyed in chemical reactions. Cassini CIRS probes the far-infrared rotational lines of the molecule and has determined a volume mixing ratio of $(4.7 \pm 0.2) \times 10^{-3}$, corresponding to a C/H enrichment relative to solar of 10.4 [Fletcher et al. 2009b]. This is more than a factor of 2 greater than that for Jupiter but consistent with conventional models of the formation and evolution of the giant planets, which predict increasing ratios to H of the heavy element abundances relative to the Sun from Jupiter to Neptune [Atreya et al. 2019].

Saturn's greater enrichment is also qualitatively consistent with the masses and radii of the two giant planets. These, coupled with the gravitational moments, rotation rate, and an equation of state, give information about the core mass and amount of heavy elements in the molecular envelope [Guillot 1999; Nettelmann et al. 2013]. Chemical models preceding the arrival of Galileo and Cassini listed many gases that were potentially observable in the atmospheres of Jupiter and Saturn [Fegley and Lodders 1994].

The high C/H ratio is taken as evidence of heavy element enrichment in general and has implications for possible differential sedimentation in the planet's interior over its lifetime [Mousis et al. 2006]. Measurements of NH_3, PH_3, C_2H_2, C_2H_6, and CH_4 all are consistent with these gases trapped as clathrate hydrate in the feeding zone of Saturn as the planets were forming [Hersant et al. 2008]. Clathrate hydrates require water, and our lack of knowledge of the oxygen abundance allows for a number of interior models with a range of values for the C/O ratio [Lunine 2011]. Cassini CIRS measurements suggest that Saturn's D/H ratio is less than that for Jupiter, which mostly reminds us that our understanding planetary formation and evolution is incomplete [Pierel et al. 2017].

Although ammonia is the main carrier of nitrogen on Jupiter and Saturn, the isotopic ratio $^{15}N/^{14}N$ can reveal insights into the molecular carrier (N_2 versus NH_3) in the protoplanetary nebula. The Saturnian and Jovian isotopic ratios appear indistinguishable [Fletcher et al. 2014; Fouchet et al. 2004a]. That result favors accretion of primordial N_2 on both planets, either in the gas phase from the solar nebula or as ices formed at very low temperature [Fletcher et al. 2014].

- **Saturn's Rotation Rate (SN1a)** – Determine Saturn's rotation rate and internal structure despite the planet's unexpected high degree of axisymmetry.

The periodic variation of the dynamo field has been used to estimate the interior rotation rates of Jupiter, Uranus, and Neptune. However, Saturn's magnetic field axis is so closely aligned with its rotation axis that is has no periodic variation. Taking the misalignment of the other three giant

planets, 10° for Jupiter, 60° for Uranus, and 47° for Neptune, the 0.1° upper bound for Saturn is highly improbable (1 chance in 10^4 or 10^5), given that the probability of the magnetic axis aligning with the rotation axis goes as the square of the angle between them [Dougherty 2017]. The close alignment means that there is no detectable wobble in the field as the planet rotates and therefore no periodic signal with which to estimate the rotation period of the planet's interior. The SKR radio emissions are tied to currents in the magnetosphere and ionosphere, and the period is variable from year to year [Fischer et al. 2014], which rules out a direct tie to the interior of Saturn.

There have been various attempts to use the atmospheric periods to estimate the interior rotation rate. They use the data in different ways, but they all derive a period that is near the midpoint of the atmospheric periods. Smith et al. [1982] use cloud tracking and choose a reference frame that minimizes the variance of the cloud-tracked zonal wind with respect to latitude, with 10 h 31 m 30 ±30 s as the result. Anderson and Schubert [2007] chose the reference frame that minimizes the measured shape of the 100 mbar surface from an equipotential, with 10 h 32 m 35 ±13 s as the result. Read et al. [2009b] use the reference frame in which the atmosphere is marginally stable with respect to Arnol'd's second stability criterion, with 10 h 34 m 13 ±20 s as the result. Their method uses ISS and CIRS wind and temperature data to estimate potential vorticity in the range 2–270 mbar. The problem with these approaches is that they ignore the thermal wind equation, which allows vertical shear in the zonal winds. Thus the speed at depth might not match the average speed at the tops of the clouds where the winds and temperatures are measured. Read et al. [2009b] argue that the stability criterion depends on the speed of the longest Rossby waves, which are deeply rooted, but still the problem remains. For instance, the midpoint of the wind distribution at Earth's upper troposphere would give a period between 22 hours and 23 hours for the rotation of the planet, because the average wind at the top of the troposphere is to the east.

Saturn is a fluid planet, and if it were in equilibrium only the zonal harmonics with even *n* would be present.

The gravity field [Jacobson et al. 2006] also has information about the rotation rate of the interior [Hubbard 2009]. As with all planets, Saturn's gravitational potential can be expanded into spherical harmonics, the leading term of which is the spherically symmetric potential −GM/R, followed by the zonal harmonics and the tesseral harmonics. The zonal harmonics are axially symmetric, and each term is proportional to a Legendre polynomial of degree n and a dimensionless amplitude factor J_n. The tesseral harmonics are the longitudinally-varying part of the gravitational potential. Saturn is a fluid planet, and if it were in equilibrium only the zonal harmonics with even n would be present. The J_n reflect the response of the planet to its own rotation, so one could use them to infer the interior rotation rate if the interior structure were known. Conversely, one could infer the interior structure, e.g., core mass, metallic hydrogen, degree of helium separation, heavy elements in the molecular envelope, etc., if the rotation rate were known [Helled and Guillot 2013; Helled et al. 2015; Hubbard 2009]. Further information about the interior could come from the tidal Love number—the magnitude of the planet's response to tidal forces [Lainey et al. 2017]. The observations are astrometric data on the orbits of Saturn's moons spanning more than a century and include a large set of Cassini data. The study indicates significant tidal

dissipation inside the planet. In all cases, an independent measure of the rotation rate is important for probing the internal structure.

The tesseral harmonics have an effect on the rings, which are a sensitive seismometer for detecting the non-zonal gravity field [Hedman and Nicholson 2013, 2014]. The harmonics are of two types. One type has pattern speeds ranging from 807 to 834 degrees per day, for which the corresponding periods are 10 h 42 m to 10 h 22 m, respectively (Figure SATURN-15). These nearly bracket the periods derived from tracking the clouds at various latitudes in Saturn's atmosphere, and could be due to non-zonal structures rotating with the planet. The large range of periods prevents improving on cloud tracking estimates alone. The other types of tesseral harmonics have pattern speeds near five hours and are thought to be due to normal mode oscillations inside the planet. The precise frequencies of these normal modes depend both on the interior structure and the interior rotation rate, but as with the zonal harmonics, it is difficult to separate the two effects. This is an ongoing effort.

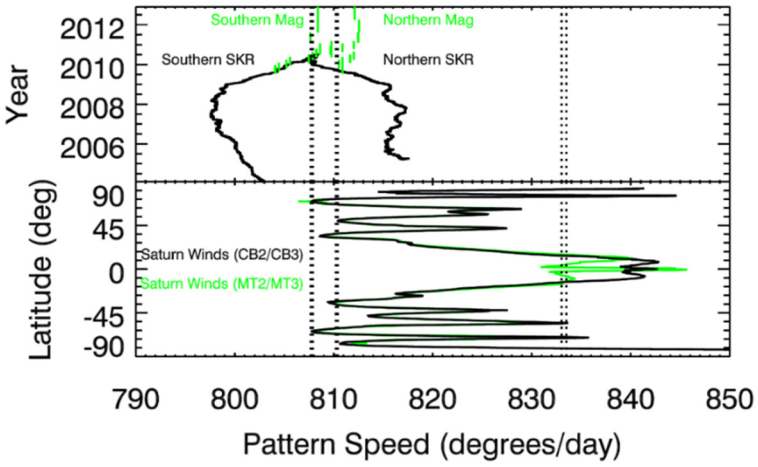

Figure SATURN-15. Ring seismology. The vertical dotted lines are the speeds of non-axisymmetric patterns in Saturn's rings. Only the patterns that match the planet's rotation are shown. They could be due to floating masses in the interior of Saturn. For comparison, periods of exterior magnetic fields, radio emissions, and clouds in the atmosphere are shown. Other patterns with speeds twice as fast are likely due to normal mode oscillations of the planet [Hedman and Nicholson 2014].

The precise frequencies of the normal modes depend both on the interior structure and the interior rotation rate. Parameters of the interior structure include the mass of the core, the helium mass fraction and the heavy-element mass fraction in the metallic and molecular envelopes, and the pressure at the metallic-molecular transition [Mankovich et al. 2019]. For a given rotation rate, the interior parameters are adjusted to give the observed values of J_2 and J_4. The rotation rate is varied to give the best fit to the observed frequencies of the ~20 normal modes whose resonant effect on the ring orbits makes them detectable. The planet's rotation affects the frequencies through the Coriolis and centrifugal forces and the ellipticity of level surfaces. The distribution of rotation periods resulting from a broad sample of interior models can be summarized as $10^h\ 33^m\ 38s^{+1m52s}_{-1m19s}$ [Mankovich et al. 2019]. The residuals of the fit do not exhibit any strong evidence of differential rotation inside the planet, but differential rotation cannot be ruled out. The rotation period

is consistent with predictions by Militzer et al. [2019] who combined interior models, which were constrained by Cassini's gravity measurements, with observations of the planet's oblateness by the Voyager spacecraft. Based on this analysis, a rotation period of 10:33:34 ±55 s is predicted for the planet's deep interior.

The even zonal harmonics, especially n = 6 and above, can be used to detect differential rotation inside the planet [Galanti and Kaspi 2017; Kaspi 2013]. This method is being used both with Cassini at Saturn and with Juno at Jupiter. The odd harmonics have been used only at Jupiter. The software to analyze these data was developed to be used on both planets [Galanti and Kaspi 2016; Galanti et al. 2017; Kaspi et al. 2016]. Cassini produced its best gravity data during six dives between the planet and the innermost ring during the final five months of the mission [Iess et al. 2019]. On these dives the spacecraft skimmed 2600–3900 km above the cloud tops while the radio link to Earth was monitored to determine the gravitational field of the planet and the mass of the rings. The gravity measurements yielded unexpectedly large values of the even zonal harmonics J_6, J_8 and J_{10}. These values do not match any interior model that assumes uniform rotation and makes reasonable assumptions about the equation of state and helium rain [Iess et al. 2019]. Galanti et al. [2019] confirmed that an acceptable solution can only be found for J_2 and J_4.

One can fit all the even harmonics J_2-J_{10} with a model where unknown winds extend through the planet on cylinders. The best fit is where the atmosphere at the equator rotates 4% faster than the deep interior, but the models also require a region that rotates more slowly than the deep interior, which is surprising because it is not seen in the cloud tracking data. One can also fit the harmonics by assuming the observed cloud-top winds extend to a finite depth. The best fit is with a finite depth of 9000 km. Qualitatively the two results are the same, since the cloud-top winds are fastest at the equator. The depth of the winds for Saturn is 2–3 times deeper than that for Jupiter, but the difference is explained by the more rapid increase of electrical conductivity with depth on Jupiter and the shallower point where magnetic drag suppresses differential rotation [Guillot et al. 2018].

Once the gravity signal of the deep winds is adequately incorporated into models for Saturn's interior, reasonable structures are obtained: The conditions of helium rain are compatible with predictions from ab initio computer simulations. Cores of heavy elements with 15–18 Earth masses are compatible with the core-accretion hypothesis, which requires a ~8 Earth mass core to trigger run-away gas accretion. The enrichment of heavy elements in the planet's molecular envelope of 1–3 times solar is lower than expected but still reasonable. This contrasts with the persistent conundrum for Jupiter, for which the inferred heavy abundances are near or subsolar.

A puzzling feature of this analysis is that the same model of the gravitational field cannot fit all of the six passes in a combined, multi-arc orbital solution [Iess et al. 2019]. The residuals represent unmodeled accelerations acting on Cassini over time scales of 20–60 min and could be due to time-varying tesseral harmonics. Convection in Saturn's interior is one possible source. Normal modes varying in amplitude and frequency is another. The data were eventually fit by assuming random accelerations of 10 minute duration acting within ±1 hour from pericenter [Iess

et al. 2019]. The hope is that these high-frequency accelerations do not significantly affect the determination of the even harmonics J_2-J_{10}.

Aurora, Chemistry, and Upper Atmosphere (SC2a)

Observe the upper atmosphere and the aurora as it changes on all time scales—minutes to years—and is affected by seasonal and solar cycle forcing.

- **Upper atmosphere (SC2a)**

The stratosphere entered in the discussion in the sections entitled Composition and chemistry, Seasonal variations, and Saturn's winds. To reduce the overlap between those sections and this one, we focus here on theoretical models and on the parts of the atmosphere above the stratosphere. The entire subject, upper atmosphere and ionosphere, is reviewed in the book chapter by Nagy [2009]. Species like C_2H_2 and C_2H_6 have chemical lifetimes in the stratosphere that are comparable to a season on Saturn, so they can be used as tracers of the meridional circulation and its annual reversal from north to south. At the equator the zonal winds in the stratosphere exhibit a 15-year oscillation that is accompanied by an oscillation of the temperature distribution symmetric about the equator to maintain thermal wind balance.

The simplest chemical model is a diurnally averaged 1D photochemical model with eddy diffusion chosen to represent dynamical processes. Moses et al. [2000a] developed a model that couples hydrocarbon and oxygen photochemistry, molecular and eddy diffusion, radiative transfer, and condensation to better constrain the chemical species and to identify the important physical processes that control the abundances. Moses et al. [2000b] consider the role of oxygen by comparing their model results with the observed abundances of H_2O and CO_2. They find that an external source of oxygen is necessary, and they estimate its magnitude. They mention micrometeoroid ablation and ring particle diffusion as likely sources.

In particular, electrostatic charging could lead to ejection of nanograins out of the ring plane and into the atmosphere by the electromagnetic force [Ip et al. 2016]. Further evidence of ring rain is seen in enhanced H_3^+ emissions at latitudes tied to magnetic field lines that cross the equatorial plane at the locations of the inner edges of the A-ring and B-ring and at the orbit of Enceladus [O'Donoghue et al. 2013, 2017].

Hesman et al. [2009] compare the output of the static photochemical model with observations of C_2H_2 and C_2H_6, and they find evidence of a meridional circulation. Guerlet et al. [2014] compare the temperatures computed from a radiative equilibrium model with temperatures observed by Cassini CIRS, and they find evidence that other processes, presumably related to dynamics, control Saturn's stratospheric thermal structure. Teanby et al. [2006] place new upper limits on halides in Saturn's stratosphere, but they advise that the abundances in the troposphere could be much larger. Sinclair et al. [2014] compare temperatures and gaseous abundances from Cassini with those from Voyager exactly one Saturn year later. They find that most of the change is due to the opposite phase of the 15-year oscillation and that other types of interannual variability are small.

Above the stratosphere, diffusive separation takes over and each gas's density falls off with altitude at its own individual scale height, which depends on its molecular weight. The altitude of the transition is called the homopause. Below the homopause, one finds gaseous hydrocarbons ranging in molecular weight at least up to benzene [Koskinen et al. 2016; Vervack and Moses 2015]. These hydrocarbons are the source of stratospheric haze particles at non-auroral latitudes [Moses et al. 2000a; Kim et al. 2012]. Above the homopause the major constituent is H_2, which continues into the exosphere where the molecules don't collide with each other except at the exobase [Koskinen et al. 2013]. The relatively high (380 K to 590 K) exospheric temperature at low to mid latitudes is a long-standing mystery [Shemansky and Liu 2012; Stallard et al. 2012b]. Despite the changing seasons, the high temperatures have persisted from the period of the Voyager flybys through the Cassini era [Koskinen et al. 2015]. High temperatures do occur in the auroral zones, but dynamical models strongly suggest that the upper atmosphere is geostrophically balanced and cannot convey the high-temperature air to lower latitudes (Figure SATURN-16). One possibility is that atmospheric gravity waves, which are often overlooked in models, could supply enough torque to overcome the Coriolis force and allow enough meridional overturning to warm the equatorial thermosphere [Müeller-Wodarg et al. 2019].

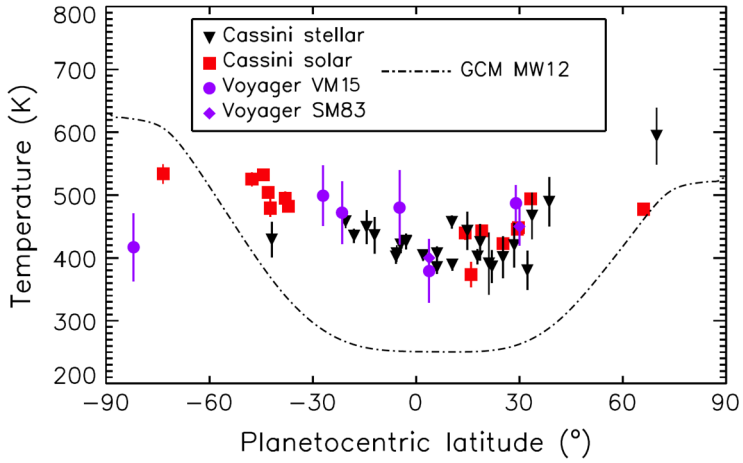

Figure SATURN-16. Comparison of Cassini UVIS observations with Voyager observations and with a 3-D general circulation model. The model result is represented by the smooth dot-dashed line, and it is significantly low (colder) equatorward of ±60° in both hemispheres. The problem is that the air from the polar regions, heated by auroral currents, cools before it reaches the lower latitudes. What keeps it warm is an ongoing mystery [Koskinen et al. 2015].

The first in situ measurements of the equatorial thermosphere occurred during the final month of the Cassini mission, when the spacecraft skimmed through the upper atmosphere on four periapses and also during the final plunge. The Ion Neutral Mass Spectrometer (INMS) measured the profiles of temperature and composition [Yelle et al. 2018]. The best fit to the exospheric temperature is in the range 340 to 370 K, with a value during the final plunge of 354 K. The helium profiles are consistent with diffusive equilibrium, but the methane profiles are not. Even well above the homopause, the CH_4/H_2 ratio is nearly constant with height. This points to an external source, the most likely being Saturn's rings [Yelle et al. 2018].

- **Aurora (SC2a)**

The aurora is caused by precipitating electrons striking the upper atmosphere. The source of the electrons is in the magnetosphere, and the subject is covered mainly in the section entitled Magnetospheres and Plasma Science (MAPS) Discipline Science Results. Some of the questions involve the energy and source of the electrons, how deep they penetrate into the atmosphere, and what effects they have on the temperatures, chemistry, and electromagnetic emissions associated with the aurora.

The aurora is observed in the ultraviolet [Gerard et al. 2013; Gustin et al. 2009, 2010, 2017], visible [Dyudina et al. 2016], infrared [Melin et al. 2011, 2016; O'Donoghue et al. 2014; Stallard et al. 2012a], and radio wavelengths [Lamy et al. 2009, 2013; Ye et al. 2016]. The currents associated with the electrons can be observed when the spacecraft flies through an auroral flux tube [Bunce et al. 2014]. And although the magnetosphere of Saturn is much less energetic than that of Jupiter, the footprint of the Enceladus flux tube has detectable emissions [Pryor et al. 2011], though not so bright as those of the Jovian moons: The geysers of Enceladus are weaker than the volcanoes of Io, and the magnetic field of Saturn is weaker than the magnetic field of Jupiter.

For a short, broad-brush summary of the magnetosphere, ionosphere, and atmosphere, we recommend Gombosi and Ingersoll [2010].

- **Ionosphere (S_AO4)** – Study the diurnal variations and magnetic control of the ionosphere of Saturn.

This science objective is captured in detail in the Magnetospheres and Plasma Science (MAPS) Discipline Science Results under the following AO and TM science objectives: **MN1b:** Conduct in situ studies of Saturn's ionosphere and inner radiation belt; **MN1c:** Investigate magnetospheric periodicities, their coupling to the ionosphere, and how the SKR periods are imposed from close to the planet (3–5 R_S) out to the deep tail; **MN2a:** Determine the coupling between Saturn's rings and ionosphere; and **MC1a:** Determine the temporal variability of Enceladus' plume (relevant to the Enceladus auroral footprint).

Further Science Objectives for Saturn Science

- **Water.** Measure the global water abundance and determine its role in bringing heat to the surface. Determine the role of moist convection in maintaining the large-scale motions. A Saturn probe to the base of the water cloud is a challenging but possible objective.
- **Rotation.** Determine Saturn's rotation period if such a number exists, or determine the spread of periods if differential rotation persists into the interior.
- **Noble gases.** Determine Saturn's noble gas abundances including helium, as done for Jupiter by the Galileo probe. A Saturn probe could measure noble gases to exquisite precision.

- **Weather layer.** Determine the vertical profiles of temperature, winds, clouds, condensable gases, longwave and shortwave radiation, and turbulence levels. A cloud-resolving model like those used in tropical meteorology, but tailored to the giant planets, is both timely and valuable. Again, a Saturn probe is needed.
- **Interior.** Using the power of ring seismometry and gravity sounding, improve the understanding of Saturn's internal equation of state, mass distribution, composition, and temperature distribution. Develop a fully coupled interior/weather-layer model as done for Earth's oceans and atmosphere.

SATURN DWG NON-SATURN SCIENCE RESULTS

- **Jupiter atmospheric dynamics (J_AO1)** – Extend the time for studies of atmospheric dynamics beyond the period accessible to the Galileo nominal mission.

Jupiter has a photogenic atmosphere; its colorful clouds provide ideal tracers of the winds (Figure SATURN-17). The light and dark bands—the zones and belts—and their associated jet streams have been observed from Earth for more than 100 years. The Great Red Spot (GRS) and its smaller cousins have been observed for just as long. Thus Jupiter is an atmospheric dynamics laboratory, where dynamical phenomena like waves, jets, eddies, and vortices can be studied without the complications of continents, oceans, and large seasonal swings. As it approached and flew past Jupiter in late 2000, Cassini provided three months of valuable data about the atmosphere. A 70-day movie shows the clouds in motion at all longitudes and latitudes up to within ~10 degrees of the poles. That movie in cylindrical and polar projections is PIA03452, PIA03453, and PIA03454, and is available at https://photojournal.jpl.nasa.gov/.

The GRS is at least 150 years old, although it could be much older. The three white ovals to the south of the GRS formed in the late 1930s and merged into one oval named BA in the late 1990s. All of these features are anticyclones with circumferential winds greater than 100 m s^{-1}. They drift slowly in longitude but stay fixed in latitude. Combined with Hubble Space Telescope and Galileo data, Cassini data were used to show that the GRS shrank by 15% from 1996 to 2006, both in terms of its visible appearance and its ring of circumferential winds [Asay-Davis et al. 2009; Shetty and Marcus 2010].

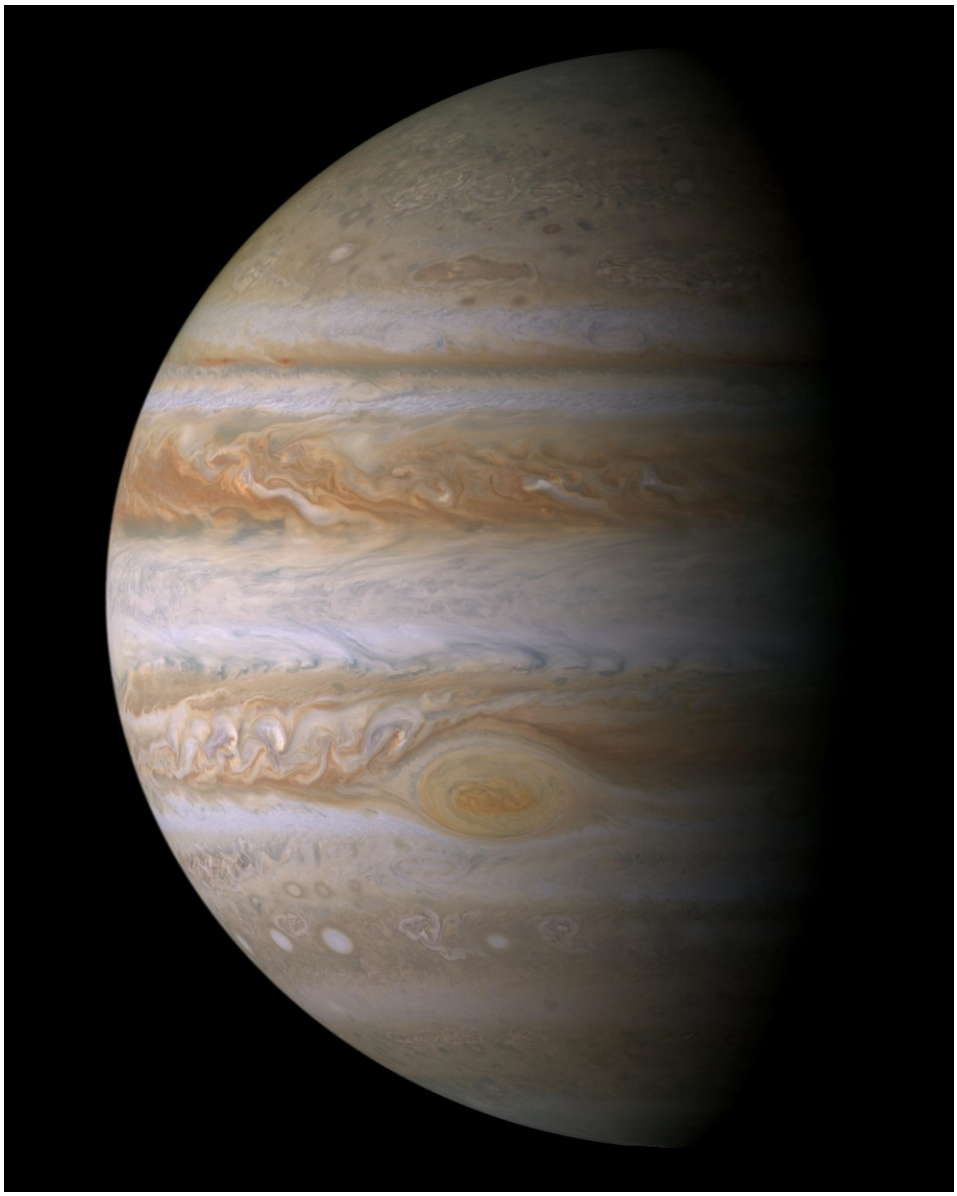

Figure SATURN-17. The highest-resolution, full-disk color mosaic of Jupiter ever taken. Jupiter more than filled the field of view of the ISS, so the mosaic was assembled from over 30 individual images, allowing for the planet's rotation as the images were taken.

The white ovals occupied a single latitude band with anticyclonic vorticity. They avoided each other for 60 years because they were separated by cyclonic regions encroaching into the band from the equatorward side [Youssef and Marcus 2003]. When the cyclonic regions got pushed out, the ovals merged. Peak velocities around oval BA remained steady while the color changed from white to red several years later. Using different techniques to measure winds and different definitions of the oval's edge, different groups have documented small changes in the properties of

BA over similar time periods [Hueso et al. 2009; Choi et al. 2010; Sussman et al. 2010]. The combination of Cassini ISS data and Hubble methane band data was used to understand the changes in vertical cloud structure as BA changed from white to red [Wong et al. 2011]. Using ISS data from the Cassini flyby [Li et al. 2004; Choi et al. 2013] and amateur telescopic data [Rogers et al. 2006], several authors have documented the life cycles—formation, shape, lifetime, mergers—of the more numerous smaller spots on Jupiter.

Jupiter's zonal jets are remarkably steady in comparison with Earth's jet streams, which change on time scales of one or two weeks (Figure SATURN-18). Cassini ISS documented only one latitude outside the equator, near 21° planetocentric, where the jet speed had changed by a modest amount from Voyager in 1979 to Cassini in 2000 [Porco et al. 2003; Asay-Davis et al. 2011]. Most of the observed variability is at the equator [Garcia-Melendo et al. 2011a] and is part of a regular ~4-year oscillation similar to the QBO on Earth [Simon-Miller et al. 2007; Simon-Miller and

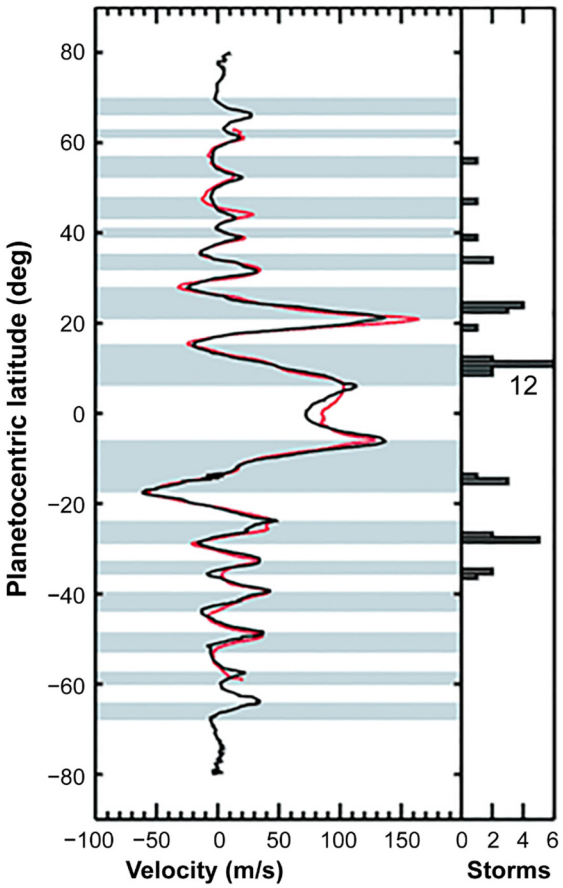

Figure SATURN-18. Atmospheric zonal velocity for Jupiter. The black curve is from Cassini ISS data in late 2000, and the red curve is from Voyager data in mid1979. The jets are remarkably steady over this 21-year interval [Porco et al. 2003].

Gierasch 2010]. Meridional transport is inferred indirectly from Cassini CIRS data that give the latitudinal distribution of C_2H_2 and C_2H_6, which have known chemical lifetimes and thereby track

the age of air masses in the stratosphere [Liang et al. 2005; Zhang et al. 2013b]. Vertical wind shear of the zonal winds is studied by tracking features at different wavelengths that probe different altitudes [Li et al. 2006c].

Waves in a planetary atmosphere provide information about the medium in which they propagate and also about the sources that excite them. Mesoscale waves—wavelengths ~100 km—are visible from space if the crests and troughs are marked by clouds. The thunder following a lightning strike and the sonic boom following a meteor impact are examples of intense sound waves. Cassini could not detect sound waves, but it did detect thunderstorms and lightning [Dyudina et al. 2004; Porco et al. 2003; Baines et al. 2007]. Voyager, Galileo, and New Horizons detected mesoscale wave trains with crests and troughs aligned north-south and wavelengths of ~300 km. Cassini apparently did not detect mesoscale waves [Arregi et al. 2009]. They may have been absent at the time of the Cassini flyby or perhaps the waves were unobservable due to lack of cloud tracers. One theory says the mesoscale waves are propagating gravity waves [Flasar and Gierasch 1986], and another theory says they are shear instabilities [Bosak and Ingersoll 2002]. The measured phase velocities seem inconsistent with both models [Simon et al. 2015] given reasonable assumptions about the vertical wind shears, so the nature of the mesoscale waves is uncertain.

Cassini also detected large scale periodic patterns with wavelengths ranging up to 20,000 km. Circumpolar waves have wavelengths and phase speeds that suggest they are Rossby waves [Barrado-Izagirre et al. 2008, 2009]. Simultaneous observations by ISS, UVIS, and CIRS allow one to probe the vertical structure and opacity sources of the waves [Li et al. 2006b]. Radio observations allow one to study how the passage of a wave affects the distribution of ammonia [Cosentino et al. 2017]. Cassini observations have been used to support various theories of wave-like features in the South Equatorial Belt—that they are either inertia-gravity waves or Rossby waves [Simon-Miller et al. 2012] or a pattern associated with baroclinic instability at that latitude [Rogers et al. 2016].

Wave mean-flow interactions and cascades of energy from one scale to another are fundamental processes in the dynamics of planetary atmospheres. One theory says that the zonal mean flow forms into a potential vorticity (PV) staircase. PV is a conserved dynamical tracer and the staircase consists of latitude bands with constant PV and sharp boundaries in between. However, quantitative analysis of the Cassini 70-day movie shows that the PV gradient reverses sign and is not zero as the staircase model predicts [Li et al. 2004; Read et al. 2006; Shetty and Marcus 2010]. The 70-day movie was also used to show that the eddy momentum transport is into the jets from neighboring latitudes, meaning that the eddies are supplying energy to the jets and not the reverse (Figure SATURN-19) [Salyk et al. 2006]. The eddies could be getting their energy from convection [Li et al. 2006a] or the latitudinal gradient of radiative heating, or both [Schneider and Liu 2009]. Fourier spectra of the 70-day movie data generally reveal an inverse energy cascade, where kinetic energy flows from intermediate scales to large scales [Choi and Showman 2011; Galperin et al. 2014; Hadjighasem and Haller 2016], but there is evidence of a forward cascade from intermediate scales down to small scales, which has been interpreted as energy input at the intermediate scales, perhaps associated with the radius of

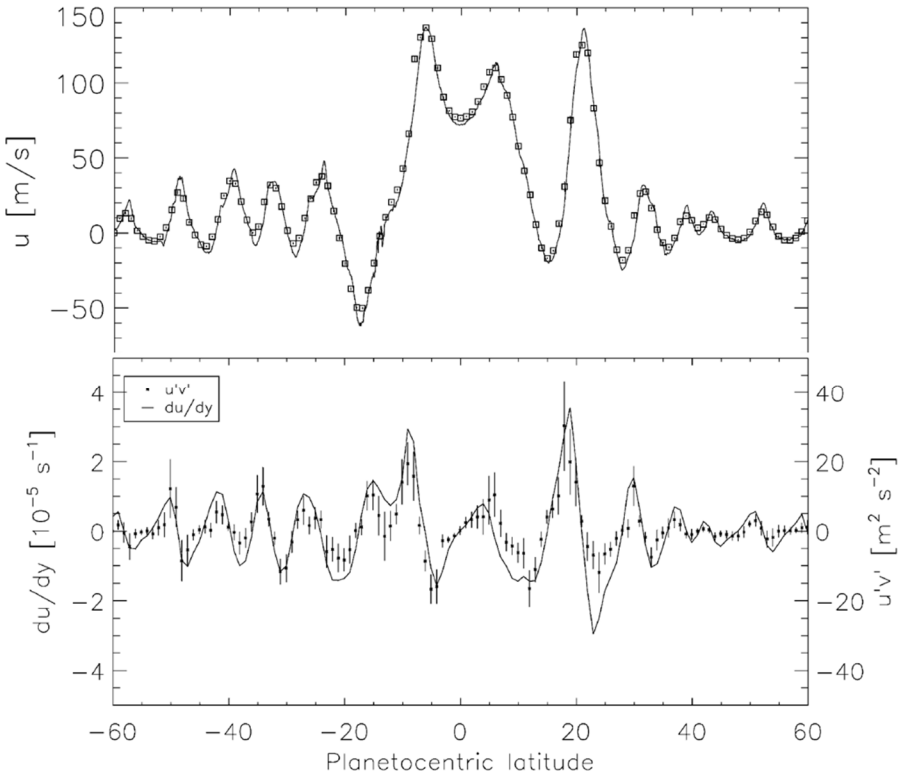

Figure SATURN-19. Eddy momentum transport for Jupiter from Cassini ISS. The eastward and northward eddy winds u′ and v′ are the departures from the zonal means. Their product $\overline{u'v'}$ averaged over longitude and multiplied by density is the northward eddy flux of eastward momentum. The fact that this quantity has the same sign as $\partial\overline{u}/\partial y$, which is the increase of the mean eastward wind with latitude, says that the eddies are putting energy into the jets and not the reverse [Salyk et al. 2006].

deformation through baroclinic instability [Young and Read 2017]. Others have compared visible features in the 70-day movie with fine-scale features in their 3-dimensional numerical models to test the models' treatment of unknown processes and parameters [Heimpel et al. 2005, 2016; Morales-Juberias and Dowling 2013].

- **Jupiter Global Atmospheric Structure and Composition (J_AO2)** – Infer global atmospheric thermal structure and composition with instrumentation not carried by the Galileo Orbiter, complementing the local in situ measurements of the Galileo Probe.

Reactive gases can serve as tracers that reveal regions of upwelling, downwelling, and meridional motion (Figure SATURN-20). During the Jupiter flyby, Cassini CIRS measured the latitude distributions of C_2H_2 and C_2H_6, which are produced in the upper stratosphere by photodissociation of methane. The rate of production is greatest at the equator where the solar ultraviolet (UV) is greatest. C_2H_2 has a chemical lifetime that is short compared to the meridional overturning, so it decreases toward the poles in response to the reduced solar UV. C_2H_6 has a longer chemical lifetime, so following a fluid parcel it increases with time the longer the parcel

spends in the stratosphere. The abundance of C_2H_6 increases toward the poles [Nixon et al. 2007, 2010], suggesting a meridional circulation in the stratosphere with upwelling at the equator and downwelling at the poles. The circulation revealed from the distributions of C_2H_2 and C_2H_6 aids in understanding the origin and chemical lifetimes of HCN and CO_2, which were also measured by CIRS [Lellouch et al. 2006].

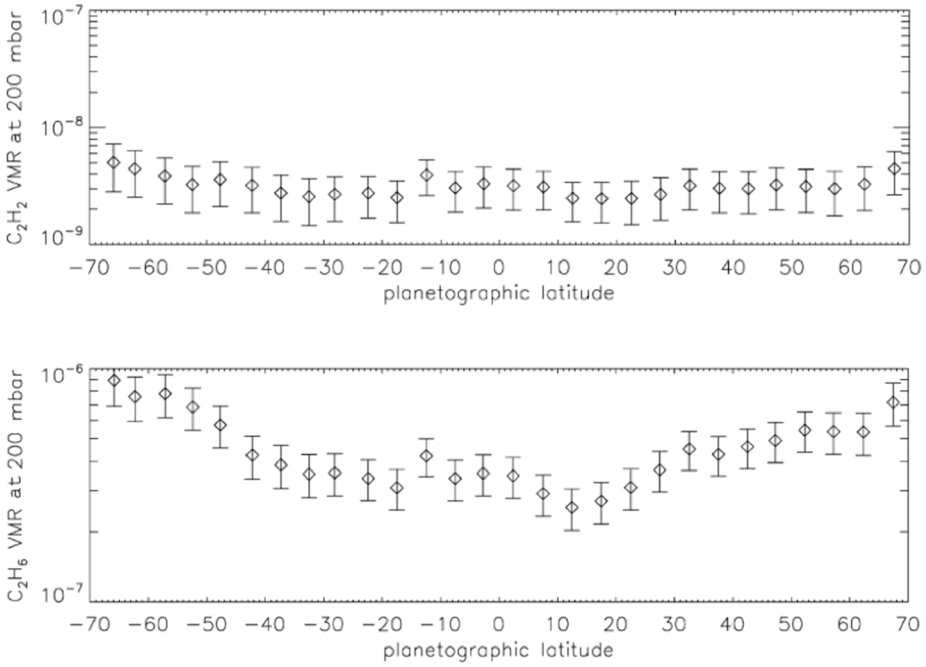

Figure SATURN-20. Chemical tracers in Jupiter's atmosphere at 200 mbar from Cassini CIRS. Both acetylene and ethane are formed at higher altitudes than these observations. C_2H_2 has a shorter lifetime once it is formed than C_2H_6 does, so it decays on the downdrafts faster than C_2H_6. The lower panel indicates downdrafts at the pole and updrafts at the equator. The upper panel shows that the time constant of this circulation is longer than the lifetime of the C_2H_2 molecule, because it has decayed before reaching the 200 mbar level [Nixon et al. 2007].

Since the stratosphere is stably stratified, to maintain steady state the updrafts must be heated and the downdrafts must be cooled. The decrease of sunlight toward the poles is consistent with updrafts at the equator and downdrafts at the poles. CIRS measurements of stratospheric temperatures and abundances of radiatively active gases are used to model the radiative forcing [Zhang et al. 2013a, 2013b], which includes the effects of stratospheric aerosols [Zhang et al. 2013c, 2015].

Cassini CIRS also measured the latitude distributions of phosphine [Irwin et al. 2004; Fletcher et al. 2009a] and ammonia [Achterberg et al. 2006]. The measurements refer to the upper troposphere, at the 100–500 mbar level, and they tell a consistent story. Both gases are removed from the atmosphere at upper levels, phosphine by photodissociation and ammonia by condensation, and both have maximum abundance at the equator and reduced abundance in the cyclonic belts on either side of the equator. This indicates rapid uplift or strong vertical mixing in

the equatorial zone and descent in the neighboring belts. Probing still deeper into the troposphere, Cassini VIMS detected a 3 μm absorption that could be a mixture of NH_4SH and NH_3 [Brown et al. 2003; Sromovsky and Fry 2010] and provided new insights into the composition of fresh ammonia clouds [Sromovsky and Fry 2018].

Gaseous abundances can provide clues to planet formation. CIRS measured the nitrogen isotopic ratio in ammonia [Abbas et al. 2004; Fouchet et al. 2004a]. The ratio is similar to that on the Sun but different from that on Earth, suggesting that the Earth was somehow isolated from the main reservoir of nitrogen during solar system formation. The hydrogen halides, on the other hand, are depleted relative to solar composition and support the halogens' condensation in ammonium salts [Fouchet et al. 2004b].

The Cassini flyby provided insights into aurora-related phenomena on Jupiter as well. UVIS observations of the He 584 Å line were used to infer enhanced eddy mixing in the polar regions, which may account for the enhancement of heavy hydrocarbons there [Parkinson et al. 2006]. Alternately, the enhancement of C_2H_2 and C_2H_6 in the polar regions could be explained by a combination of auroral-driven chemistry and advection by the meridional circulation [Sinclair et al. 2017]. CIRS observations have also been used to study the sources of heating in the polar stratosphere from 1–10 mbar [Sinclair et al. 2018]. The result is that heating by auroral soot particles dominates at 1 mbar altitude, and that heating by charged particles dominates at 10 mbar. Cassini VIMS observations have been used to produce the first maps of H_3^+ emission, temperature, and column density on Jupiter's nightside [Stallard et al. 2015]. The enhanced emission in the polar regions is produced by enhanced H_3^+ density rather than higher temperatures, which further points to the importance of auroral chemistry in that region.

Because of its high spatial and spectral resolution and full angular coverage during the flyby, Cassini obtained useful information about the clouds of Jupiter. Cloud color is a long-standing uncertainty: What chemical gives the Red Spot its redness? How many coloring agents are there? Comparison of laboratory experiments and visible spectra from Cassini VIMS suggests that the red chromophore is the product of photolyzed ammonia reacting with acetylene [Carlson et al. 2016; Baines et al. 2019]. The chromophore occurs in an optically thin layer above the main cloud deck, and may require upward displacement of the air mass to form. A principal component analysis of Cassini ISS data indicates that the red chromophore explains most of the variance across the planet, but a second coloring agent is required to explain the brownish color of the cyclones in Jupiter's North Equatorial Belt [Ordonez-Etxeberria et al. 2016].

The vertical structure of the cloud layers is another long-standing unknown. Cassini CIRS thermal spectra were used to probe into the clouds at a wavelength of 7.18 μm, where the ammonia gas is relatively transparent [Matcheva et al. 2005]. The result is that cloud base is at 0.9–1.1 bar, which is deeper than the nominal ammonia cloud base and might imply another, deeper cloud, possibly NH_4SH. Cassini VIMS covers 4.5–5.1 μm, another wavelength range where the gas is relatively transparent. Holes in the cloud allow thermal radiation to space, so the holes appear as hot spots. The cloud is found to be spectrally flat and at a pressure of 1.2 bar or deeper [Giles et al. 2015]. Pure NH_3 cloud and pure NH_4SH cloud do not match the spectra, and some kind of

coating is implied. Despite the possibility of coatings, CIRS has detected the spectral signature of NH_3 ice particles in the upper tropospheric clouds [Wong et al. 2004].

The planet's global energy budget is a key to its evolution and internal processes, including the separation of helium from hydrogen in the metallic interior. To determine the energy budget accurately, one would have to measure the thermal emission and scattered sunlight at all seasons, latitudes, longitudes, wavelengths, emission angles, incident angles, and phase angles. In practice, one samples these quantities and uses models to fill the gaps. Cassini CIRS, VIMS, and ISS all contribute to this estimate [Simon-Miller et al. 2006; Li et al. 2012; Sato et al. 2013; Mayorga et al. 2016]. North-south asymmetries and changes from Voyager to Cassini are present at the level of a few percent, but whether these are random fluctuations or systematic trends is uncertain.

Venus Atmosphere Observations

The Venus flybys yielded useful data at a variety of wavelengths. The VIMS instrument detected thermal emission from the hot surface at wavelengths of 0.85 and 0.90 μm, and thereby provided a new technique for exploring the surface mineralogy [Baines et al. 2000]. In an attempt to image the surface, the RADAR instrument was operated at 2.2 cm in both scatterometric and radiometric modes during the encounters, but only the thermal emission from the thick absorbing atmosphere was detected [Lorenz et al. 2001]. The UVIS instrument studied the airglow of Venus, focusing on N_2, C, O, and CO as clues to the excitation mechanisms and abundances [Hubert et al. 2010, 2012; Gerard et al. 2011]. Lightning on Venus is a long-standing controversial subject. The RPWS instrument on Cassini searched for lightning signals in the frequency range 0.125 to 16 MHz and found none, even though they easily detected lightning at rates of 70 s^{-1} during the Earth flyby several months later [Gurnett et al. 2001].

ACRONYMS

Note: For a complete list of Acronyms, refer to Cassini Acronyms – Attachment A.

AO	Announcement of Opportunity
CAKE	Cassini Apoapses for Kronian Exploration
CIRS	Composite Infrared Spectrometer
CSM	Cassini Solstice Mission
DWG	Discipline Working Group
GCM	General Circulation Model
GRS	Great Red Spot
HST	Hubble Space Telescope
IDS	Interdisciplinary Scientists
IR	Infrared
ISS	Imaging Science Subsystem
MAG	Magnetometer
MAPS	Magnetospheres and Plasma Science
PIE	Pre Integration Event
PSG	Project Science Group
PV	Potential Vorticity
QBO	Quasi-Biennial Oscillation
RADAR	Titan Radar Mapper
RPWS	Radio and Plasma Wave Science
SAMWG	Saturn Atmospheric Modeling Working Group
SED	Saturn Electrostatic Discharges
SKR	Saturn Kilometric Radiation
SWG	Saturn Working Group
TM	Traceability Matrix
TWT	Target Working Team
UV	Ultraviolet
UVIS	Ultraviolet Imaging Spectrograph
VIMS	Visual and Infrared Mapping Spectrometer
WG	Working Group

REFERENCES

Disclaimer: The partial list of references below correspond with in-text references indicated in this report. For all other Cassini references, refer to Attachment B – References & Bibliographies; Attachment C – Cassini Science Bibliographies; the sections entitled References contributed by individual Cassini instrument and discipline teams located in Volume 1 Sections 3.1 and 3.2 Science Results; and other resources outside of the Cassini Final Mission Report.

Abbas, M. M., A. LeClair, E. Woodard, M. Young, M. Stanbro, F. M. Flasar, et al., (2013), Distribution of CO2 in Saturn's atmosphere from Cassini/CIRS infrared observations, The Astrophysical Journal, 776, 2, 73, doi: 10.1088/0004-637x/776/2/73.

Abbas, M. M., A. LeClair, T. Owen, B. J. Conrath, F. M. Flasar, V. G. Kunde, et al., (2004), The nitrogen isotopic ratio in Jupiter's atmosphere from observations by the Composite Infrared Spectrometer on the Cassini spacecraft, The Astrophysical Journal, 602, 1063–1074, doi: 10.1086/381084.

Achterberg, R. K., Flasar, F. M., Bjoraker, G. L., Hesman, B. E., Gorius, N. J. P., Mamoutkine, A. A., et al., (2018), Thermal emission from Saturn's polar cyclones, Geophysical Research Letters, 45, 11, 5312–5319, doi: 10.1029/2018GL078157.

Achterberg, R. K., P. J. Gierasch, B. J. Conrath, L. N. Fletcher, B. E. Hesman, G. L. Bjoraker, F. M. Flasar, (2014), Changes to Saturn's zonal-mean tropospheric thermal structure after the 2010-2011 northern hemisphere storm, The Astrophysical Journal, 786, 2, 92, doi: 10.1088/0004-637x/786/2/92.

Achterberg, R. K., B. J. Conrath, P. J. Gierasch, (2006), Cassini CIRS retrievals of ammonia in Jupiter's upper troposphere, Icarus, 182, 169–180, doi: 10.1016/j.icarus.2005.12.020.

Adriani, A., M. L. Moriconi, E. D'Aversa, F. Oliva, G. Filacchione, (2015), Faint luminescent ring over Saturn's polar hexagon, The Astrophysical Journal, 808, L16, doi: 10.1088/2041-8205/808/1/l16.

Aguiar, A. C. B., P. L. Read, R. D. Wordsworth, T. Salter, Y. H. Yamazaki, (2010), A laboratory model of Saturn's north polar hexagon, Icarus, 206, 2, 755-763, doi: 10.1016/j.icarus.2009.10.022.

Anderson, J. D., and G. Schubert, (2007), Saturn's gravitational field, internal rotation, and interior structure. Science, 317, 1384–1387, doi: 10.1126/science.1144835.

Antunano, A., T. del Río-Gaztelurrutia, A. Sánchez-Lavega, P. L. Read, L. N. Fletcher, (2019), Potential vorticity of Saturn's polar regions, J. Geophys. Res., 124, 186-201, doi: 10.1029/2018JE005764.

Antunano, A., T. del Rio-Gaztelurrutia, A. Sanchez-Lavega, J. Rodriguez-Aseguinolaza, (2018), Cloud morphology and dynamics in Saturn's northern polar region, Icarus, 299, 117–132, doi: 10.1016/j.icarus.2017.07.017.

Antunano, A., T. del Rio-Gaztelurrutia, A. Sanchez-Lavega, R. Hueso, (2015), Dynamics of Saturn's polar regions, Journal of Geophysical Research-Planets, 120, 2, 155–176, doi: 10.1002/2014je004709.

Arregi, J., J. F. Rojas, R. Hueso, A. Sanchez-Lavega, (2009), Gravity waves in Jupiter's equatorial clouds observed by the Galileo orbiter, Icarus, 202, 358–360, doi: 10.1016/j.icarus.2009.03.028.

Asay-Davis, X. S., P. S. Marcus, M. H. Wong, I. de Pater, (2011), Changes in Jupiter's zonal velocity between 1979 and 2008, Icarus, 211, 1215–1232, doi: 10.1016/j.icarus.2010.11.018.

Asay-Davis, X. S., P. S. Marcus, M. H. Wong, I. de Pater, (2009), Jupiter's shrinking Great Red Spot and steady Oval BA: Velocity measurements with the "Advection Corrected Correlation Image Velocimetry" automated cloud-tracking method, Icarus, 203, 164–188, doi: 10.1016/j.icarus.2009.05.001.

Atreya, S. K., A. Crida, T. Guillot, J. I. Lunine, N. Madhusudhan, M. Mousis, (2019), The origin and evolution of Saturn, with exoplanet perspective, in Saturn in the 21st Century, (eds.) K. Baines, M. Flasar, N. Krupp, T. Stallard), Cambridge University Press, pp. 5–43.

Atreya, S. K., P. R. Mahaffy, H. B. Niemann, M. H. Wong, T. C. Owen, (2003), Composition and origin of the atmosphere of Jupiter - an update, and implications for the extrasolar giant planets, Planetary and Space Science 51, 2, 105–112, doi: 10.1016/s0032-0633(02)00144-7.

Atreya, S. K., M. H. Wong, T. C. Owen, P. R. Mahaffy, H. B. Niemann, I. de Pater, P. Drossart, T. Encrenaz, (1999), A comparison of the atmospheres of Jupiter and Saturn: deep atmospheric composition, cloud structure, vertical mixing, and origin, Planetary and Space Science, 47,10–11, 1243–1262, doi: 10.1016/s0032-0633(99)00047-1.

Aurnou, J., M. Heimpel, L. Allen, E. King, J. Wicht, (2008), Convective heat transfer and the pattern of thermal emission on the gas giants, Geophysical Journal International, 173, 3, 793–801, doi: 10.1111/j.1365-246X.2008.03764.x.

Auwera, J. V., N. Moazzen-Ahmadi, J. M. Flaud, (2007), Toward an accurate database for the 12 μm region of the ethane spectrum, Astrophysical Journal, 662, 1, 750–757.

Baines, K. H., L. A. Sromovsky, R. W. Carlson, T. W. Momary, T. W., P. M. Fry, (2019), The visual spectrum of Jupiter's Great Red Spot accurately modeled with aerosols produced by photolyzed ammonia reacting with acetylene, Icarus 330, 217–229.

Baines, K. H., M. L. Delitsky, T. W. Momary, R. H. Brown, B. J. Buratti, R. N. Clark, P. D. Nicholson, (2009a), Storm clouds on Saturn: Lightning-induced chemistry and associated materials consistent with Cassini/VIMS spectra, Planetary and Space Science, 57, 14–15, 1650–1658, doi: 10.1016/j.pss.2009.06.025.

Baines, K. H., T. W. Momary, L. N. Fletcher, A. P. Showman, M. Roos-Serote, R. H. Brown, B. J. Buratti, R. N. Clark, P. D. Nicholson, (2009b), Saturn's north polar cyclone and hexagon at depth revealed by Cassini/VIMS, Planetary and Space Science, 57, 14–15, 1671–1681, doi: 10.1016/j.pss.2009.06.026.

Baines, K. H., A. A. Simon-Miller, G. S. Orton, H. A. Weaver, A. Lunsford, T. W. Momary, et al., (2007), Polar lightning and decadal-scale cloud variability on Jupiter, Science, 318, 226–229, doi: 10.1126/science.1147912.

Baines, K. H., P. Drossart, T. W. Momary, V. Formisano, C. Griffith, G. Bellucci, J. P. Bibring, et al., (2005), The atmospheres of Saturn and Titan in the near-infrared: First results of Cassini/VIMS, Earth Moon and Planets, 96, 3–4, 119–147, doi: 10.1007/s11038-005-9058-2.

Baines, K. H., G. Bellucci, J. P. Bibring, R. H. Brown, B. J. Buratti, E. Bussoletti, et al., (2000), Detection of sub-micron radiation from the surface of Venus by Cassini/VIMS, Icarus, 148, 307–311, doi: 10.1006/icar.2000.6519.

Banfield, D., B. J. Conrath, P. J. Gierasch, P. D. Nicholson, K. Matthews, (1998), Near-IR spectrophotometry of Jovian aerosols - Meridional and vertical distributions, Icarus, 134, 1, 11–23, doi: 10.1006/icar.1998.5942.

Barrado-Izagirre, N., S. Perez-Hoyos, A. Sanchez-Lavega, (2009), Brightness power spectral distribution and waves in Jupiter's upper cloud and hazes, Icarus, 202, 181–196, doi: 10.1016/j.icarus.2009.02.015.

Barrado-Izagirre, N., A. Sanchez-Lavega, S. Perez-Hoyos, R. Hueso, (2008), Jupiter's polar clouds and waves from Cassini and HST images: 1993-2006. Icarus, 194, 173–185, doi: 10.1016/j.icarus.2007.08.025.

Barstow, J. K., P. G. J. Irwin, L. N. Fletcher, R. S. Giles, C. Merlet, (2016), Probing Saturn's tropospheric cloud with Cassini/VIMS, Icarus, 271, 400–417, doi: 10.1016/j.icarus.2016.01.013.

Beebe, R. F., (2005), Comparative study of the dynamics of the outer planets, Space Science Reviews, 116, 1–2, 137–154, doi: 10.1007/s11214-005-1952-4.

Bosak, T., and A. P. Ingersoll, (2002), Shear instabilities as a probe of Jupiter's atmosphere, Icarus, 158, 2, 401–409, doi: 10.1006/icar.2002.6886.

Brown, R. H., K. H. Baines, G. Bellucci, J. P. Bibring, B. J. Buratti, F. Capaccioni, et al., (2003), Observations with the Visual and Infrared Mapping Spectrometer (VIMS) during Cassini's flyby of Jupiter, Icarus, 164, 461–470, doi: 10.1016/s0019-1035(03)00134-9.

Brueshaber, S. R., K. M. Sayanagi, T. E. Dowling, (2019), Dynamical regimes of giant planet polar vortices, Icarus 323, 46–61.

Bunce, E. J., D. C. Grodent, S. L. Jinks, David J. Andrews, S. V. Badman, Andrew J. Coates, S. W. H. Cowley, et al., (2014), Cassini nightside observations of the oscillatory motion of Saturn's northern auroral oval, Journal of Geophysical Research-Space Physics, 119, 5, 3528–3543, doi: 10.1002/2013ja019527.

Cao, Hao, C. T. Russell, U. R. Christensen, M. K. Dougherty, M. E. Burtonm (2011), Saturn's very axisymmetric magnetic field: No detectable secular variation or tilt, Earth and Planetary Science Letters 304, no. 1–2, 22–28.

Carlson, R. W., K. H. Baines, M. S. Anderson, G. Filacchione, A. A. Simon, (2016), Chromophores from photolyzed ammonia reacting with acetylene: Application to Jupiter's Great Red Spot, Icarus, 274, 106–115, doi: 10.1016/j.icarus.2016.03.008.

Cavalie, T., M. Dobrijevic, L. N. Fletcher, J. C. Loison, K. M. Hickson, V. Hue, P. Hartogh, (2015), Photochemical response to the variation of temperature in the 2011–2012 stratospheric vortex of Saturn, Astronomy & Astrophysics, 580, doi: 10.1051/0004-6361/201425444.

Choi, D. S., A. P. Showman, A. R. Vasavada, A. A. Simon-Miller, (2013), Meteorology of Jupiter's equatorial hot spots and plumes from Cassini, Icarus, 223, 832–843, doi: 10.1016/j.icarus.2013.02.001.

Choi, D. S., and A. P. Showman, (2011), Power spectral analysis of Jupiter's clouds and kinetic energy from Cassini, Icarus, 216, 597–609, doi: 10.1016/j.icarus.2011.10.001.

Choi, D. S., A. P. Showman, A. R. Vasavada, (2010), The evolving flow of Jupiter's White Ovals and adjacent cyclones, Icarus, 207, 359–372, doi: 10.1016/j.icarus.2009.10.013.

Choi, D. S., A. P. Showman, R. H. Brown, (2009), Cloud features and zonal wind measurements of Saturn's atmosphere as observed by Cassini/VIMS, Journal of Geophysical Research-Planets, 114, doi: 10.1029/2008je003254.

Conrath, B. J., and D. Gautier, (2000), Saturn helium abundance: A reanalysis of Voyager measurements, Icarus, 144, 1, 124–134, doi: 10.1006/icar.1999.6265.

Conrath, B. J., D. Gautier, R. A. Hanel, J. S. Hornstein, (1984), The helium abundance of Saturn from Voyager measurements, Astrophysical Journal, 282, 2, 807-815, doi: 10.1086/162267.

Cosentino, R. G., B. Butler, B. Sault, R. Morales-Juberias, A. Simon, I. de Pater, (2017), Atmospheric waves and dynamics beneath Jupiter's clouds from radio wavelength observations, Icarus, 292, 168–181, doi: 10.1016/j.icarus.2017.01.006.

Del Genio, A. D., and J. M. Barbara, (2016), An objective classification of Saturn cloud features from Cassini ISS images, Icarus, 271, 222–236, doi: 10.1016/j.icarus.2016.02.011.

Del Genio, A. D., and J. M. Barbara, (2012), Constraints on Saturn's tropospheric general circulation from Cassini ISS images, Icarus, 219, 2, 689–700, doi: 10.1016/j.icarus.2012.03.035.

Del Genio, A. D., R. K. Achterberg, K. H. Baines, F. M. Flasar, P. L. Read, A. Sanchez-Lavega, A. P. Showman, (2009), Saturn atmospheric structure and dynamics, In Saturn from Cassini-Huygens, (eds.) M. K. Doughterty, L. W. Esposito, S. M. Krimigis, pp. 113–159, Springer, Dordrecht, Netherlands.

Del Genio, A. D., J. M. Barbara, J. Ferrier, A. P. Ingersoll, R. A. West, A. R. Vasavada, J. Spitale, C. C. Porco, (2007), Saturn eddy momentum fluxes and convection: First estimates from Cassini images, Icarus, 189, 2, 479–492, doi: 10.1016/j.icarus.2007.02.013.

del Rio-Gaztelurrutia, T., A. Sanchez-Lavega, A. Antunano, J. Legarreta, E. Garcia-Melendo, K. M. Sayanagi, et al., (2018), A planetary-scale disturbance in a long living three vortex coupled system in Saturn's atmosphere, Icarus, 302, 499–513, doi: 10.1016/j.icarus.2017.11.029.

del Rio-Gaztelurrutia, T., J. Legarreta, R. Hueso, S. Perez-Hoyos, A. Sanchez-Lavega, (2010), A long-lived cyclone in Saturn's atmosphere: Observations and models, Icarus, 209, 2, 665–681, doi: 10.1016/j.icarus.2010.04.002.

Desch, M. D., and M. L. Kaiser, (1981), Voyager measurement of the rotation period of Saturn's magnetic field, Geophysical Research Letters, 8, 3, 253–256, doi: 10.1029/GL008i003p00253.

Devi, V. M., I. Kleiner, R. L. Sams, L. R. Brown, D. C. Benner, L. N. Fletcher, (2014), Line positions and intensities of the phosphine (PH3) pentad near 4.5 μm, Journal of Molecular Spectroscopy, 298, 11–23, doi: 10.1016/j.jms.2014.01.0130022-2852.

Dobrijevic, M., T. Cavalie, F. Billebaud, (2011), A methodology to construct a reduced chemical scheme for 2D-3D photochemical models: Application to Saturn, Icarus, 214, 1, 275–285, doi: 10.1016/j.icarus.2011.04.027.

Dougherty, M., and Cassini Magnetometer Team, (2017), Cassini's magnetometer at Saturn, Astronomy & Geophysics, 58, 4, 36–42, doi: 10.1093/astrogeo/atx140.

Dowling, T. E., (1995), Dynamics of Jovian atmospheres, Annual Review of Fluid Mechanics, 27, 293–334, doi: 10.1146/annurev.fl.27.010195.001453.

Dubrovin, D., A. Luque, F. J. Gordillo-Vazquez, Y. Yair, F. C. Parra-Rojas, U. Ebert, C. Price, (2014), Impact of lightning on the lower ionosphere of Saturn and possible generation of halos and sprites, Icarus, 241, 313–328, doi: 10.1016/j.icarus.2014.06.025.

Dyudina, U. A., X. Zhang, L. Li, P. Kopparla, A. P. Ingersoll, L. Dones, A. Verbiscer, Y. L. Yung, (2016), Reflected light curves, spherical and Bond albedos of Jupiter- and Saturn-like exoplanets, The Astrophysical Journal, 822, 2, 76, doi: 10.3847/0004-637x/822/2/76.

Dyudina, U. A., A. P. Ingersoll, S. P. Ewald, C. C. Porco, G. Fischer, Y. Yair, (2013), Saturn's visible lightning, its radio emissions, and the structure of the 2009-2011 lightning storms, Icarus, 226, 1, 1020–1037, doi: 10.1016/j.icarus.2013.07.013.

Dyudina, U. A., A. P. Ingersoll, S. P. Ewald, C. C. Porco, G. Fischer, W. S. Kurth, R. A. West, (2010), Detection of visible lightning on Saturn, Geophysical Research Letters, 37, doi: 10.1029/2010gl043188.

Dyudina, U. A., A. P. Ingersoll, S. P. Ewald, A. R. Vasavada, R. A. West, K. H. Baines, T. W. Momary, et al., (2009), Saturn's south polar vortex compared to other large vortices in the Solar System, Icarus, 202, 1, 240–248, doi: 10.1016/j.icarus.2009.02.014.

Dyudina, U. A., A. P. Ingersoll, S. P. Ewald, A. R. Vasavada, R. A. West, A. D. Del Genio, J. M. Barbara, et al., (2008), Dynamics of Saturn's south polar vortex, Science, 319, 5871, 1801–1801, doi: 10.1126/science.1153633.

Dyudina, U. A., A. P. Ingersoll, S. P. Ewald, C. C. Porco, G. Fischer, W. Kurth, M. Desch, A. Del Genio, J. Barbara, J. Ferrier, (2007), Lightning storms on Saturn observed by Cassini ISS and RPWS during 2004-2006, Icarus, 190(2), 545-555, doi: 10.1016/j.icarus.2007.03.035.

Dyudina, U. A., A. D. Del Genio, A. P. Ingersoll, C. C. Porco, R. A. West, A. R. Vasavada, J. M. Barbara, (2004), Lightning on Jupiter observed in the H-alpha line by the Cassini imaging science subsystem, Icarus, 172, 24–36, doi: 10.1016/j.icarus.2004.07.014.

Farrell, W. M., M. L. Kaiser, G. Fischer, P. Zarka, W. S. Kurth, D. A. Gurnett, (2007), Are Saturn electrostatic discharges really superbolts? A temporal dilemma, Geophysical Research Letters, 34, 6, doi: 10.1029/2006gl028841.

Fegley, B., and K. Lodders, (1994), Chemical Models of the deep atmospheres of Jupiter and Saturn, Icarus, 110, 1, 117–154, doi: 10.1006/icar.1994.1111.

Fischer, G., S. Y. Ye, J. B. Groene, A. P. Ingersoll, K. M. Sayanagi, J. D. Menietti, W. S. Kurth, D. A. Gurnett, (2014), A possible influence of the Great White Spot on Saturn kilometric radiation periodicity, Annales Geophysicae, 32, 12, 1463–1476, doi: 10.5194/angeo-32-1463-2014.

Fischer, G., W. S. Kurth, D. A. Gurnett, P. Zarka, U. A. Dyudina, A. P. Ingersoll, S. P. Ewald, et al., (2011), A giant thunderstorm on Saturn, Nature, 475, 7354, 75–77, doi: 10.1038/nature10205.

Fischer, G., D. A. Gurnett, W. S. Kurth, F. Akalin, P. Zarka, U. A. Dyudina, W. M. Farrell, M. L. Kaiser, (2008), Atmospheric electricity at Saturn, Space Science Reviews, 137, 1–4, 271–285, doi: 10.1007/s11214-008-9370-z.

Fischer, G., W. S. Kurth, U. A. Dyudina, M. L. Kalser, P. Zarka, A. Lecacheux, A. P. Ingersoll, D. A. Gurnett, (2007), Analysis of a giant lightning storm on Saturn, Icarus, 190, 2, 528–544, doi: 10.1016/j.icarus.2007.04.002.

Fischer, G., M. D. Desch, P. Zarka, M. L. Kaiser, D. A. Gurnett, W. S. Kurth, W. Macher, et al., (2006a), Saturn lightning recorded by Cassini/RPWS in 2004, Icarus, 183, 1, 135–152, doi: 10.1016/j.icarus.2006.02.010.

Fischer, G., W. Macher, D. A. Gurnett, M. D. Desch, A. Lecacheux, P. Zarka, W. S. Kurth, M. L. Kaiser, (2006b), Discrimination between Jovian radio emissions and Saturn electrostatic discharges, Geophysical Research Letters, 33, 21, doi: 10.1029/2006gl026766.

Flasar, F. M., (2005), Temperatures, winds, and composition in the Saturnian system, Science, 307, 5713, 1247–1251. doi: 10.1126/science.1105806.

Flasar, F., and P. Gierasch, (1986), Mesoscale waves as a probe of Jupiter's deep atmosphere, Journal of the Atmospheric Sciences, 43, 22, 2683–2707, doi: 10.1175/1520-0469(1986)043<2683:MWAAPO>2.0.CO;2.

Fletcher, L. N., T. K. Greathouse, S. Guerlet, J. I. Moses, R. A. West, (2018), Saturn’s seasonally changing atmosphere: thermal structure, composition and aerosols. In Saturn in the 21st Century, (eds.) K. H. Baines, F. M. Flasar, N. Krupp, T. Stallard, Cambridge University Press, pp. 251–294, doi: 10.1017/9781316227220.010.

Fletcher, L. N., S. Guerlet, G. S. Orton, R. G. Cosentino, T. Fouchet, P. G. J. Irwin, L. M. Li, F. M. Flasar, N. Gorius, R. Morales-Juberias, (2017), Disruption of Saturn's quasi-periodic equatorial oscillation by the great northern storm, Nature Astronomy, 1, 11, 765–770, doi: 10.1038/s41550-017-0271-5.

Fletcher, L. N., P. G. J. Irwin, R. K. Achterberg, G. S. Orton, F. M. Flasar, (2016), Seasonal variability of Saturn's tropospheric temperatures, winds and para-H2 from Cassini far-IR spectroscopy, Icarus, 264, 137–159, doi: 10.1016/j.icarus.2015.09.009.

Fletcher, L. N., P. G. J. Irwin, J. A. Sinclair, G. S. Orton, R. S. Giles, J. Hurley, N. Gorius, R. K. Achterberg, B. E. Hesman, G. L. Bjoraker, (2015), Seasonal evolution of Saturn's polar temperatures and composition, Icarus, 250, 131–153, doi: 10.1016/j.icarus.2014.11.022.

Fletcher, L. N., T. K. Greathouse, G. S. Orton, P. G. J. Irwin, O. Mousis, J. A. Sinclair, R. S. Giles, (2014), The origin of nitrogen on Jupiter and Saturn from the 15N/14N ratio, Icarus, 238, 170–190, doi: 10.1016/j.icarus.2014.05.007.

Fletcher, L. N., B. E. Hesman, R. K. Achterberg, P. G. J. Irwin, G. Bjoraker, N. Gorius, J. Hurley, et al., (2012), The origin and evolution of Saturn's 2011-2012 stratospheric vortex, Icarus, 221, 2, 560–586, doi: 10.1016/j.icarus.2012.08.024.

Fletcher, L. N., B. E. Hesman, P. G. J. Irwin, K. H. Baines, T. W. Momary, A. Sanchez-Lavega, F. M. Flasar, P. L. Read, G. S. Orton, A. Simon-Miller, R. Hueso, G. L. Bjoraker, A. Mamoutkine, T. del Rio-Gaztelurrutia, J. M. Gomez, B. Buratti, R. N. Clark, P. D. Nicholson, C. Sotin, (2011), Thermal structure and dynamics of Saturn’s northern springtime disturbance, Science 332, no. 6036, 1413–1417, doi: 10.1126/science.1204774.

Fletcher, L. N., K. H. Baines, T. W. Momary, A. P. Showman, P. G. J. Irwin, G. S. Orton, M. Roos-Serote, C. Merlet, (2011a), Saturn's tropospheric composition and clouds from Cassini/VIMS 4.6-5.1 μm nightside spectroscopy, Icarus, 214, 2, 510-533, doi: 10.1016/j.icarus.2011.06.006.

Fletcher, L. N., B. E. Hesman, P. G. J. Irwin, K. H. Baines, T. W. Momary, A. Sanchez-Lavega, F. M. Flasar, et al., (2011b), Thermal structure and dynamics of Saturn's northern springtime disturbance, Science, 332, 6036, 1413–1417, doi: 10.1126/science.1204774.

Fletcher, L. N., R. K. Achterberg, T. K. Greathouse, G. S. Orton, B. J. Conrath, A. A. Simon-Miller, N. Teanby, S. Guerlet, P. G. J. Irwin, F. M. Flasar, (2010), Seasonal change on Saturn from Cassini/CIRS observations, 2004–2009, Icarus, 208, 1, 337-352, doi: 10.1016/j.icarus.2010.01.022.

Fletcher, L. N., G. S. Orton, N. A. Teanby, P. G. J. Irwin, (2009a), Phosphine on Jupiter and Saturn from Cassini/CIRS, Icarus, 202, 543–564, doi: 10.1016/j.icarus.2009.03.023.

Fletcher, L. N., G. S. Orton, N. A. Teanby, P. G. J. Irwin, G. L. Bjoraker, (2009b), Methane and its isotopologues on Saturn from Cassini/CIRS observations, Icarus, 199, 2, 351–367, doi: 10.1016/j.icarus.2008.09.019.

Fletcher, L. N., P. G. J. Irwin, G. S. Orton, N. A. Teanby, R. K. Achterberg, G. L. Bjoraker, P. L. Read, A. A. Simon-Miller, C. Howett, R. de Kok, N. Bowles, S. B. Calcutt, B. Hesman, F. M. Flasar, (2008), Temperature and composition of Saturn’s polar hot spots and hexagon, Science, 319, 5859, 79–81.

Fletcher, L. N., P. G. J. Irwin, N. A. Teanby, G. S. Orton, P. D. Parrish, S. B. Calcutt, N. Bowles, R. de Kok, C. Howett, F. W. Taylor, (2007a), The meridional phosphine distribution in Saturn's upper troposphere from Cassini/CIRS observations, Icarus, 188, 1, 72–88, doi: 10.1016/j.icarus.2006.10.029.

Fletcher, L. N., P. G. J. Irwin, N. A. Teanby, G. S. Orton, P. D. Parrish, R. de Kok, C. Howett, S. B. Calcutt, N. Bowles, F. W. Taylor, (2007b), Characterizing Saturn's vertical temperature structure from Cassini/CIRS, Icarus, 189, 2, 457–478, doi: 10.1016/j.icarus.2007.02.006.

Fouchet, T., T. K. Greathouse, A. Spiga, L. N. Fletcher, S. Guerlet, J. Leconte, G. S. Orton, (2016), Stratospheric aftermath of the 2010 Storm on Saturn as observed by the TEXES instrument. I. Temperature structure, Icarus, 277, 196–214, doi: 10.1016/j.icarus.2016.04.030.

Fouchet, T., J. I. Moses, B. J. Conrath, (2009), Saturn: Composition and chemistry, In Saturn from Cassini-Huygens, (eds.) M. K. Doughterty, L. W. Esposito, S. M. Krimigis, pp. 83–112, Springer, Dordrecht, Netherlands.

Fouchet, T., S. Guerlet, D. F. Strobel, A. A. Simon-Miller, B. Bézard, F. M. Flasar, (2008), An equatorial oscillation in Saturn’s middle atmosphere, Nature, 453, 7192, 200–202, doi: 10.1038/nature06912.

Fouchet, T., P. G. J. Irwin, P. Parrish, S. B. Calcutt, F. W. Taylor, C. A. Nixon, T. Owen, (2004a), Search for spatial variation in the jovian 15N/14N ratio from Cassini/CIRS observations, Icarus, 172, 1, 50–58, doi: 10.1016/j.icarus.2003.11.011.

Fouchet, T., G. Orton, P. G. J. Irwin, S. B. Calcutt, C. A. Nixon, (2004b), Upper limits on hydrogen halides in Jupiter from Cassini/CIRS observations, Icarus, 170, 237–241, doi: 10.1016/j.icarus.2004.03.013.

Friedson, A. J., and J. I. Moses, (2012), General circulation and transport in Saturn's upper troposphere and stratosphere, Icarus, 218, 2, 861–875, doi: 10.1016/j.icarus.2012.02.004.

Galanti, E., Y. Kaspi, Y. Miguel, T. Guillot, D. Durante, P. Racioppa, L. Iess, (2019), Saturn’s deep atmospheric flows revealed by the Cassini grand finale gravity measurements, Geophysical Research Letters, 46, 2, 616–624, doi: 10.1029/2018GL078087.

Galanti, E., and Y. Kaspi, (2017), Prediction for the flow-induced gravity field of Saturn: Implications for Cassini's Grand Finale, Astrophysical Journal Letters, 843, 2, doi: 10.3847/2041-8213/aa7aec.

Galanti, E., Y. Kaspi, E. Tziperman, (2017), A full, self-consistent treatment of thermal wind balance on oblate fluid planets, Journal of Fluid Mechanics, 810, 175–195, doi: 10.1017/jfm.2016.687.

Galanti, E., and Y. Kaspi, (2016), An adjoint-based method for the inversion of the Juno and Cassini gravity measurements into wind fields, The Astrophysical Journal, 820, 2, 91, doi: 10.3847/0004-637x/820/2/91.

Galperin, B., R. M. B. Young, S. Sukoriansky, N. Dikovskaya, P. L. Read, A. J. Lancaster, D. Armstrong, (2014), Cassini observations reveal a regime of zonostrophic macroturbulence on Jupiter, Icarus, 229, 295–320, doi: 10.1016/j.icarus.2013.08.030.

Garcia-Melendo, E., and A. Sanchez-Lavega, (2017), Shallow water simulations of Saturn's giant storms at different latitudes, Icarus, 286, 241–260, doi: 10.1016/j.icarus.2016.10.006.

Garcia-Melendo, E., R. Hueso, A. Sanchez-Lavega, J. Legarreta, T. del Rio-Gaztelurrutia, S. Perez-Hoyos, J. F. Sanz-Requena, (2013), Atmospheric dynamics of Saturn's 2010 giant storm, Nature Geoscience, 6, 7, 525–529, doi: 10.1038/ngeo1860.

Garcia-Melendo, E., Arregi, J., Rojas, J. F., Hueso, R., Barrado-Izagirre, N., Gomez-Forrellad, J. M., et al., (2011a), Dynamics of Jupiter's equatorial region at cloud top level from Cassini and HST images, Icarus, 211, 1242–1257, doi: 10.1016/j.icarus.2010.11.020.

Garcia-Melendo, E., S. Perez-Hoyos, A. Sanchez-Lavega, R. Hueso, (2011b), Saturn's zonal wind profile in 2004-2009 from Cassini ISS images and its long-term variability, Icarus, 215, 1, 62–74, doi: 10.1016/j.icarus.2011.07.005.

Garcia-Melendo, E., A. Sanchez-Lavega, J. Legarreta, S. Perez-Hoyos, R. Hueso, (2010), A strong high altitude narrow jet detected at Saturn's equator, Geophysical Research Letters, 37, doi: 10.1029/2010gl045434.

Garcia-Melendo, E., A. Sanchez-Lavega, J. F. Rojas, S. Perez-Hoyos, R. Hueso, (2009), Vertical shears in Saturn's eastward jets at cloud level, Icarus, 201, 2, 818–820, doi: 10.1016/j.icarus.2009.02.022.

Garcia-Melendo, E., A. Sanchez-Lavega, R. Hueso, (2007), Numerical models of Saturn's long-lived anticyclones, Icarus, 191, 2, 665–677, doi: 10.1016/j.icarus.2007.05.020.

Gerard, J. C., J. Gustin, W. R. Pryor, D. Grodent, B. Bonfond, A. Radioti, G. R. Gladstone, J. T. Clarke, J. D. Nichols, (2013), Remote sensing of the energy of auroral electrons in Saturn's atmosphere: Hubble and Cassini spectral observations, Icarus, 223, 1, 211–221, doi: 10.1016/j.icarus.2012.11.033.

Gerard, J. C., B. Hubert, J. Gustin, V. I. Shematovich, D. Bisikalo, G. R. Gladstone, L. W. Esposito, (2011), EUV spectroscopy of the Venus dayglow with UVIS on Cassini, Icarus, 211, 70–80. doi: 10.1016/j.icarus.2010.09.020.

Gierasch, P. J., A. P. Ingersoll, D. Banfield, S. P. Ewald, P. Helfenstein, A. Simon-Miller, A. Vasavada, H. H. Breneman, D. A. Senske, Galileo Imaging Team, (2000), Observation of moist convection in Jupiter's atmosphere, Nature, 403, 6770, 628–630, doi: 10.1038/35001017.

Giles, R. S., L. N. Fletcher, P. G. J. Irwin, (2015), Cloud structure and composition of Jupiter's troposphere from 5 μm Cassini VIMS spectroscopy, Icarus, 257, 457–470, doi: 10.1016/j.icarus.2015.05.030.

Gombosi, T. I., and A. P. Ingersoll, (2010), Saturn: atmosphere, ionosphere, and magnetosphere, Science, 327, 5972, 1476–1479, doi: 10.1126/science.1179119.

Guerlet, S., A. Spiga, M. Sylvestre, M. Indurain, T. Fouchet, J. Leconte, E. Millour, et al., (2014), Global climate modeling of Saturn's atmosphere. Part I: Evaluation of the radiative transfer model, Icarus, 238, 110-124, doi: 10.1016/j.icarus.2014.05.010.

Guerlet, S., T. Fouchet, B. Bezard, F. M. Flasar, A. A. Simon-Miller, (2011), Evolution of the equatorial oscillation in Saturn's stratosphere between 2005 and 2010 from Cassini/CIRS limb data analysis, Geophysical Research Letters, 38, doi: 10.1029/2011gl047192.

Guerlet, S., T. Fouchet, B. Bezard, J. I. Moses, L. N. Fletcher, A. A. Simon-Miller, F. M. Flasar, (2010), Meridional distribution of CH_3C_2H and C_4H_2 in Saturn's stratosphere from CIRS/Cassini limb and nadir observations, Icarus, 209, 2, 682-695, doi: 10.1016/j.icarus.2010.03.033.

Guerlet, S., T. Fouchet, B. Bezard, A. A. Simon-Miller, F. M. Flasar, (2009), Vertical and meridional distribution of ethane, acetylene and propane in Saturn's stratosphere from CIRS/Cassini limb observations, Icarus, 203, 214–232, doi: 10.1016/j.icarus.2009.04.002.

Guillot, T., Y. Miguel, B. Militzer, W. B. Hubbard, Y. Kaspi, E. Galanti, et al., (2018), A suppression of differential rotation in Jupiter's deep interior, Nature, 555(7695), 227, doi: 10.1038/nature25775.

Guillot, T., (1999), A comparison of the interiors of Jupiter and Saturn, Planetary and Space Science, 47, 10–11, 1183-1200, doi: 10.1016/s0032-0633(99)00043-4.

Gunnarson, J. L., K. M. Sayanagi, J. J. Blalock, L. N. Fletcher, A. P. Ingersoll, U. A. Dyudina, et al., (2018), Saturn's new ribbons: Cassini observations of planetary waves in Saturn's 42N atmospheric jet, Geophysical Research Letters, 45, 15, 7399–7408, doi: 10.1029/2018GL078156.

Gurnett, D. A., P. Zarka, R. Manning, W. S. Kurth, G. B. Hospodarsky, T. F. Averkamp, et al., (2001), Non-detection at Venus of high-frequency radio signals characteristic of terrestrial lightning, Nature, 409, 313–315, doi: 10.1038/35053009.

Gustin, J., D. Grodent, A. Radioti, W. Pryor, L. Lamy, J. Ajello, (2017), Statistical study of Saturn's auroral electron properties with Cassini/UVIS FUV spectral images, Icarus, 284, 264–283, doi: 10.1016/j.icarus.2016.11.017.

Gustin, J., I. Stewart, J. C. Gerard, L. Esposito, (2010), Characteristics of Saturn's FUV airglow from limb-viewing spectra obtained with Cassini-UVIS, Icarus, 210, 1, 270–283, doi: 10.1016/j.icarus.2010.06.031.

Gustin, J., J. C. Gerard, W. Pryor, P. D. Feldman, D. Grodent, G. Holsclaw, (2009), Characteristics of Saturn's polar atmosphere and auroral electrons derived from HST/STIS, FUSE and Cassini/UVIS spectra, Icarus, 200, 1, 176–187, doi: 10.1016/j.icarus.2008.11.013.

Hadjighasem, A., and G. Haller, (2016), Geodesic transport barriers in Jupiter's atmosphere: A video-based analysis, Siam Review, 58, 69–89, doi: 10.1137/140983665.

Hanel, R. A., B. J. Conrath, V. G. Kunde, J. C. Pearl, J. A. Pirraglia, (1983), Albedo, internal heat flux, and energy balance of Saturn, Icarus, 53, 2, 262–285, doi: 10.1016/0019-1035(83)90147-1.

Hanley, T. R., P. G. Steffes, B. M. Karpowicz, (2009), A new model of the hydrogen and helium-broadened microwave opacity of ammonia based on extensive laboratory measurements, Icarus, 202, 1, 316–335, doi: 10.1016/j.icarus.2009.02.002.

Hedman, M. M., and P. D. Nicholson, (2014), More kronoseismology with Saturn's rings, Monthly Notices of the Royal Astronomical Society, 444, 2, 1369–1388, doi: 10.1093/mnras/stu1503.

Hedman, M. M., and P. D. Nicholson, (2013), Kronoseismology: Using density waves in Saturn's C ring to probe the planet's interior, Astronomical Journal, 146, 1, doi: 10.1088/0004-6256/146/1/12.

Heimpel, M., T. Gastine, J. Wicht, (2016), Simulation of deep-seated zonal jets and shallow vortices in gas giant atmospheres, Nature Geoscience, 9, 19, doi: 10.1038/ngeo2601.

Heimpel, M., and J. Aurnou, (2007), Turbulent convection in rapidly rotating spherical shells: A model for equatorial and high latitude jets on Jupiter and Saturn, Icarus, 187, 2, 540–557, doi: 10.1016/j.icarus.2006.10.023.

Heimpel, M., J. Aurnou, J. Wicht, (2005), Simulation of equatorial and high-latitude jets on Jupiter in a deep convection model, Nature, 438, 193–196, doi: 10.1038/nature04208.

Helled, R., E. Galanti, Y. Kaspi, (2015), Saturn's fast spin determined from its gravitational field and oblateness, Nature, 520, 7546, 202-U140, doi: 10.1038/nature14278.

Helled, R., and T. Guillot, (2013), Interior models of Saturn: Including the uncertainties in shape and rotation, The Astrophysical Journal, 767, 2, 113, doi: 10.1088/0004-637x/767/2/113.

Hersant, F., D. Gautier, G. Tobie, J. I. Lunine, (2008), Interpretation of the carbon abundance in Saturn measured by Cassini, Planetary and Space Science, 56, 8, 1103–1111, doi: 10.1016/j.pss.2008.02.007.

Hesman, B. E., G. L. Bjoraker, P. V. Sada, R. K. Achterberg, D. E. Jennings, P. N. Romani, A. W. Lunsford, et al., (2012), Elusive ethylene detected in Saturn's northern storm region, The Astrophysical Journal, 760, 1, 24, doi: 10.1088/0004-637x/760/1/24.

Hesman, B. E., D. E. Jennings, P. V. Sada, G. L. Bjoraker, R. K. Achterberg, A. A. Simon-Miller, C. M. Anderson, et al., (2009), Saturn's latitudinal C_2H_2 and C_2H_6 abundance profiles from Cassini/CIRS and ground-based observations, Icarus, 202, 1, 249–259, doi: 10.1016/j.icarus.2009.02.013.

Hodosan, G., C. Helling, R. Asensio-Torres, I. Vorgul, P. B. Rimmer, (2016), Lightning climatology of exoplanets and brown dwarfs guided by Solar system data, Monthly Notices of the Royal Astronomical Society, 461, 4, 3927–3947, doi: 10.1093/mnras/stw1571.

Howett, C. J. A., P. G. J. Irwin, N. A. Teanby, A. Simon-Miller, S. B. Calcutt, L. N. Fletcher, R. de Kok, (2007), Meridional variations in stratospheric acetylene and ethane in the southern hemisphere of the saturnian atmosphere as determined from Cassini/CIRS measurements, Icarus, 190, 2, 556–572, doi: 10.1016/j.icarus.2007.03.009.

Hubbard, W. B., M. K. Dougherty, D. Gautier, R. Jacobson, (2009), The interior of Saturn, In Saturn from Cassini-Huygens,(eds.) M. K. Doughterty, L. W. Esposito, S. M. Krimigis, pp. 75–81, Springer, Dordrecht, Netherlands.

Hubert, B., J. C. Gerard, J. Gustin, D. V. Bisikalo, V. I. Shematovich, G. R. Gladstone, (2012), Cassini-UVIS observation of dayglow FUV emissions of carbon in the thermosphere of Venus, Icarus, 220, 635–646, doi: 10.1016/j.icarus.2012.06.002.

Hubert, B., J. C. Gerard, J. Gustin, V. I. Shematovich, D. V. Bisikalo, A. I. Stewart, G. R. Gladstone, (2010), UVIS observations of the FUV OI and CO 4P Venus dayglow during the Cassini flyby, Icarus, 207, 549–557, doi: 10.1016/j.icarus.2009.12.029.

Hue, V., T. K. Greathouse, T. Cavalie, M. Dobrijevic, F. Hersant, (2016), 2D photochemical modeling of Saturn's stratosphere. Part II: Feedback between composition and temperature, Icarus, 267, 334–343, doi: 10.1016/j.icarus.2015.12.007.

Hue, V., T. Cavalie, M. Dobrijevic, F. Hersant, T. K. Greathouse, (2015), 2D photochemical modeling of Saturn's stratosphere. Part I: Seasonal variation of atmospheric composition without meridional transport, Icarus, 257, 163–184, doi: 10.1016/j.icarus.2015.04.001.

Hueso, R., J. Legarreta, E. Garcia-Melendo, A. Sanchez-Lavega, S. Perez-Hoyos, (2009), The Jovian anticyclone BA II. Circulation and interaction with the zonal jets, Icarus, 203, 499–515, doi: 10.1016/j.icarus.2009.05.004.

Hurley, J., P. G. J. Irwin, L. N. Fletcher, J. I. Moses, B. Hesman, J. Sinclair, C. Merlet, (2012a), Observations of upper tropospheric acetylene on Saturn: No apparent correlation with 2000 km-sized thunderstorms, Planetary and Space Science, 65, 21–37. doi: 10.1016/j.pss.2011.12.026.

Hurley, J., L. N. Fletcher, P. G. J. Irwin, S. B. Calcutt, J. A. Sinclair, C. Merlet, (2012b), Latitudinal variation of upper tropospheric NH3 on Saturn derived from Cassini/CIRS far-infrared measurements, Planetary and Space Science, 73, 1, 347–363, doi: 10.1016/j.pss.2012.08.003.

Iess, L., B. Militzer, Y. Kaspi, P. Nicholson, D. Durante, P. Pacioppa, A. Anabtawi, E. Galanti, W. Hubbard, M. J. Mariani, P. Tortora, S. Wahl, M. Zannoni, (2019), Measurement and implications of Saturn's gravity field and ring mass, Science, doi: 10.1125/science.aat2965.

Ingersoll, A. P., S. P. Ewald, K. M. Sayanagi, J. J. Blalock, (2018), Saturn’s atmosphere at 1-10 kilometer resolution, Geophysical Research Letters, 45, 15, 7851–7856, doi: 10.1029/2018GL079255.

Ingersoll, A. P., V. Adumitroaie, M. D. Allison, S. Atreya, A. A. Bellotti, S. J. Bolton, et al., (2017), Implications of the ammonia distribution on Jupiter from 1 to 100 bars as measured by the Juno microwave radiometer, Geophysical Research Letters, 44, 15, 7676–7685, doi: 10.1002/2017GL074277.

Ingersoll, A. P., P. J. Gierasch, D. Banfield, A. R. Vasavada, Galileo Imaging Team, (2000), Moist convection as an energy source for the large-scale motions in Jupiter’s atmosphere, Nature, 403, 6770, 630–632, doi: 10.1038/35001021.

Ip, W. H., C. M. Liu, K. C. Pan, (2016), Transport and electrodynamical coupling of nano-grains ejected from the Saturnian rings and their possible ionospheric signatures, Icarus, 276, 163–169, doi: 10.1016/j.icarus.2016.04.004.

Irwin, P. G. J., P. Parrish, T. Fouchet, S. B. Calcutt, F. W. Taylor, A. A. Simon-Miller, C. A. Nixon, (2004), Retrievals of Jovian tropospheric phosphine from Cassini/CIRS, Icarus, 172, 37–49, doi: 10.1016/j.icarus.2003.09.027.

Jacobson, R. A., P. G. Antreasian, J. J. Bordi, K. E. Criddle, R. Ionasescu, J. B. Jones, R. A. Mackenzie, et al., (2006), The gravity field of the Saturnian system from satellite observations and spacecraft tracking data, Astronomical Journal, 132, 6, 2520–2526, doi: 10.1086/508812.

Janssen, M. A., A. P. Ingersoll, M. D. Allison, S. Gulkis, A. L. Laraia, K. H. Baines, S. G. Edgington, Y. Z. Anderson, K. Kelleher, F. A. Oyafuso, (2013), Saturn's thermal emission at 2.2-cm wavelength as imaged by the Cassini RADAR radiometer, Icarus, 226, 1, 522–535, doi: 10.1016/j.icarus.2013.06.008.

Jennings, D. E., F. M. Flasar, V. G. Kunde, C. A. Nixon, M. E. Segura, P. N. Romani, N. Gorius, et al., (2017), Composite infrared spectrometer (CIRS) on Cassini, Applied Optics, 56, 18, 5274-5294, doi: 10.1364/ao.56.005274.

Kaspi, Y., J. E. Davighi, E. Galanti, W. B. Hubbard, (2016), The gravitational signature of internal flows in giant planets: Comparing the thermal wind approach with barotropic potential-surface methods, Icarus, 276, 170–181, doi: 10.1016/j.icarus.2016.04.001.

Kaspi, Y., (2013), Inferring the depth of the zonal jets on Jupiter and Saturn from odd gravity harmonics, Geophysical Research Letters, 40, 4, 676–680, doi: 10.1029/2012gl053873.

Kim, S. J., C. K. Sim, D. W. Lee, R. Courtin, J. I. Moses, Y. C. Minh, (2012), The three-micron spectral feature of the Saturnian haze: Implications for the haze composition and formation process, Planetary and Space Science, 65, 122–129, doi: 10.1016/j.pss.2012.02.013.

Kim, S. J., and T. R. Geballe, (2005), The 2.9-4.2 micron spectrum of Saturn: Clouds and CH4, PH3, and NH3, Icarus, 179, 2, 449–458, doi: 10.1016/j.icarus.2005.06.015.

Koskinen, T. T., and S. Guerlet, (2018), Atmospheric structure and helium abundance on Saturn from Cassini/UVIS and CIRS observations, Icarus, 307, 161–171, doi: 10.1016/j.icarus.2018.02.020.

Koskinen, T. T., J. I. Moses, R. A. West, S. Guerlet, A. Jouchoux, (2016), The detection of benzene in Saturn's upper atmosphere, Geophysical Research Letters, 43, 15, 7895–7901, doi: 10.1002/2016gl070000.

Koskinen, T. T., B. R. Sandel, R. V. Yelle, D. F. Strobel, I. C. F. Müeller-Wodarg, J. T. Erwin, (2015), Saturn's variable thermosphere from Cassini/UVIS occultations, Icarus, 260, 174-189, doi: 10.1016/j.icarus.2015.07.008.

Koskinen, T. T., B. R. Sandel, R. V. Yelle, F. J. Capalbo, G. M. Holsclaw, W. E. McClintock, S. Edgington, (2013), The density and temperature structure near the exobase of Saturn from Cassini UVIS solar occultations, Icarus, 226, 2, 1318-1330, doi: 10.1016/j.icarus.2013.07.037.

Lainey, V., R. A. Jacobson, R. Tajeddine, N. J. Cooper, C. Murray, V. Robert, et al., (2017), New constraints on Saturn’s interior from Cassini astrometric data, Icarus, 281, 286–296, doi: 10.1016/j.icarus.2016.07.014.

Lamy, L., R. Prange, W. Pryor, J. Gustin, S. V. Badman, H. Melin, T. Stallard, D. G. Mitchell, P. C. Brandt, (2013), Multispectral simultaneous diagnosis of Saturn's aurorae throughout a planetary rotation, Journal of Geophysical Research-Space Physics, 118, 8, 4817–4843, doi: 10.1002/jgra.50404.

Lamy, L., B. Cecconi, R. Prange, P. Zarka, J. D. Nichols, J. T. Clarke, (2009), An auroral oval at the footprint of Saturn's kilometric radio sources, colocated with the UV aurorae, Journal of Geophysical Research-Space Physics, 114, doi: 10.1029/2009ja014401.

Laraia, A. L., A. P. Ingersoll, M. A. Janssen, S. Gulkis, F. Oyafuso, M. Allison, (2013), Analysis of Saturn's thermal emission at 2.2-cm wavelength: Spatial distribution of ammonia vapor, Icarus, 226, 1, 641–654, doi: 10.1016/j.icarus.2013.06.017.

Lellouch, E., B. Bezard, D. F. Strobel, G. L. Bjoraker, F. M. Flasar, P. N. Romani, (2006), On the HCN and CO2 abundance and distribution in Jupiter's stratosphere. Icarus, 184, 478–497, doi: 10.1016/j.icarus.2006.05.018.

Li, C., and A. P. Ingersoll, (2015), Moist convection in hydrogen atmospheres and the frequency of Saturn's giant storms, Nature Geoscience, 8, 5, 398–403, doi: 10.1038/ngeo2405.

Li, L. M., X. Jiang, H. J. Trammell, Y. F. Pan, J. Hernandez, B. J. Conrath, et al., (2015), Saturn's giant storm and global radiant energy, Geophysical Research Letters, 42, 2144–2148, doi: 10.1002/2015gl063763.

Li, L. M., R. K. Achterberg, B. J. Conrath, P. J. Gierasch, M. A. Smith, A. A. Simon-Miller, C. A. Nixon, et al., (2013), Strong temporal variation over one saturnian year: From Voyager to Cassini, Scientific Reports, 3, doi: 10.1038/srep02410.

Li, L. M., K. H. Baines, M. A. Smith, R. A. West, S. Perez-Hoyos, H. J. Trammell, et al., (2012), Emitted power of Jupiter based on Cassini CIRS and VIMS observations, Journal of Geophysical Research-Planets, 117, doi: 10.1029/2012je004191.

Li, L. M., X. Jiang, A. P. Ingersoll, A. D. Del Genio, C. C. Porco, R. A. West, A. R. Vasavada, et al., (2011), Equatorial winds on Saturn and the stratospheric oscillation, Nature Geoscience, 4, 11, 750–752, doi: 10.1038/ngeo1292.

Li, L. M., B.J. Conrath, P. J. Gierasch, R. K. Achterberg, C. A. Nixon, A. A. Simon-Miller, F. M. Flasar, et al., (2010), Saturn's emitted power, Journal of Geophysical Research-Planets, 115, doi: 10.1029/2010je003631.

Li, L. M., P. J. Gierasch, R. K. Achterberg, B. J. Conrath, F. M. Flasar, A. R. Vasavada, A. P. Ingersoll, D. Banfield, A. A. Simon-Miller, L. N. Fletcher, (2008), Strong jet and a new thermal wave in Saturn's equatorial stratosphere, Geophysical Research Letters, 35, 23, doi: 10.1029/2008gl035515.

Li, L. M., A. P. Ingersoll, X. L. Huang, (2006a), Interaction of moist convection with zonal jets on Jupiter and Saturn, Icarus, 180, 113–123. doi: 10.1016/j.icarus.2005.08.016.

Li, L. M., A. P. Ingersoll, A. R. Vasavada, A. A. Simon-Miller, R. K. Achterberg, S. P. Ewald, et al., (2006b), Waves in Jupiter's atmosphere observed by the Cassini ISS and CIRS instruments, Icarus, 185, 416–429, doi: 10.1016/j.icarus.2006.08.005.

Li, L. M., A. P. Ingersoll, A. R. Vasavada, A. A. Simon-Miller, A. D. Del Genio, S. P. Ewald, et al., (2006c), Vertical wind shear on Jupiter from Cassini images, Journal of Geophysical Research-Planets, 111, doi: 10.1029/2005je002556.

Li, L. M., A. P. Ingersoll, A. R. Vasavada, C. C. Porco, A. D. Del Genio, S. P. Ewald, (2004), Life cycles of spots on Jupiter from Cassini images, Icarus, 172, 9–23, doi: 10.1016/j.icarus.2003.10.015.

Liang, M. C., R. L. Shia, A. Y. T. Lee, M. Allen, A. J. Friedson, Y. L. Yung, (2005), Meridional transport in the stratosphere of Jupiter, Astrophysical Journal, 635, L177–L180, doi: 10.1086/499624.

Liao, X. H., T. H. Feng, K. K. Zhang, (2007), On the saturation and temporal variation of mean zonal flows: An implication for equatorial jets on giant planets, Astrophysical Journal, 666, 1, L41-L44, doi: 10.1086/521526.

Little, B., C. D. Anger, A. P. Ingersoll, A. R. Vasavada, D. A. Senske, H. H. Breneman, W. J. Borucki, S. S. I. T. Galileo, (1999), Galileo images of lightning on Jupiter, Icarus, 142, 2, 306-323, doi: 10.1006/icar.1999.6195.

Liu, J. J., and T. Schneider (2015), Scaling of off-equatorial jets in giant planet atmospheres, Journal of the Atmospheric Sciences, 72, 1, 389–408, doi: 10.1175/jas-d-13-0391.1.

Liu, J. J., T. Schneider, L. N. Fletcher, (2014), Constraining the depth of Saturn's zonal winds by measuring thermal and gravitational signals, Icarus, 239, 260–272, doi: 10.1016/j.icarus.2014.05.036.

Lorenz, R. D., C. Elachi, R. D. West, W. T. K. Johnson, M. A. Janssen, M. Moghaddam, et al., (2001), Cassini Radio Detection and Ranging (RADAR): Earth and Venus observations. Journal of Geophysical Research-Space Physics, 106, 30271–30279, doi: 10.1029/2001ja900035.

Lunine, J., (2011), Chemistry of the Solar System revealed in the interiors of the giant planets, Proceedings of the International Astronomical Union, The Molecular Universe, 7(S280), 249–260, doi: 10.1017/S1743921311025026.

Mankovich, C., M. S. Marley, J. J. Fortney, N. Movshovitz, (2019), Cassini ring seismology as a probe of Saturn’s interior. I. Rigid Rotation. Astrophysical Journal, 871, 1, 1, doi: 10.3847/1538-4357/aaf798.

Matcheva, K. I., B. J. Conrath, P. J. Gierasch, F. M. Flasar, (2005), The cloud structure of the Jovian atmosphere as seen by the Cassini/CIRS experiment. Icarus, 179, 432–448. doi: 10.1016/j.icarus.2005.06.020.

Mayorga, L. C., J. Jackiewicz, K. Rages, R. A. West, B. Knowles, N. Lewis, M. S. Marley, (2016), Jupiter’s phase variations from Cassini: A testbed for future direct-imaging missions, The Astronomical Journal, 152, 209, doi: 10.3847/0004-6256/152/6/209.

Melin, H., S. V. Badman, T. S. Stallard, Stanley William Herbert Cowley, U. Dyudina, J. D. Nichols, G. Provan, et al., (2016), Simultaneous multi-scale and multi-instrument observations of Saturn's aurorae during the 2013 observing campaign, Icarus, 263, 56–74, doi: 10.1016/j.icarus.2015.08.021.

Melin, H., T. Stallard, S. Miller, J. Gustin, M. Galand, S. V. Badman, W. R. Pryor, J. O'Donoghue, R. H. Brown, K. H. Baines, (2011), Simultaneous Cassini VIMS and UVIS observations of Saturn's southern aurora: Comparing emissions from H, H-2 and H-3(+) at a high spatial resolution, Geophysical Research Letters, 38, doi: 10.1029/2011gl048457.

Militzer, B., S. Wahl, W. B. Hubbard, (2019), Models of Saturn's interior constructed with an accelerated concentric Maclaurin spheroid method, Astrophysical Journal 879, 78.

Morales-Juberias, R., K. M. Sayanagi, A. A. Simon, L. N. Fletcher, R. G. Cosentino, (2015), Meandering shallow atmospheric jet as a model of saturn's north-polar hexagon, Astrophysical Journal Letters, 806, 1, doi: 10.1088/2041-8205/806/1/l18.

Morales-Juberias, R., and T. E. Dowling, (2013), Jupiter's Great Red Spot: Fine-scale matches of model vorticity patterns to prevailing cloud patterns, Icarus, 225, 216–227, doi: 10.1016/j.icarus.2013.03.026.

Morales-Juberias, R., K. M. Sayanagi, T. E. Dowling, A. P. Ingersoll, (2011), Emergence of polar-jet polygons from jet instabilities in a Saturn model, Icarus, 211, 2, 1284–1293, doi: 10.1016/j.icarus.2010.11.006.

Moses, J. I., E. S. Armstrong, L. N. Fletcher, A. J. Friedson, P. G. J. Irwin, J. A. Sinclair, B. E. Hesman, (2015), Evolution of stratospheric chemistry in the Saturn storm beacon region, Icarus, 261, 149–168, doi: 10.1016/j.icarus.2015.08.012.

Moses, J. I., B. Bezard, E. Lellouch, G. R. Gladstone, H. Feuchtgruber, M. Allen, (2000a), Photochemistry of Saturn's atmosphere - I. Hydrocarbon chemistry and comparisons with ISO observations, Icarus, 143, 244–298, doi: 10.1006/icar.1999.6270.

Moses, J. I., E. Lellouch, B. Bezard, G. R. Gladstone, H. Feuchtgruber, M. Allen, (2000b), Photochemistry of Saturn's atmosphere II. Effects of an influx of external oxygen, Icarus, 145, 1, 166–202, doi: 10.1006/icar.1999.6320.

Mousis, O., Y. Alibert, W. Benz, (2006), Saturn's internal structure and carbon enrichment, Astronomy & Astrophysics, 449, 1, 411–415, doi: 10.1051/0004-6361:20054224.

Müeller-Wodarg, I. C. F., T. T. Koskinen, L. Moore, J. Serigano, R. V. Yelle, S. Horst, et al., (2019), Atmospheric Waves and Their Possible Effect on the Thermal Structure of Saturn's Thermosphere, Geophysical Research Letters, 46, 5, 2372–2380, doi: 10.1029/2018GL081124.

Nagy, A. F., A. J. Kliore, M. Mendillo, S. Miller, L. Moore, J. I. Moses, I. Müeller-Wodarg, D. Shemansky, (2009), Upper atmosphere and ionosphere of Saturn, In Saturn from Cassini-Huygens, (eds.) M. K. Doughterty, L. W. Esposito, S. M. Krimigis, pp. 181–201, Springer, Dordrecht, Netherlands.

NASA/JPL/Southwest Research Institute, PhotoJournal, (2001), Jupiter Polar Winds Movie, PIA03452, https://photojournal.jpl.nasa.gov/catalog/PIA03452

NASA/JPL/Southwest Research Institute, PhotoJournal, (2001), Jupiter Polar Winds Movie Blownup, PIA03453, https://photojournal.jpl.nasa.gov/catalog/PIA03453

NASA/JPL/Southwest Research Institute, PhotoJournal, (2001), 70 Days of Jupiter Winds, PIA03454, https://photojournal.jpl.nasa.gov/catalog/PIA03454

Nettelmann, N., R. Pustow, R. Redmer, (2013), Saturn layered structure and homogeneous evolution models with different EOSs, Icarus, 225, 1, 548–557, doi: 10.1016/j.icarus.2013.04.018.

Nixon, C. A., R. K. Achterberg, P. N. Romani, M. Allen, X. Zhang, N. A. Teanby, et al., (2010), Abundances of Jupiter's trace hydrocarbons from Voyager and Cassini. Planetary and Space Science, 58, 1667–1680, doi: 10.1016/j.pss.010.05.008.

Nixon, C. A., R. K. Achterberg, B. J. Conrath, P. G. J. Irwin, N. A. Teanby, T. Fouchet, et al., (2007), Meridional variations of C_2H_2 and C_2H_6 in Jupiter's atmosphere from Cassini CIRS infrared spectra, Icarus, 188, 47–71, doi: 10.1016/j.icarus.2006.11.016.

O'Donoghue, J., L. Moore, J. E. P. Connerney, H. Melin, T. S. Stallard, S. Miller, K. H. Baines, (2017), Redetection of the Ionospheric H-3(+) Signature of Saturn's ring rain, Geophysical Research Letters, 44, 11762–11769, doi.org/10.1002/2017gl075932.

O'Donoghue, J., T. S. Stallard, H. Melin, S. W. H. Cowley, S. V. Badman, L. Moore, S. Miller, C. Tao, K. H. Baines, J. S. D. Blake, (2014), Conjugate observations of Saturn's northern and southern H3+ aurorae, Icarus, 229, 214–220, doi: 10.1016/j.icarus.2013.11.009.

O'Donoghue, J., T. S. Stallard, H. Melin, G. H. Jones, S. W. H. Cowley, S. Miller, et al., (2013), The domination of Saturn's low-latitude ionosphere by ring rain, Nature, 496, 7444, 193–195, doi: 10.1038/nature12049.

O'Neill, M. E., K. A. Emanuel, G. R. Flierl, (2016), Weak jets and strong cyclones: shallow water modeling of giant planet polar caps, Journal of the Atmospheric Sciences, 73, 1841–1855, doi: 10.1175/JAS-D-15-0314.1.

O'Neill, M. E., K. A. Emanuel, G. R. Flierl, (2015), Polar vortex formation in giant-planet atmospheres dues to moist convection, Nature Geoscience, 8, 7, 523-U118, doi: 10.1038/ngeo2459.

Oliva, F., A. Adriani, M. L. Moriconi, G. L. Liberti, E. D'Aversa, G. Filacchione, (2016), Clouds and hazes vertical structure of a Saturn's giant vortex from Cassini/VIMS-V data analysis, Icarus, 278, 215–237, doi: 10.1016/j.icarus.2016.06.021.

Ordonez-Etxeberria, I., R. Hueso, A. Sanchez-Lavega, S. Perez-Hoyos, (2016), Spatial distribution of Jovian clouds, hazes and colors from Cassini ISS multi-spectral images, Icarus, 267, 34–50, doi: 10.1016/j.icarus.2015.12.008.

Owen, T., and T. Encrenaz, (2003), Element abundances and isotope ratios in the Giant Planets and Titan, Space Science Reviews, 106, 1–4, 121–138, doi: 10.1023/a:1024633603624.

Parkinson, C. D., A. I. F. Stewart, A. S. Wong, Y. L. Yung, J. M. Ajello, (2006), Enhanced transport in the polar mesosphere of Jupiter: Evidence from Cassini UVIS helium 584 angstrom airglow, Journal of Geophysical Research-Planets, 111, doi: 10.1029/2005je002539.

Perez-Hoyos, S., J. F. Sanz-Requena, A. Sanchez-Lavega, P. G. J. Irwin, A. Smith, (2016), Saturn's tropospheric particles phase function and spatial distribution from Cassini ISS 2010-11 observations, Icarus, 277, 1–18, doi: 10.1016/j.icarus.2016.04.022.

Perez-Hoyos, S., and A. Sanchez-Lavega, (2006), On the vertical wind shear of Saturn's Equatorial Jet at cloud level, Icarus, 180, 1, 161–175, doi: 10.1016/j.icarus.2005.07.011.

Perez-Hoyos, S., A. Sanchez-Lavega, R. G. French, (2006), Short-term changes in the belt/zone structure of Saturn's Southern Hemisphere (1996-2004), Astronomy & Astrophysics, 460, 2, 641–645, doi: 10.1051/0004-6361:20065972.

Pierel, J. D. R., C. A. Nixon, E. Lellouch, L. N. Fletcher, G. L. Bjoraker, R. K. Achterberg, B. Bezard, B. E. Hesman, P. G. J. Irwin, F. M. Flasar, (2017), D/H Ratios on Saturn and Jupiter from Cassini CIRS, Astronomical Journal, 154, 5, doi: 10.3847/1538-3881/aa899d.

Porco, C. C., E. Baker, J. Barbara, K. Beurle, A. Brahic, J. A. Burns, S. Charnoz, et al., (2005), Cassini Imaging Science: Initial results on Saturn's atmosphere, Science, 307, 5713, 1243–1247, doi: 10.1126/science.1107691.

Porco, C. C., R. A. West, A. McEwen, A. D. Del Genio, A. P. Ingersoll, P. Thomas, et al., (2003), Cassini imaging of Jupiter's atmosphere, satellites, and rings, Science, 299, 1541–1547, doi: 10.1126/science.1079462.

Pryor, W. R., A. M. Rymer, D. G. Mitchell, T. W. Hill, D. T. Young, J. Saur, G. H. Jones, et al., (2011), The auroral footprint of Enceladus on Saturn, Nature, 472(7343), 331–333, doi: 10.1038/nature09928.

Read, P. L., B. J. Conrath, L. N. Fletcher, P. J. Gierasch, A. A. Simon-Miller, L. C. Zuchowski, (2009a), Mapping potential vorticity dynamics on Saturn: Zonal mean circulation from Cassini and Voyager data, Planetary and Space Science, 57, 1682–1698, doi: 10.1016/j.pss.2009.03.004.

Read, P. L., T. E. Dowling, G. Schubert, (2009b), Saturn's rotation period from its atmospheric planetary-wave configuration, Nature, 460, 7255, 608–610, doi: 10.1038/nature08194.

Read, P. L., P. J. Gierasch, B. J. Conrath, A. Simon-Miller, T. Fouchet, Y. H. Yamazaki, (2006), Mapping potential-vorticity dynamics on Jupiter. I: Zonal-mean circulation from Cassini and Voyager 1 data, Quarterly Journal of the Royal Meteorological Society, 132, 1577–1603, doi: 10.1256/qj.05.34.

Rogers, J. H., L. N. Fletcher, G. Adamoli, M. Jacquesson, M. Vedovato, G. S. Orton, (2016), A dispersive wave pattern on Jupiter's fastest retrograde jet at 20°S, Icarus, 277, 354–369, doi: 10.1016/j.icarus.2016.05.028.

Rogers, J. H., H. J. Mettig, A. Cidadao, P. C. Sherrod, D. Peach, (2006), Merging circulations on Jupiter: Observed differences between cyclonic and anticyclonic mergers, Icarus, 185, 244–257, doi: 10.1016/j.icarus.2006.05.022.

Roman, M. T., D. Banfield, P. J. Gierasch, (2013), Saturn's cloud structure inferred from Cassini ISS, Icarus, 225, 1, 93–110, doi: 10.1016/j.icarus.2013.03.015.

Salyk, C., A. P. Ingersoll, J. Lorre, A. Vasavada, A. D. Del Genio, (2006), Interaction between eddies and mean flow in Jupiter's atmosphere: Analysis of Cassini imaging data, Icarus, 185, 430–442, doi: 10.1016/j.icarus.2006.08.007.

Sánchez-Lavega, A., G. Fischer, L. Fletcher, E. García-Melendo, B. Hesman, S. Pérez-Hoyos, L. Sromovsky, (2018), The Great Saturn Storm of 2010–2011, In Saturn in the 21st Century, (eds.) K. Baines, F. Flasar, N. Krupp, T. Stallard, Cambridge Planetary Science, Cambridge University Press, pp. 377–416, doi: 10.1017/9781316227220.013.

Sanchez-Lavega, A., E. García-Melendo, S. Perez-Hoyos, R. Hueso, M. H. Wong, A. Simon, J. F. Sanz-Requena, et al., (2016), An enduring rapidly moving storm as a guide to Saturn's Equatorial jet's complex structure, Nature Communications, 7, doi: 10.1038/ncomms13262.

Sanchez-Lavega, A., T. del Río-Gaztelurrutia, R. Hueso, S. Pérez-Hoyos, E. García-Melendo, A. Antuñano, I. Mendikoa, et al., (2014), The long- term steady motion of Saturn's hexagon and the stability of its enclosed jet stream under seasonal changes, Geophysical Research Letters, 41, 5, 1425–1431, doi: 10.1002/2013gl059078.

Sanchez-Lavega, A., T. del Río-Gaztelurrutia, M. Delcroix, J. J. Legarreta, J. M. Gómez-Forrellad, R. Hueso, E. García-Melendo, et al., (2012), Ground-based observations of the long-term evolution and death of Saturn's 2010 Great White Spot, Icarus, 220, 2, 561–576, doi: 10.1016/j.icarus.2012.05.033.

Sanchez-Lavega, A., T. del Río-Gaztelurrutia, R. Hueso, J. M. Gómez-Forrellad, J. F. Sanz-Requena, J. Legarreta, E. García-Melendo, et al., (2011), Deep winds beneath Saturn's upper clouds from a seasonal long-lived planetary-scale storm, Nature, 475, 7354, 71–74, doi: 10.1038/nature10203.

Sanchez-Lavega, A., R. Hueso, S. Perez-Hoyos, (2007), The three-dimensional structure of Saturn's equatorial jet at cloud level, Icarus, 187, 2, 510–519, doi: 10.1016/j.icarus.2006.10.022.

Sanchez-Lavega, A., R. Hueso, S. Perez-Hoyos, J. F. Rojas, (2006), A strong vortex in Saturn's South Pole, Icarus, 184, 2, 524–531, doi: 10.1016/j.icarus.2006.05.020.

Sanchez-Lavega, A., R. Hueso, S. Perez-Hoyos, J. F. Rojas, R. G. French, (2004), Saturn's cloud morphology and zonal winds before the Cassini encounter, Icarus, 170, 2, 519–523, doi: 10.1016/j.icarus.2004.05.002.

Sanchez-Lavega, A., J. F. Rojas, P. V. Sada, P. V. Sada, (2000), Saturn's zonal winds at cloud level, Icarus, 147, 2, 405–420, doi: 10.1006/icar.2000.6449.

Sanchez-Lavega, A., (1994), Saturn's Great White Spots, Chaos: An Interdisciplinary Journal of Nonlinear Science, 4, 2, 341–353, doi: 10.1063/1.166012.

Sanz-Requena J. F., S. Pérez-Hoyos, A. Sánchez-Lavega, T. del Rio-Gaztelurrutia, P. G. J. Irwin, (2019), Hazes and clouds in a singular triple vortex in Saturn's atmosphere from HST/WFC3 multispectral imaging, Icarus, 333, 22–36, doi: 10.1016/j.icarus.2019.05.037.

Sanz-Requena J. F. , S. Pérez-Hoyos, A. Sánchez-Lavega, A. Antuñano, P. G. J. Irwin, (2018), Haze and cloud structure of Saturn’s north pole and hexagon wave from Cassini/ISS imaging, Icarus, 305, 284–300, doi.org/10.1016/j.icarus.2017.12.043.

Sato, T. M., T. Satoh, Y. Kasaba, (2013), Retrieval of Jovian cloud structure from the Cassini ISS limb-darkening data I. Continuum scattering phase functions for cloud and haze in the South Tropical Zone, Icarus, 222, 100–121, doi: 10.1016/j.icarus.2012.09.035.

Sayanagi, K. M., K. H. Baines, U. Dyudina, L. N. Fletcher, A. Sánchez-Lavega, R. A. West, (2018), Saturn’s polar atmosphere, In Saturn in the 21st Century, (eds.) K. H. Baines, F. M. Flasar, N. Krupp, T. Stallard, Cambridge University Press, pp. 337–376, doi: 10.1017/9781316227220.012.

Sayanagi, K. M., J. J. Blalock, U. A. Dyudina, S. P. Ewald, A. P. Ingersoll, (2017), Cassini ISS observation of Saturn's north polar vortex and comparison to the south polar vortex, Icarus, 285, 68–82, doi: 10.1016/j.icarus.2016.12.011.

Sayanagi, K. M., U. A. Dyudina, S. P. Ewald, G. D. Muro, A. P. Ingersoll, (2014), Cassini ISS observation of Saturn's String of Pearls, Icarus, 229, 170–180, doi: 10.1016/j.icarus.2013.10.032.

Sayanagi, K. M., U. A. Dyudina, S. P. Ewald, G. Fischer, A. P. Ingersoll, W. S. Kurth, G. D. Muro, C. C. Porco, R. A. West, (2013), Dynamics of Saturn's great storm of 2010–2011 from Cassini ISS and RPWS, Icarus, 223, 1, 460–478, doi: 10.1016/j.icarus.2012.12.013.

Sayanagi, K. M., R. Morales-Juberias, A. P. Ingersoll, (2010), Saturn's northern hemisphere ribbon: Simulations and comparison with the meandering Gulf Stream, Journal of the Atmospheric Sciences, 67, 2658–2678, doi: 10.1175/2010jas3315.1.

Sayanagi, K. M., and A. P. Showman, (2007), Effects of a large convective storm on Saturn's equatorial jet, Icarus, 187, 2, 520–539, doi: 10.1016/j.icarus.2006.10.020.

Schinder, P. J., F. M. Flasar, E. A. Marouf, R. G. French, A. Anabtawi, E. Barbinis, A. J. Kliore, (2015), A numerical technique for two-way radio occultations by oblate axisymmetric atmospheres with zonal winds, Radio Science, 50, 7, 712–727, doi: 10.1002/2015rs005690.

Schinder, P. J., F. M. Flasar, E. A. Marouf, R. G. French, C. A. McGhee, A. J. Kliore, N. J. Rappaport, E. Barbinis, D. Fleischman, and A. Anabtawi, (2011), Saturn's equatorial oscillation: Evidence of descending thermal structure from Cassini radio occultations, Geophysical Research Letters, 38, doi: 10.1029/2011gl047191.

Schneider, T., and J. Liu, (2009), Formation of jets and equatorial superrotation on Jupiter, Journal of the Atmospheric Sciences, 66, 3, 579–601, doi.org/10.1175/2008JAS2798.1.

Shemansky, D. E., and X. Liu, (2012), Saturn upper atmospheric structure from Cassini EUV and FUV occultations, Canadian Journal of Physics, 90, 8, 817–831, doi: 10.1139/p2012-036.

Shetty, S., and P. S. Marcus, (2010), Changes in Jupiter's Great Red Spot (1979-2006) and Oval BA (2000-2006), Icarus, 210, 182–201, doi: 10.1016/j.icarus.2010.06.026.

Showman, A. P., A. P. Ingersoll, R. Achterberg, Y. Kaspi, (2018), The global atmospheric circulation of Saturn, In Saturn in the 21st Century, (eds.) K. H. Baines, F. M. Flasar, N. Krupp, T. Stallard, Cambridge University Press, pp. 295–336, doi: 10.1017/9781316227220.011.

Showman, A. P., and I. de Pater, (2005), Dynamical implications of Jupiter's tropospheric ammonia abundance, Icarus, 174, 1, 192–204, doi.org/10.1016/j.icarus.2004.10.004.

Simon, A. A., L. Li, D. C. Reuter, (2015), Small-scale waves on Jupiter: A reanalysis of New Horizons, Voyager, and Galileo data, Geophysical Research Letters, 42, 8, 2612–2618, doi: 10.1002/2015GL063433.

Simon-Miller, A. A., J. H. Rogers, P. J. Gierasch, D. Choi, M. D. Allison, G. Adamoli, H. J. Mettig, (2012), Longitudinal variation and waves in Jupiter's south equatorial wind jet, Icarus, 218, 817–830, doi: 10.1016/j.icarus.2012.01.022.

Simon-Miller, A. A., and P. J. Gierasch, (2010), On the long-term variability of Jupiter's winds and brightness as observed from Hubble, Icarus, 210, 258–269. doi: 10.1016/j.icarus.2010.06.020.

Simon-Miller, A. A., B. W. Poston, G. S. Orton, B. Fisher, (2007), Wind variations in Jupiter's equatorial atmosphere: A QQO counterpart?, Icarus, 186, 192–203. doi: 10.1016/j.icarus.2006.08.009.

Simon-Miller, A. A., B. J. Conrath, P. J. Gierasch, G. S. Orton, R. K. Achterberg, F. M. Flasar, B. M. Fisher, (2006), Jupiter's atmospheric temperatures: From Voyager IRIS to Cassini CIRS, Icarus, 180, 98–112. doi: 10.1016/j.icarus.2005.07.019.

Sinclair, J. A., G. S. Orton, T. K. Greathouse, L. N. Fletcher, J. I. Moses, V. Hue, P. G. J. Irwin, (2018), Jupiter's auroral-related stratospheric heating and chemistry II: Analysis of IRTF-TEXES spectra measured in December 2014, Icarus, 300, 305–326, doi: 10.1016/j.icarus.2017.09.016.

Sinclair, J. A., G. S. Orton, T. K. Greathouse, L. N. Fletcher, J. I. Moses, V. Hue, P. G. J. Irwin, (2017), Jupiter's auroral-related stratospheric heating and chemistry I: Analysis of Voyager-IRIS and Cassini-CIRS spectra, Icarus, 292, 182–207, doi: 10.1016/j.icarus.2016.12.033.

Sinclair, J. A., P. G. J. Irwin, L. N. Fletcher, T. Greathouse, S. Guerlet, J. Hurley, C. Merlet, (2014), From Voyager-IRIS to Cassini-CIRS: Interannual variability in Saturn's stratosphere?, Icarus, 233, 281–292, doi: 10.1016/j.icarus.2014.02.009.

Sinclair, J. A., P. G. J. Irwin, L. N. Fletcher, J. I. Moses, T. K. Greathouse, A. J. Friedson, B. Hesman, J. Hurley, C. Merlet, (2013), Seasonal variations of temperature, acetylene and ethane in Saturn's atmosphere from 2005 to 2010, as observed by Cassini-CIRS, Icarus, 225, 1, 257–271, doi: 10.1016/j.icarus.2013.03.011.

Smith, B. A., L. Soderblom, R. M. Batson, P. M. Bridges, J. L. Inge, H. Masursky, E. Shoemaker, R. F. Beebe, J. Boyce, G. Briggs, A. Bunker, S. A. Collins, C. Hansen, T. V. Johnson, J. L. Mitchell, R. J. Terrile, A. F. Cook, J. N. Cuzzi, J. B. Pollack, G. E. Danielson, A. P. Ingersoll, M. E. Davies, G. E. Hunt, D. Morrison, T. Owen, C. Sagan, J. Veverka, R. Strom, V. E. Suomi, (1982), A new look at the Saturn system: The Voyager 2 Images, Science, 215, 4532, 504–537, doi.org/10.1126/science.215.4532.504.

Sromovsky, L. A., K. H. Baines, P. M. Fry, (2019), Saturn's south polar cloud composition and structure inferred from 2006 Cassini/VIMS spectra and ISS images, Icarus in press, doi: 10.1016/j.icarus.2019.113398.

Sromovsky, L. A. and P. M. Fry, (2019), Interpretation of shadows and antishadows on Saturn and the evidence against south polar eyewalls, Icarus in press, doi: 10.1016/j.icarus.2019.113399.

Sromovsky, L. A., K. H. Baines, P. M. Fry, (2018), Models of bright storm clouds and related dark ovals in Saturn's Storm Alley as constrained by 2008 Cassini/VIMS spectra, Icarus 302, 360.

Sromovsky, L. A., and P. M. Fry, (2018), Composition and structure of fresh ammonia clouds on Jupiter based on quantitative analysis of Galileo/NIMS and New Horizons/LEISA spectra, Icarus 307, 347.

Sromovsky, L. A., K. H. Baines, P. M. Fry, R. W. Carlson, (2017), A possibly universal red chromophore for modeling color variations on Jupiter, Icarus, 291, 232–244, doi: 10.1016/j.icarus.2016.12.014.

Sromovsky, L. A., K. H. Baines, P. M. Fry, T. W. Momary, (2016), Cloud clearing in the wake of Saturn's Great Storm of 2010-2011 and suggested new constraints on Saturn's He/H2 ratio, Icarus, 276, 141–162, doi: 10.1016/j.icarus.2016.04.031.

Sromovsky, L. A., K. H. Baines, P. M. Fry, (2013), Saturn's Great Storm of 2010-2011: Evidence for ammonia and water ices from analysis of VIMS spectra, Icarus, 226, 1, 402–418, doi: 10.1016/j.icarus.2013.05.043.

Sromovsky, L. A., and P. M. Fry, (2010), The source of widespread 3 μm absorption in Jupiter's clouds: Constraints from 2000 Cassini VIMS observations, Icarus, 210, 230–257, doi: 10.1016/j.icarus.2010.06.039.

Stallard, T. S., H. Melin, S. Miller, S. V. Badman, K. H. Baines, R. H. Brown, et al., (2015), Cassini VIMS observations of H3+ emission on the nightside of Jupiter, Journal of Geophysical Research-Space Physics, 120, 6948–6973, doi: 10.1002/2015ja021097.

Stallard, T. S., H. Melin, S. Miller, S. V. Badman, R. H. Brown, K. H. Baines, (2012a), Peak emission altitude of Saturn's H3+ aurora, Geophysical Research Letters, 39, doi: 10.1029/2012gl052806.

Stallard, T. S., H. Melin, S. Miller, J. O'Donoghue, S. W. Cowley, S. V. Badman, A. Adriani, R. H. Brown, K. H. Baines, (2012b), Temperature changes and energy inputs in giant planet atmospheres: what we are learning from H3+, Philos Trans A Math Phys Eng Sci, 370, 1978, 5213–5224, doi: 10.1098/rsta.2012.0028.

Sugiyama, K., K. Nakajima, M. Odaka, K. Kuramoto, Y. Y. Hayashi, (2014), Numerical simulations of Jupiter's moist convection layer: Structure and dynamics in statistically steady states, Icarus, 229, 71–91, doi: 10.1016/j.icarus.2013.10.016.

Sussman, M. G., N. J. Chanover, A. A. Simon-Miller, A. R. Vasavada, R. F. Beebe, (2010), Analysis of Jupiter's Oval BA: A streamlined approach, Icarus, 210, 202–210, doi: 10.1016/j.icarus.2010.06.044.

Sylvestre, M., S. Guerlet, T. Fouchet, A. Spiga, F. M. Flasar, B. Hesman, G. L. Bjoraker, (2015), Seasonal changes in Saturn's stratosphere inferred from Cassini/CIRS limb observations, Icarus, 258, 224–238, doi: 10.1016/j.icarus.2015.05.025.

Teanby, N. A., L. N. Fletcher, P. G. J. Irwin, T. Fouchet, G. S. Orton, (2006), New upper limits for hydrogen halides on Saturn derived from Cassini-CIRS data, Icarus, 185, 2, 466–475, doi: 10.1016/j.icarus.2006.07.011.

Tejfel, V. G., (2005), Latitudinal variations of the molecular absorption on Saturn and seasonal changes of the atmospheric state at S- and N-hemispheres, Terrestrial Atmospheric and Oceanic Sciences, 16, 1, 231–240, doi: 10.3319/tao.2005.16.1.231(aa).

Temma, T., N. J. Chanover, A. A. Simon-Miller, D. A. Glenar, J. J. Hillman, D. M. Kuehn, (2005), Vertical structure modeling of Saturn's equatorial region using high spectral resolution imaging, Icarus, 175, 2, 464–489, doi: 10.1016/j.icarus.2004.11.006.

Trammell, H. J., L. Li, X. Jiang, Y. Pan, M. A. Smith, E. A. Bering III, S. M. Hörst, et al., (2016), Vortices in Saturn's Northern Hemisphere (2008–2015) observed by Cassini ISS, Journal of Geophysical Research-Planets, 121, 9, 1814–1826, doi: 10.1002/2016je005122.

Trammell, H. J., L. M. Li, X. Jiang, M. Smith, S. Horst, A. Vasavada, (2014), The global vortex analysis of Jupiter and Saturn based on Cassini Imaging Science Subsystem, Icarus, 242, 122–129, doi: 10.1016/j.icarus.2014.07.019.

Vasavada, A. R., S. M. Horst, M. R. Kennedy, A. P. Ingersoll, C. C. Porco, A. D. Del Genio, R. A. West, (2006), Cassini imaging of Saturn: Southern hemisphere winds and vortices, Journal of Geophysical Research-Planets, 111, E5, doi: 10.1029/2005je002563.

Vervack, R. J., and J. I. Moses, (2015), Saturn's upper atmosphere during the Voyager era: Reanalysis and modeling of the UVS occultations, Icarus, 258, 135–163, doi: 10.1016/j.icarus.2015.06.007.

West, R. A., K.H. Baines, E. Karkoschka, A. Sanchez-Lavega, (2009), Clouds and aerosols in Saturn's atmosphere, In Saturn from Cassini-Huygens, (eds.) M. K. Doughterty, L.W. Esposito, S.M. Krimigis, pp. 161–179, Springer, Dordrecht, Netherlands.

Wong, M. H., I. de Pater, X. Asay-Davis, P. S. Marcus, C. Y. Go, (2011), Vertical structure of Jupiter’s Oval BA before and after it reddened: What changed?, Icarus, 215, 211–225, doi: 10.1016/j.icarus.2011.06.032.

Wong, M. H., G. L. Bjoraker, M. D. Smith, F. M. Flasar, C. A. Nixon, (2004), Identification of the 10-μm ammonia ice feature on Jupiter, Planetary and Space Science, 52, 385–395, doi: 10.1016/j.pss.2003.06.005.

Yair, Y., (2012), New results on planetary lightning, Advances in Space Research, 50, 3, 293–310, doi: 10.1016/j.asr.2012.04.013.

Yair, Y., G. Fischer, F. Simoes, N. Renno, P. Zarka, (2008), Updated review of planetary atmospheric electricity, Space Science Reviews, 137, 1–4, 29–49, doi: 10.1007/s11214-008-9349-9.

Ye, S. Y., G. Fischer, W. S. Kurth, J. D. Menietti, D. A. Gurnett, (2016), Rotational modulation of Saturn's radio emissions after equinox, Journal of Geophysical Research-Space Physics, 121, 12, 11714–11728, doi: 10.1002/2016ja023281.

Yelle, R. V., J. Serigano, T. T. Koskinen, S. M. Horst, M. E. Perry, R. S. Perryman, J. H, Waite, (2018), Thermal Structure and Composition of Saturn’s Upper Atmosphere From Cassini/Ion Neutral Mass Spectrometer Measurements, Geophysical Research Letters, 45, 20, 10951–10958, doi: 10.1029/2018GL078454.

Young, R. M. B., and P. L. Read, (2017), Forward and inverse kinetic energy cascades in Jupiter’s turbulent weather layer, Nature Physics, 13, 1135, doi: 10.1038/nphys4227.

Youssef, A., and P. S. Marcus, (2003), The dynamics of Jovian white ovals from formation to merger, Icarus, 162, 1, 74–93, doi: 10.1016/S0019-1035(02)00060-X.

Zarka, P., W. Farrell, G. Fischer, A. Konovalenko, (2008), Ground-based and space-based radio observations of planetary lightning, Space Science Reviews, 137, 1–4, 257–269, doi: 10.1007/s11214-008-9366-8.

Zhang, X., R. A. West, P. G. J. Irwin, C. A. Nixon, Y. L. Yung, (2015), Aerosol influence on energy balance of the middle atmosphere of Jupiter, Nature Communications, 6, doi: 10.1038/ncomms10231.

Zhang, X., C. A. Nixon, R. L. Shia, R. A. West, P. G. J. Irwin, R. V. Yelle, et al., (2013a), Radiative forcing of the stratosphere of Jupiter, Part I: Atmospheric cooling rates from

Voyager to Cassini, Planetary and Space Science, 88, 3–25, doi: 10.1016/j.pss.2013.07.005.

Zhang, X., R.-L. Shia, Y. L. Yung, (2013b), Jovian stratosphere as a chemical transport system: Benchmark analytical solutions, The Astrophysical Journal, 767, 172, doi: 10.1088/0004-637x/767/2/172.

Zhang, X., R. A. West, D. Banfield, Y. L. Yung, (2013c), Stratospheric aerosols on Jupiter from Cassini observations, Icarus, 226, 159–171, doi: 10.1016/j.icarus.2013.05.020.

Zuchowski, L. C., Y. H. Yamazaki, P. L. Read, (2009), Modeling Jupiter's cloud bands and decks 1, Jet scale meridional circulations, Icarus, 200, 548–562, doi: 10.1016/j.icarus.2008.11.024.